LBL-20043 c.2

Lawrence Berkeley Laboratory
UNIVERSITY OF CALIFORNIA

Materials & Molecular Research Division

THE CHEMISTRY AND DYNAMICS OF NO_3 PRODUCED BY PHOTOLYSIS OF N_2O_5

D.M. Swanson
(Ph.D. Thesis)

TWO-WEEK LOAN COPY
This is a Library Circulating Copy which may be borrowed for two weeks.

July 1984

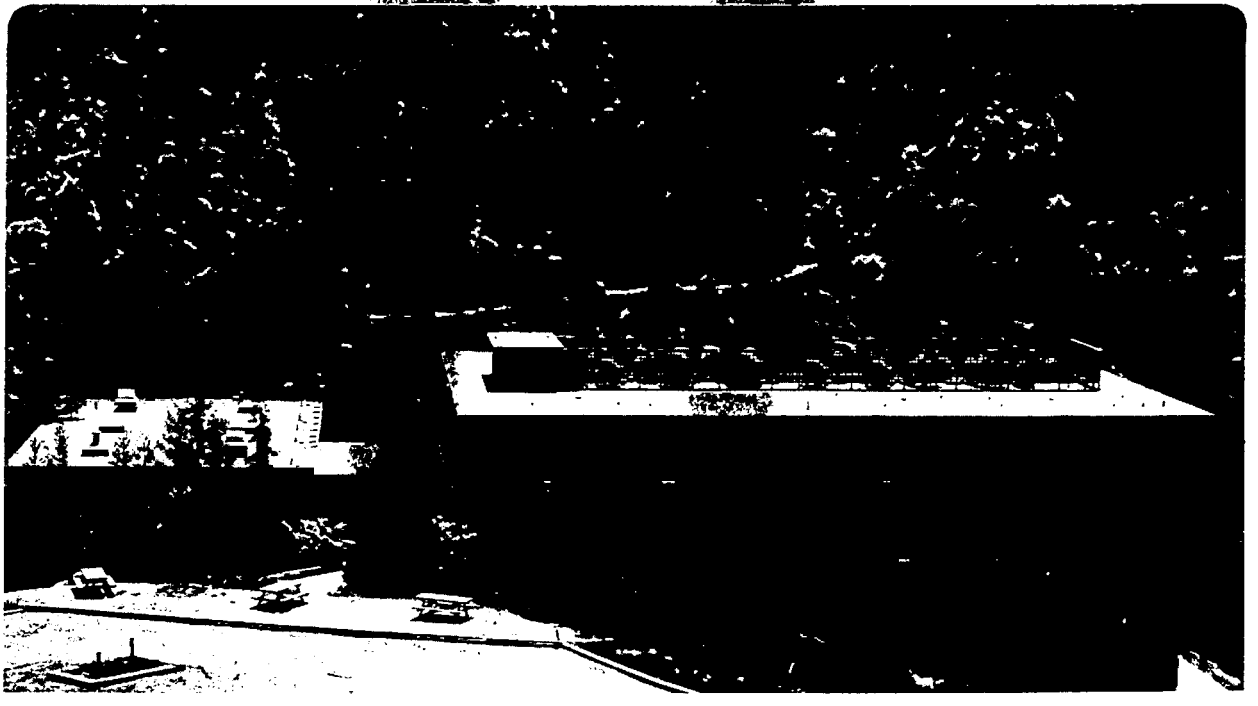

LBL-20043 c.2

Prepared for the U.S. Department of Energy under Contract DE-AC03-76SF00098

DISCLAIMER

This document was prepared as an account of work sponsored by the United States Government. While this document is believed to contain correct information, neither the United States Government nor any agency thereof, nor the Regents of the University of California, nor any of their employees, makes any warranty, express or implied, or assumes any legal responsibility for the accuracy, completeness, or usefulness of any information, apparatus, product, or process disclosed, or represents that its use would not infringe privately owned rights. Reference herein to any specific commercial product, process, or service by its trade name, trademark, manufacturer, or otherwise, does not necessarily constitute or imply its endorsement, recommendation, or favoring by the United States Government or any agency thereof, or the Regents of the University of California. The views and opinions of authors expressed herein do not necessarily state or reflect those of the United States Government or any agency thereof or the Regents of the University of California.

LBL-20043

THE CHEMISTRY AND DYNAMICS OF NO_3 PRODUCED BY PHOTOLYSIS OF N_2O_5

Diane M. Swanson

Ph.D. Thesis

Lawrence Berkeley Laboratory
University of California
Berkeley, California 94720

July 1985

THE CHEMISTRY AND DYNAMICS OF NO_3 PRODUCED BY PHOTOLYSIS OF N_2O_5

Diane M. Swanson

ABSTRACT

The results of several different studies involving the nitrate radical (NO_3) are reported in this work. The method of Flash Photolysis/Laser Absorption was used to measure directly the quantum yield for NO_3 production from UV photolysis of N_2O_5. Several product channels are possible at UV wavelengths. Although previous indirect studies indicated that the major products were 2 NO_2 + O, this work has shown that NO_3 is a primary product. The quantum yield of NO_3 obtained for photolysis at 249 nm was 0.90±0.14 independent of pressure and N_2O_5 concentration. A fast rise in the concentration of NO_3 was observed which was dependent on both pressure and N_2O_5 concentration. The rate constants obtained for the deactivation process $NO_3(\nu>0) + M \rightarrow NO_3(\nu=0) + M$ were $k(N_2O_5)=4.0\pm1.0 \times 10^{-12}$ cm^3sec^{-1} and $k(N_2) = 1.6 \pm 0.3 \times 10^{-13}$ cm^3sec^{-1}.

The appearance of NO_3 with up to 615 cm^{-1} excess energy was studied. Instantaneous production ($\leq$500 ns) of $NO_3(\nu=1)$ was followed by a fast initial decay. The rate constant for the deactivation process $NO_3(\nu=1) + M \rightarrow NO_3(\nu=0) + M$ was obtained, $k(N_2)=$

$6.3 \pm 1.5 \times 10^{-14}$ $cm^3 sec^{-1}$. The average quantum yield of NO_3 was found to be greater than unity, indicating an enhanced population at short times. About 40% of the deactivation was found to occur through this vibrational mode.

The rate of reaction of $O + NO_3 \rightarrow NO_2 + O_2$ was determined using the FP/LA technique. Variation of the oxygen atom concentration under psuedo-first-order conditions gave a rate constant $k = 6.2 \pm 0.5 \times 10^{-12}$ $cm^3 sec^{-1}$ (T=298K) which was independent of pressure (20-100 torr).

The method of Laser-Induced Fluorescence was used to determine the fluorescence yield of NO_3 relative to NO_2 after visible excitation at 623 nm. Although no NO_3 fluorescence was observed, an upper limit of 4×10^{-3} for the relative yield was obtained.

The structure of NO_3 was investigated by *ab initio* calculational methods. Geometry optimization gave a $^2B_2$ ground state of C_{2v} symmetry with N-O bond distances $R_1 = 1.34$Å, $R_{2,3} = 1.18$Å and unique angle $\theta = 132^o$. This structure was found to be 33.6 kcal/mole lower in energy than the optimized D_{3h} structure (R=1.21Å). Calculated vibrational frequencies were consistent with those recently observed experimentally.

Harold S. Johnston

ACKNOWLEDGEMENTS

Many people have been helpful in the course of my work here at Berkeley. This research was conducted under the guidance of Professor Harold Johnston. His patience and knowledge provided invaluable assistance to my education as a researcher.

I would like to thank Bill Marinelli for his guidance when I first began my graduate career. The other members of the Johnston group; Jim, Brian, Pierre, Francis, Tony, Baek, Doug, and Wade; have also provided much needed support and encouragement, both scientific and otherwise.

My husband, Ken, whom I met while at Berkeley, has provided great encouragement and support. In addition, he volunteered his time and typing skills in the preparation of this thesis.

Assistance in the calculations was provided by Professor Andrew Streitwieser, Professor H.F. Schaefer, and Dr. Michel DuPuis, from whom the computer programs were borrowed.

This work was financially supported by Lawrence Berkeley Laboratory and the U.S. Department of Energy, through the Materials and Molecular Research Division under Contract No. DE-AC03-76SF00098.

Table of Contents

I. Introduction 1

A. NO_3 as a Product of N_2O_5 Photolysis 1

B. Deactivation of NO_3 after N_2O_5 Photolysis 2

C. Kinetics of the Reaction O + NO_3 3

D. Laser Induced Fluorescence of NO_3 4

E. Structure of NO_3 6

II. Experimental 8

A. Flash Photolysis/Laser Absorption 8

1. Photolysis Source 8

2. Energy Measurement 10

3. Dye Laser Probe System 10

4. Precursor Monitoring 12

5. Reaction Cell and Flow System 13

6. Signal Detection and Data Acquisition 17

7. Procedure 18

a. N_2O_5 Photolysis 18

b. O-NO_3 Kinetics 19

B. Laser Induced Fluorescence 20

1. Pulse Source 20

2. Photolysis Cell and Flow System 22

3. Precursor Monitoring 23

4. Signal Detection and Data Acquisition 25

5. Procedure 26

a. NO_2 Fluorescence 26

b. NO_3 Fluorescence 26

C. Reactants and Gases 27

1. Carrier Gases 27

2. NO_2 27

3. Ozone 27

4. Di-nitrogen Pentoxide 29

III. Photolysis of Di-nitrogen Pentoxide 30

A. Introduction 30

B. NO_3 Quantum Yields 35

1. Quantum Yield versus Pressure 35

2. Quantum Yield versus Concentration 35

3. Quantum Yield versus Photolysis Wavelength 38

4. Quantum Yield versus Laser Fluence 38

5. Discussion 42

C. Decay Rates of NO_3 after Photolysis 46

1. Decay Rate versus Pressure 46

2. Decay Rate versus Concentration 46

D. Risetimes of NO_3 after N_2O_5 Photolysis 52

1. Appearance Rate versus Pressure 56

2. Appearance Rate versus Concentration 59

IV. Deactivation of NO_3 60

A. Introduction 60

B. Probe of NO_3 (υ = 1) 61

1. Quantum Yields 61

2. Risetimes 70

3. Decay Rates 71

C. Variation of Probe Beam Wavelength 77

1. Quantum Yields 78

2. Risetimes 83

3. Decay Rates 85

V. Rate of Reaction O + NO_3 88

A. Analysis 88

1. Calculation of Its Rate Constant 88

2. Calculation of Reactant Concentrations 90

B. Results 95

1. Calculation of NO_3 Concentrations 95

2. Pressure Dependence of the Rate Constant 99

C. Discussion 99

VI. NO_3 Laser Induced Fluorescence Yields 104

A. Results 104

B. Consideration of Fluorescence Lifetimes 111

C. Discussion 113

VII. *Ab initio* Calculational Studies of NO_3 114

A. Methods 114

B. Results 115

C. Discussion 117

References 121

I. INTRODUCTION

The primary molecule of interest in the current study is the NO_3 radical. Because it is a radical, direct studies of its chemical and structural properties have been difficult. Much of the work that has been done has been due to the importance of NO_3 in atmospheric chemistry. Knowledge of the photochemical and chemical properties of NO_x species is necessary for accurate models of atmospheric systems. In the present work, several different studies involving the NO_3 radical will be reported.

A. NO_3 as a Product of N_2O_5 Photolysis

Photolysis of N_2O_5 is known to occur at UV wavelengths. The possible product channels and their threshold wavelengths, calculated from thermodynamic information, are shown below:

$$N_2O_5 \xrightarrow{h\nu} NO_2 + NO_3 \qquad \lambda < 1300 \text{ nm} \qquad (1)$$

$$NO_2 + NO + O_2 \qquad \lambda < 1125 \text{ nm} \qquad (2)$$

$$2\ NO_2 + O \qquad \lambda < 401 \text{ nm} \qquad (3)$$

$$NO_3 + NO + O \qquad \lambda < 307 \text{ nm} \qquad (4)$$

Early studies[1,2] looked at pressure changes upon constant illumination under the assumption that the products were 2 NO_2 + 1/2 O_2. Molecular modulation techniques[3] have also been used to determine quantum yields for N_2O_5 disappearance by monitoring IR absorption of N_2O_5 and NO_2. Indirect methods were used to dis-

tinguish among the possible product channels. In that study, it was concluded that the primary channel was Equation 3. The only previous direct study[4] used flash photolysis/resonance fluorescence to look at the yields of NO and oxygen atoms (λ=290-300 nm). The results suggested an upper limit of 0.11 for the quantum yield of NO production. This led to the conclusion that channels 2 and 4 were unimportant. The oxygen atom yield was reported to be 0.35 ± 0.10. A mechanism involving an excited N_2O_5 deactivating to 2 NO_2 and O was postulated in order to explain all these previous results.[3]

The method of flash photolysis/laser absorption, FP/LA, was used in this work to directly determine whether channel 1 is important in N_2O_5 photolysis. Using this technique, a tunable dye laser was used as a probe in monitoring the visible absorption of NO_3 after pulsed UV photolysis.

B. Deactivation of NO_3 after N_2O_5 Photolysis

The results of the FP/LA experiments (Section III) indicated that NO_3 was a primary product of N_2O_5 photolysis. These experiments, which monitored NO_3 absorption as function of time, also provided kinetic (dynamic) information. A risetime for NO_3 appearance was observed. From the threshold wavelength for channel 1, an excess energy of 40 kcal/mol was calculated for photolysis at 249 nm. This energy must be distributed among rotational, vibrational, translational and/or electronic energies of the

products. The photolysis experiments measured NO_3 in its ground state ($\nu = 0$). However by tuning the dye laser, the same FP/LA technique could be used to probe low vibrational levels of NO_3. The aim of the experiments was to gather information on the dynamics of the deactivation of NO_3.

C. Kinetics of the Reaction of O + NO_3

The N_2O_5 photolysis results (Section III), in addition to showing an initial rise of NO_3, showed a subsequent loss of NO_3. Assuming that NO_2 and NO_3 are the major photolysis products, loss of NO_3 is expected to occur mainly by reaction 5.

$$NO_2 + NO_3 \xrightarrow{[M]} N_2O_5 \qquad (5)$$

Reaction of NO_3 with itself is much slower than (5). Under the reaction conditions used, it was found that the loss rate of NO_3 was considerably faster than the rate expected for reaction 5.[5] If in fact some oxygen atoms were produced by the photolysis of either N_2O_5 or a small O_3 impurity, reaction 6 would occur.

$$O + NO_3 \xrightarrow{k_1} NO_2 + O_2 \qquad (6)$$

The rate constant, k_1, had been measured in only one previous study.[6] A molecular modulation technique was used which gave an indirect measurement of the rate constant k_1. Assuming this rate constant and a reasonable concentration of oxygen atoms, the loss

of NO_3 after N_2O_5 photolysis in the current study (Section III) still appears to be too fast. Because the previous measurement of k_1 was indirect,[6] the rate constant k_1 was redetermined in this work using a direct method. Photolysis of a suitable mixture of N_2O_5 and O_3 gave NO_3 with excess oxygen atoms. FP/LA was again used to measure the NO_3 absorption as a function of time. From these data, the rate constant k_1 was extracted.

D. Laser Induced Fluorescence of NO_3

The work mentioned so far involves interactions of NO_3 with other species. The radical itself is also interesting and not well studied. It was mentioned that NO_3 can be monitored by its visible absorption. The visible absorption spectrum of NO_3 was first obtained by Jones and Wolf,[7] and has been reexamined by several workers.[8-13] An absorption maximum at 662 nm was observed, followed by a series of vibrational bands to shorter wavelengths. The absorption spectrum was reported to be diffuse;[8] that is, no rotational structure was seen. This diffuseness was attributed to pre-dissociation. Two product channels are possible at visible wavelengths.

$$NO_3 \xrightarrow{h\nu} NO + O_2 \qquad \lambda < 6300 \text{ nm} \qquad (7)$$

$$NO_2 + O \qquad \lambda < 580 \text{ nm} \qquad (8)$$

A study of the photolysis products[4] (oxygen atoms and NO) indicated for wavelengths shorter than 580 nm the quantum yield of

oxygen atoms is near unity. The yield of NO was smaller, with a maximum of 0.30 in the wavelength region λ = 600-560 nm. No dissociation products were observed in the region 662-600 nm. The conclusion drawn from these results was that predissociation was not occurring. A reinvestigation of the absorption spectrum[10] (with a resolution of 0.0003 nm) confirmed that the spectrum was diffuse. The diffuseness of the absorption spectrum can then be explained by the Douglas effect.[14] The broadening of the absorption spectrum is due to coupling of the excited electronic state to high vibrational levels of the ground state. This coupling mechanism has been used previously to explain the anomalously long fluorescence lifetime of NO_2 for example.[15] If this explanation is correct for NO_3, visible fluorescence could be observed after excitation in the region 600-662 nm. The fluorescence is expected to have a long lifetime and a fluorescence yield near unity.

The laser-induced fluorescence technique, LIF, has recently been used by two different groups.[16,17] Although there was some disagreement on the collision-free lifetimes, both groups were able to observe fluorescence. In neither case was the fluorescence yield obtained. The present work used the LIF technique in measuring the yield of NO_3 fluorescence relative to NO_2 fluorescence. Multi-path visible absorption was used to monitor the concentration of both NO_2 and NO_3.

E. Structure of NO_3

Both experimental and theoretical work has been done to try to determine the structure of NO_3,[18-27] yet the results have been inconclusive. Several ESR studies have been done,[18-22] but with conflicting results. In all cases, the g-values obtained indicated that NO_3 is planar. For planar NO_3, two different symmetries are possible, either a trigonally symmetric D_{3h} structure or a structure of C_{2v} symmetry. The ESR results did not agree with each other and were apparently dependent upon the medium used. A rotationally resolved IR spectrum has not been obtained for NO_3. Large interferences by molecules such as N_2O_5 and NO_2 which absorb in the same region as expected for NO_3 have made obtaining an IR spectrum of NO_3 difficult.

Several theoretical calculations have been carried out. The first two were done using semi-empirical methods. Walsh[23] used Hückel molecular orbital calculations to investigate whether a planar D_{3h} symmetry was more stable than a pyrimidal C_{3v} structure. He found that the planar geometry is the more stable. An INDO study[24] compared the energies of D_{3h} and C_{2v} NO_3 stuctures and found the C_{2v} to be the lower in enegry. *Ab initio* methods have also been used to study NO_3.[25,27] Calculations assuming D_{3h} symmetry[26] concluded that for this symmetry, $^2A_2'$ would be the ground state. If the ground electronic state for D_{3h} symmetry were degenerate ($^2E'$ or $^2E''$), the Jahn-Teller effect predicts

that distortion to C_{2v} symmetry would occur. For a $^2A_2'$ ground state, distortion would not be expected to occur. These studies, however, did not calculate the energy of NO_3 with C_{2v} symmetry for comparison. A partial geometry optimization was reported by Lund and Thomas[27] using *ab initio* methods ([4s,2p]). They also concluded that D_{3h} was the lower energy symmetry; however, details describing which geometrical parameters were allowed to vary were not given. Therefore, it is uncertain what the values determined correspond to. The present study uses *ab initio* methods to calculate and compare the energies of the lowest states of C_{2v} and D_{3h} symmetry. At the optimum geometry obtained, force constants were then calculated and used to predict the vibrational frequencies of the NO_3 radical.

II. EXPERIMENTAL

A. Flash-Photolysis/Laser Absorption

The method of Flash-Photolysis/Laser Absorption (FP/LA) was used both to measure the yield of NO_3 from photolysis of N_2O_5 and to measure the rate of reaction of NO_3 with oxygen atoms. A schematic of the experiment is shown in Figure 1.

1. Photolysis Source

The photolysis source used in these experiments was a Lumonics TE-860-2M rare gas halide excimer laser. For these experiments it was operated either on the KrF or XeF transitions at 248 nm and 350 nm, respectively. The typical bandwidth was about 0.4 nm,[28] and the pulse width, as reported by the manufacturer, is 10-20 ns.

The laser output was unpolarized and rectangular in shape, typically about 7 X 20 mm upon exiting the laser cavity. Because of the large divergence of the beam, a one meter quartz lens was placed in front of the cell, to more nearly collimate the beam. Pulse energies were as high as 250 mJ (KrF). A black anodized aluminum aperture (0.5 cm^2 area) was centered on the cell window to define the photolysis beam. The resulting excimer pulse energies were 10-20 mJ as measured upon exiting the cell, and varied with gas fill, age of the fill, and discharge current.

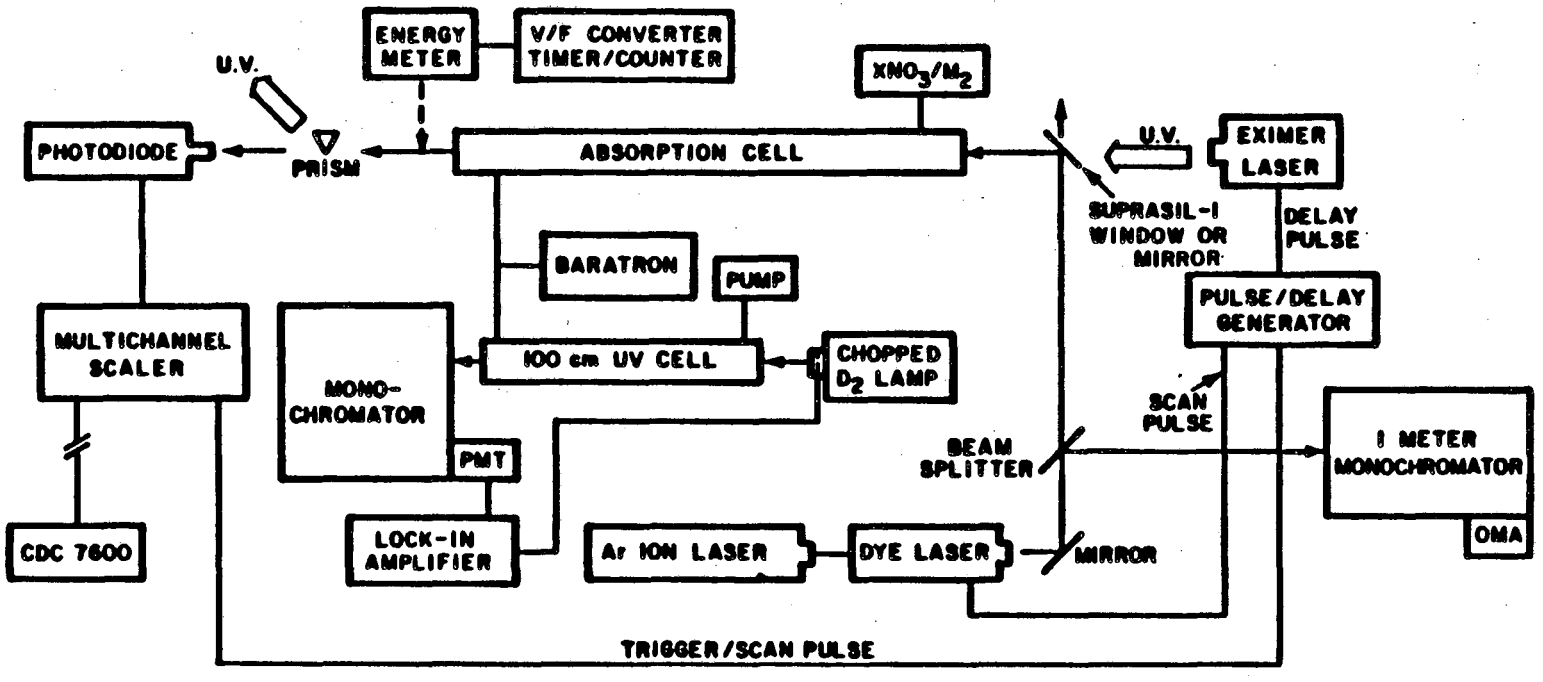

XBL 851-894

Figure 1. Schematic of Flash Photolysis/ Laser Absorption experiment

2. Energy Measurement

In order to determine quantum yields, it was necessary to measure the energy of the photolysis pulse. This was accomplished using a Gentec Model ED200 pyroelectric joulemeter, with a peak reading sample and hold (PRJ-D) digital readout. The joulemeter had been previously calibrated by Marinelli.[28] In the course of an experiment, the absorbing face was recoated with Nextel 101-C10 flat black enamel, and therefore, needed to be recalibrated. This was done by comparing it to another joulemeter which had recently been calibrated at the factory. The readout was appropriately adjusted.

3. Dye Laser Probe System

The laser used as a probe was a Spectra-Physics Model 581 A single frequency dye laser pumped by a Model 164-05, 5 watt Ar ion laser. Several dye mixtures were used in the course of these experiments, as are listed in Table 1. Concentrations and solvents were those suggested by Exciton.[29]

In these experiments the dye laser was operated with all the tuning elements removed except the 3-plate birefringent filter. The linewidth in this case was approximately 0.5 Å.[28] Current stabilization of the ion laser was used to obtain stable light levels. The output power of the dye laser was measured using an internal power meter, and was typically 30-50 mW.

Table 1 Dyes Used

Dye	Laser Region (nm)
R640/R590	614-672
DCM	608-727
LDS 698	688-808

Part of the beam was split off by reflection from a (pyrex) window (before the cell) and sent to an Interactive Technologies Model CT-103 one meter monochromator, which had a 1200 line/mm grating blazed at 5000 Å, and which was used in second order. Attached to the output port of the monochromator was a PAR model 1205D vidicon tube and model 1205A optical multichannel analyzer. A CRT then displayed the wavelength with a resolution of 0.4 Å. In addition to the dye laser beam, the output from a neon pilot lamp was focused onto the monochromator slits. The neon lines, as measured by Paschen,[30] were then displayed with the dye laser signal and were used for calibration.

The remainder of the beam then propagated to a suprasil window at approximately 45°, such that approximately 5% of this beam was reflected down the photolysis cell, colinearly with the photolysis beam. This probe beam was totally contained within the region of the photolysis laser.

4. Precursor Monitoring

The method of ultraviolet absorption spectroscopy was used to measure the precursor concentrations, which was made possible by the relatively high absorption cross section of the precursors in the 220 to 250 nm region.

The monitoring system (Figure 1) consisted of a deuterium lamp and power supply from a Beckman Model DU-2 spectrophotometer. The lamp was housed in an aluminum box which was painted

flat black and had an exit hole approximately 2 mm in diameter. The output was modulated using an American Time Products 400 Hz tuning fork chopper and was collimated with a 10 cm focal length quartz lens. The beam was sent down a 2.3 i.d. X 100 cm pyrex absorption cell equipped with Suprasil windows. After exiting the cell the beam entered a McPherson Model 218 0.3 meter monochromator with a 2400 l/mm grating blazed at 1500 Å. The slits were typically 200 µm, resulting in a resolution of approximately 6 Å. The monochromator was calibrated by using the output of a HeNe laser at 6328 Å. The output of the monochromator impinged on an RCA 1P28 photomultiplier tube. The resulting signal was amplified and sent to a lock-in amplifier, then digital voltmeter.

The spectra of the precursor molecules, N_2O_5 and O_3, are shown in Figure 2. Their absorption cross-sections are listed in Table 2 at the wavelengths of interest, along with cross-sections for the most likely impurities.

5. Reaction Cell and Flow System

All experiments were done in a flowing system. The precursor concentrations were controlled by adjusting the flow rate of carrier gas through traps at various temperatures. The trap containing N_2O_5 was typically immersed in a slush bath of either *m*-xylene or *o*-xylene, resulting in temperatures of $-48^{o}C$ and

Table 2 UV Absorption Cross-sections ($/cm^2$) of Important Species

Gas	Wavelength (nm) 220	250
N_2O_5	2.20×10^{-18}	4.0×10^{-19}
O_3	1.8×10^{-18}	1.1×10^{-17}
HNO_3	1.51×10^{-19}	1.91×10^{-20}
NO_2	3.96×10^{-19}	2.83×10^{-20}

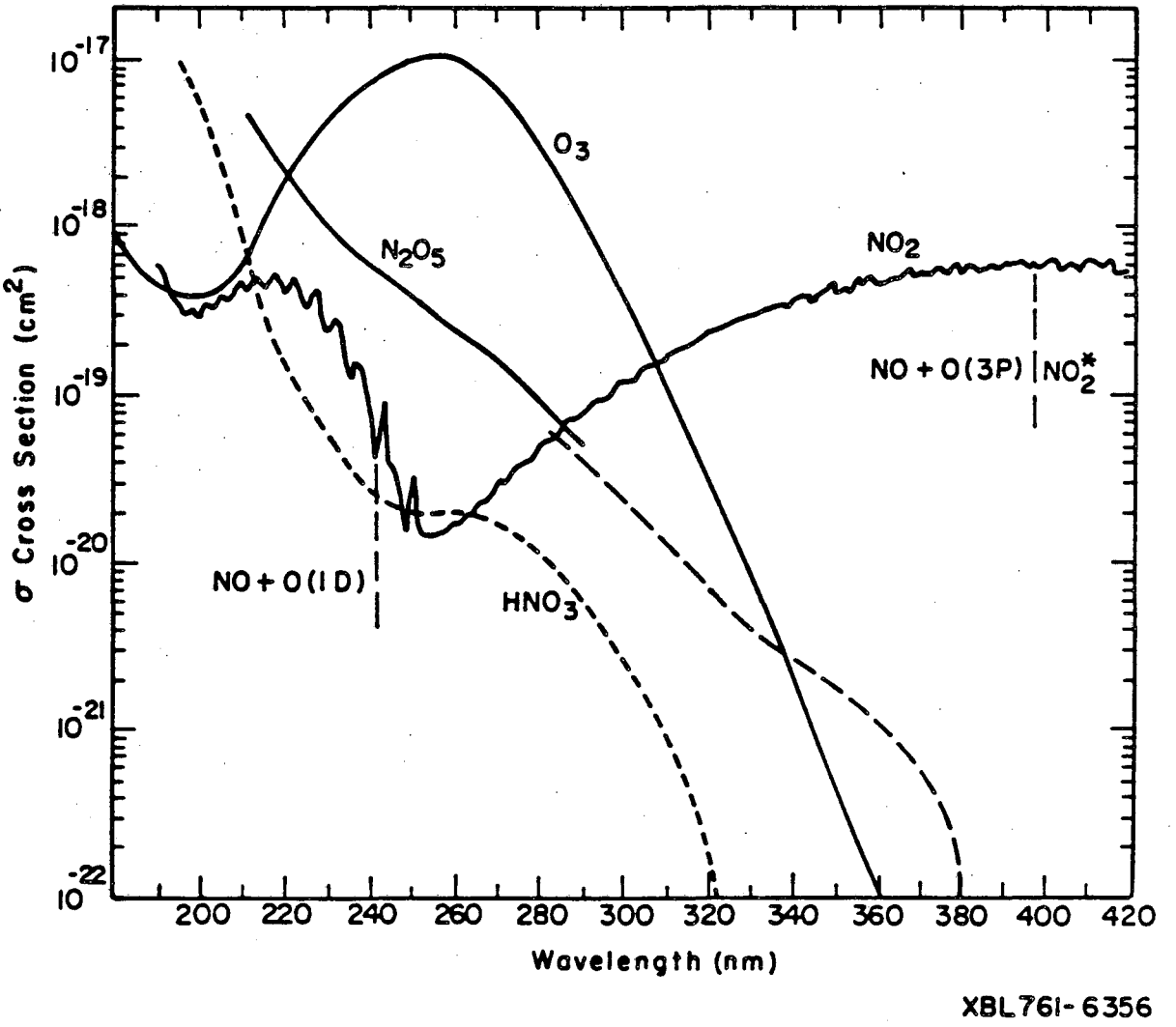

Figure 2. Ultraviolet and near ultraviolet absorption spectra of NO_2, N_2O_5, O_3, and HNO_3

-29°C, respectively. The O_3 trap (when needed) was kept in a dry ice/isopropanol slush bath at -77°C.

Either N_2 or O_2 was used as a carrier gas. After passing through a flow meter, the carrier gas was split into several streams. One of these streams bypassed the traps, while the others flowed through the separate traps and picked up the precursors. These streams were recombined before entering the absorption cell, where the concentration of the precursors was monitored.

From the absorption cell, the gases flowed through 3/4 inch tubing into the photolysis cell. The purpose of making the connecting tubing large between the two cells was to eliminate a pressure drop between them. Measurements of the pressure at either end of the system showed no difference in pressure. After the photolysis cell, the gas mixture was sent through a throttled and trapped rough pump. With flow rates measured at 200 scm^3/min, the typical residence time in the photolysis cell at 20 torr total pressure was approximately ten seconds.

The photolysis cell consisted of a 4.3 cm i.d. X 120 cm pyrex tube with stainless steel end caps connected by "ultra-torr" fittings. The cell windows were 3.75 cm Suprasil-1 flats. The total path length was measured to be 133 cm. Pressures in the cell were measured using an MKS Baratron Model 310BHS-1000 capacitance manometer.

6. Signal Detection and Data Acquisition

The photolysis and probe beams, after passing through the photolysis cell were split by a quartz prism. The probe beam was sent through a 660 or 700 nm interference filter, then through several apertures onto a photodiode detector. By adjusting the angle of the interference filter, whose bandwidth was approximately 5 nm, all wavelengths of interest could be passed.

The photodiode used was an SGD-100A, with an amplifier of in-house design (built by Marinelli[31]). The calculated bandwidth of the dectector/amplifier was reported to be 10 MHz,[28] and measured to be $\leq$50 ns.

The analog signals from this detector were then sent to a Biomation 8100 transient digitizer. Originally the signal was then sent to a Fabritek 1074 Signal Averager/PDP8 computer system for storage, display and averaging. Typically the Fabritek was used with 1024 channels at 200 ns/channel. This was later replaced by an Apple II+ computer system, with in-house software.[32] The Apple collected 2048 channels at 50 ns/channel. In either case the data could be sent to the Lawrence Berkeley Laboratory CDC 7600 computing system for analysis.

The trigger pulse was provided by a Wavetek pulse generator. This same trigger was sent to a EH Research Labs Model G710 pulse-delay generator, which then triggered the excimer laser approximately 100 channels after the beginning of a sweep. (The

actual time depended on the channel width.) Between 128 and 1024 sweeps were collected and averaged for each experiment.

Initially the excimer laser was pulsed at 0.1 Hz, such that the photolysis products were removed from the cell between pulses. However, it was found that increasing the rate to 1 Hz did not affect the results, so all subsequent experiments were done at this rate.

7. Procedures

a. N_2O_5 Photolysis

Before starting an experiment, the equipment was allowed to warm up for about one hour. The flow of carrier gas was started and adjusted such that the pressure was as desired. At least 30 minutes were allowed for stabilization. At this point, a flow of N_2O_5 through the cell was begun. After about ten minutes, the N_2O_5 was removed in order to condition the cell and remove some impurities in the N_2O_5. Meanwhile the dye laser was adjusted to an appropriate wavelength. The channel numbers of the two nearest neon lines were determined and the desired channel number for the dye laser was obtained by interpolation.

Each run consisted of the following:

1) With only buffer gas flowing, I_o from the UV absorption system was recorded.

2) The energy of 10-20 excimer laser shots was recorded by

placing the joulemeter at the rear photolysis cell window.

3) Some of the flow was then diverted through the N_2O_5 trap, and the flow rate was adjusted to give the desired N_2O_5 concentration.

4) After about ten minutes of stabilization time, the UV intensity (I), the energies of another 10-20 pulses, and the total pressure were recorded.

5) Data collection was then started. After the desired number of sweeps, I was recorded again. The system was then purged of N_2O_5 with pure carrier gas.

When the pressure was changed between runs, the flow was allowed to equilibrate for about 30 minutes. When the wavelength was changed, the dye laser was readjusted for peak power, and the angle of the interference filter was changed slightly. In many of the early runs, an interference filter was not used, but a 640 nm high-pass cut-off filter was placed before the photodiode.

b. $O-NO_3$ Kinetics

The procedure for these experiments was similar to the N_2O_5 photolysis experiments except for the following:

The flow of carrier gas was diverted by two separate paths through an N_2O_5 and an O_3 (on silica gel) trap. The N_2O_5 was added first and allowed to stabilize, then an appropriate amount of O_3 was added, again controlled by the flow rate. I_o and I in

the UV absorption cell were measured at both 220 and 250 nm. After a kinetic run, the system was again purged with pure carrier gas and both I_o and I were again recorded.

B. Laser Induced Fluorescence

The method of laser induced fluorescence was used to try to quantify the fluorescence of NO_3. In order to measure the concentration of NO_3 in the cell, a long path length was needed. An existing multipass White cell[33] originally designed for use in the IR was modified to accomodate this experiment. A schematic is shown in Figure 3.

1. Pulse Source

The excitation source was a Lumonics EPD-330 dye laser pumped by the same Lumonics TE-860 Excimer as used as a photolysis source in the FP/LA experiments. In this case the excimer laser was used at the XeF (350 nm) transition, with pulse energies of up to 70 mJ. The dye laser was operated on DCM in propylene glycol (about 3×10^{-3} M). The pulse width is given by the manufacturer as $\leq$ 10 ns. The beam upon exiting the laser was roughly triangular in shape, about 2 mm wide. The linewidth as reported by the manufacturer is 3×10^{-3} nm. The wavelength was measured by sending the beam through the monochromator after exiting the photolysis cell. A black anodized aluminum aperture (about 4 mm diameter) was placed at the exit port of the laser to

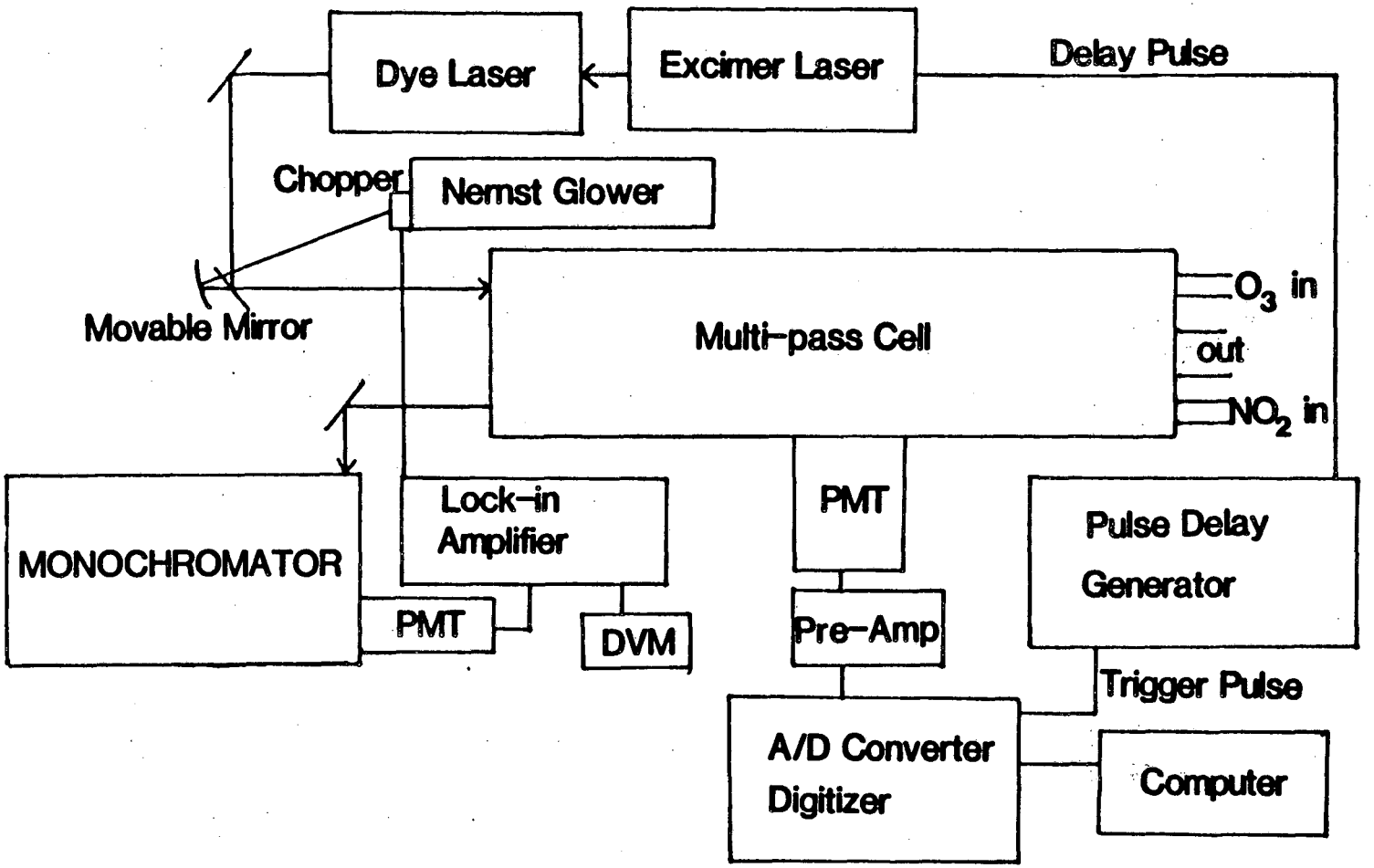

Figure 3. Schematic of Laser Induced Fluorescence experiment

reduce stray light. The conversion rate for the dye laser was about 10-15%, i.e., the output energy was typically 7 mJ/pulse, as measured by the same Gentec joulemeter described previously.

2. Photolysis Cell and Flow System

The photolysis cell was a 100 X 40 cm diameter quartz tube with stainless steel end caps. On one end were beam entrance and exit ports consisting of 5 cm diameter NaCl windows. Gases entered through two ports at the other end, connected to 3/8" o.d. disperser tubes running the length of the cell. At that end was also attached a large port to a trapped rough pump.

The internal mirrors were set up in a White type arrangement.[33] Because the cell had previously been used in the IR, the mirrors were removed and recoated with Al/MgF_2 for maximum reflection at 650 nm. Adjustment of the two end mirrors to get the desired number of passes was accomplished by turning a single threaded rod, which ensured that these two mirrors turned to the same degree. (For further details of the construction consult Littlejohn.[34])

The experiments were carried out in a slowly flowing system. Because of the large volume of the cell the residence time of gases in the cell was long, and estimated to be approximately ten minutes.

NO_3 was produced by the reaction of NO_2 with excess ozone. NO_2 was introduced at one port by simple expansion. Ozone (kept

at $-77^{o}C$ in a dry ice/isopropanol bath) was introduced at the other port.

3. Precursor Monitoring

The concentrations of NO_3 and NO_2 (used for calibration) were measured by visible absorption. The visible absorption spectra[4] of these molecules and of O_3 (a precursor) are shown in Figure 4.

The system had been set up to measure IR absorption with a Nernst glower. It was found that this same source also provided enough visible light to be used in a visible absorption experiment. The Nernst glower and power supply was that of a Beckman IR spectrophotometer. The black aluminum housing had a rectangular aperture. The light was chopped at 400 Hz (National Time Products) and focused onto the white cell entrance by a cylindrical mirror.

After making multiple passes, and exiting the cell, the beam was refocused onto the slits of a MacPherson one meter monochromator with a 1200 l/in grating blazed at 5000 Å. The signal was then detected by a RCA C31034A photomultiplier in a thermoelectrically cooled housing. The amplified signal was sent to a PAR lock-in amplifier. The monochromator was then scanned, and the output of the lock-in amplifier was recorded on a chart recorder.

It was found that the probe beam could still be detected

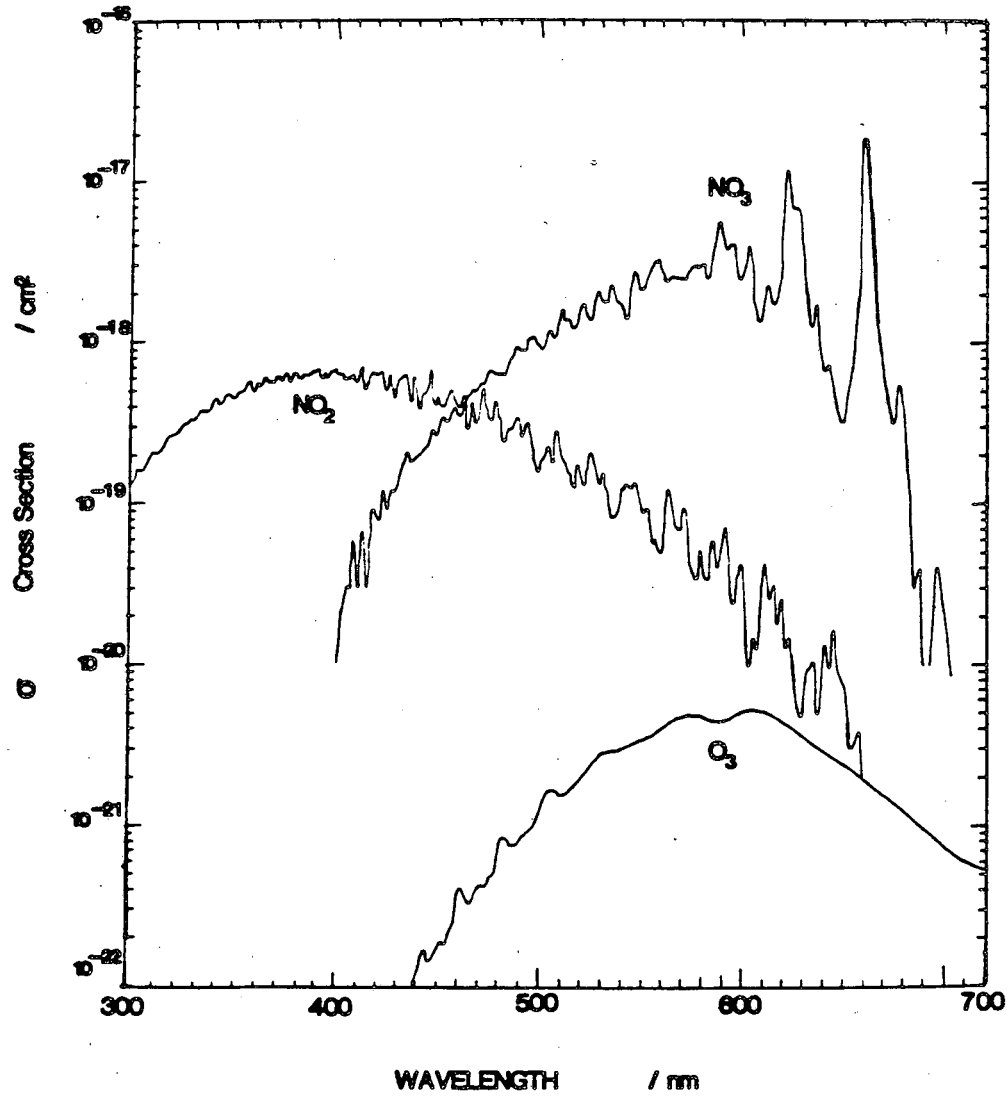

Figure 4. Visible absorption spectra of NO_2, NO_3, and O_3

after making 32 passes of the cell; however, the signal-to-noise was significantly better after only 12 passes, so this was used for the experiments.

Calibration of the monochromator was accomplished using a HeNe laser at 6328 Å. With this calibration, the NO_3 absorption peak occurred at 6620 Å, as expected.

4. Signal Detection and Data Acquisition

Visible fluorescence was observed perpendicular to the cell using an RCA C31034A photomultiplier, with a dry ice cooled housing. At the face of the PMT was a 6600 Å glass filter, a 0.5 cm^2 aperture, a 10 cm long piece of baffling, and another 0.5 cm^2 aperture just before the cell. This was required in order to minimize stray light from the dye laser pulse.

The signal was sent for preamplification to a Keithley amplifier with a bandwidth of 100 MHz and from there to the Biomation 8100 digitizer/Apple II+ computer system as described in the FP/LA experiments (Section II.A.6). Triggering of the digitizer/laser was also done as before, such that the laser fired after the beginning of an individual sweep. Typically 256 shots were taken for an experiment.

5. Procedure

a. NO_2 Fluorescence

Measurements of NO_2 fluorescence were done in order to compare to the intensity of NO_3 fluorescence observed. With the cell empty, a baseline visible absorption spectrum was taken in the region 6400-6600 Å.

NO_2 was admitted into the cell, and the flow was allowed to stabilize. The energy of the dye laser was measured and about 10 shots recorded. A visible spectrum of NO_2 in the cell was then taken such that the concentration could later be calculated. An internal mirror in the monochromator was rotated such that the dye laser beam would be deflected from the PMT. The laser was fired and data collected.

b. NO_3 Fluorescence

These experiments were carried out as with the NO_2 fluorescence (Section II.B.a), except for the following: In this case, after taking an empty cell spectrum in the region 6500-6700 Å, O_3 was admitted to the cell to a total pressure of about 0.5 torr. This was done to correct for the small absorption due to O_3 in this region. A small amount of NO_2 (approx. 50 µm) was then admitted and the concentration was adjusted until the maximum amount of NO_3 was produced.

C. Reactants and Gases

1. Carrier Gases

The carrier gases and excimer laser helium were supplied by Lawrence Berkeley Laboratory and were used without further purification. The 10% F_2 in He mixture used for the excimer laser was supplied by Matheson. The other laser gases, Kr and Xe, were Airco grade 4.5 (99.995%) which met or exceeded the manufacturer's stated purity requirements.

2. NO_2

The NO_2 needed in these experiments was also supplied by Matheson and was trapped as a solid at 77 K (liquid N_2) and allowed to warm to a liquid at room temperature before being used. Typical impurity levels for the gases supplied by LBL and the NO_2 are shown in Table 3.

3. Ozone

A stream of O_2 was purified by passing through a silica tube with copper turnings heated to 900 K, then through a column of 5% palladium or alumina at 620 K. This was done in order to convert hydrocarbon impurities to CO_2 and H_2O, which were then removed by absorption in columns of ascarite and P_2O_5 coated glass beads. The purified O_2 was then passed through an Ozone Reasearch and

Table 3 Typical Impurity Levels of Gases Used

Gas	High Dry N_2[a]	Pure He[a]	High Purity He[b]	High Dry O_2[a]	NO_2[c]
N_2	99.999	1 ppm	14 ppm	500 ppm	---
He	---	99.998	99.995	---	---
Ar	5 ppm	0.1 ppm	1 ppm	4000 ppm	---
O_2	1.5 ppm	0.2 ppm	1 ppm	99.5	---
H_2O	1.5 ppm	0.3 ppm	12 ppm	1.5 ppm	0.06
CO_2	---	0.1 ppm	1 ppm	10 ppm	---
Ne	---	---	14 ppm	---	---
THC[d]	---	---	1 ppm	3 ppm	---
H_2	---	---	1 ppm	---	---
NO	---	---	---	---	<5 ppm
ClNO	---	---	---	---	---
NO_2	---	---	---	---	99.9

[a] LBL issue.

[b] Used in Halogen/Helium mixtures.

[c] Matheson Co., supplier.

[d] Total hydrocarbons.

Equipment Company silent discharge ozonator. Typically about seven percent of the O_2 was converted to O_3. The O_3 was then preferentially trapped out by passing the O_3/O_2 mixture through a silica gel trap at 196 K in which the O_3 could be stored for later use.

4. Di-Nitrogen Pentoxide

Di-nitrogen pentoxide was prepared by the method of Schott and Davidson.[9] Part of the stream of high purity oxygen was bubbled through a trap containing NO_2. This stream was merged with the O_3/O_2 stream coming from the ozonator. The flow of O_2 through the NO_2 was adjusted such that O_3 was in excess, as evidenced by the disappearance of the brown NO_2 color after the mixing tee. The $N_2O_5/O_3/O_2$ mixture was passed through a trap held at 196 K where the N_2O_5 was deposited as thin white needle-like crystals. Production of N_2O_5 in this manner also produced a large (10-20%) impurity of HNO_3, formed in the reaction of N_2O_5 and H_2O.

III. PHOTOLYSIS OF DINITROGEN PENTOXIDE

A. Introduction

A series of experiments was done to investigate the production of NO_3 as a product of N_2O_5 photolysis under various conditions. Although indirect determinations of N_2O_5 photolysis products seemed to indicate that NO_3 was not produced,[3,4] the current results of a typical experiment (Figure 5) show a high yield of NO_3. The quantum yield of NO_3 production is given by the ratio of NO_3 produced per photon absorbed.

$$\phi = [NO_3]/\text{photons} \tag{9}$$

The amount of photons absorbed can be calculated from Beer's law and a knowledge of the incident photolysis energy. For these experiments, the N_2O_5 concentration was measured by UV absorption according to Equation 2

$$\Delta I = I_o - I = I_o(1 - e^{-\sigma[N_2O_5]L}) \tag{10}$$

where I is the absorbed and I_o the incident light intensities in units of photons/cm^3, L is the path length (128 cm), and σ is the cross-section. The incident intensity was determined by dividing the average pulse energy by the photolysis volume (0.5 cm^2 aperture by 128 cm). N_2O_5 cross-sections are given in Table 4.

The NO_3 produced was measured by laser absorption, in this case at the NO_3 absorption maximum at 662 nm. The NO_3 cross-

Table 4 UV Absorption Cross-sections for N_2O_5 at the Photolysis Wavelengths Used[40]

λ/nm	$\sigma_{N_2O_5}$ /cm^2
249	4.0×10^{-19}
308	1.8×10^{-20}
350	2.2×10^{-21}

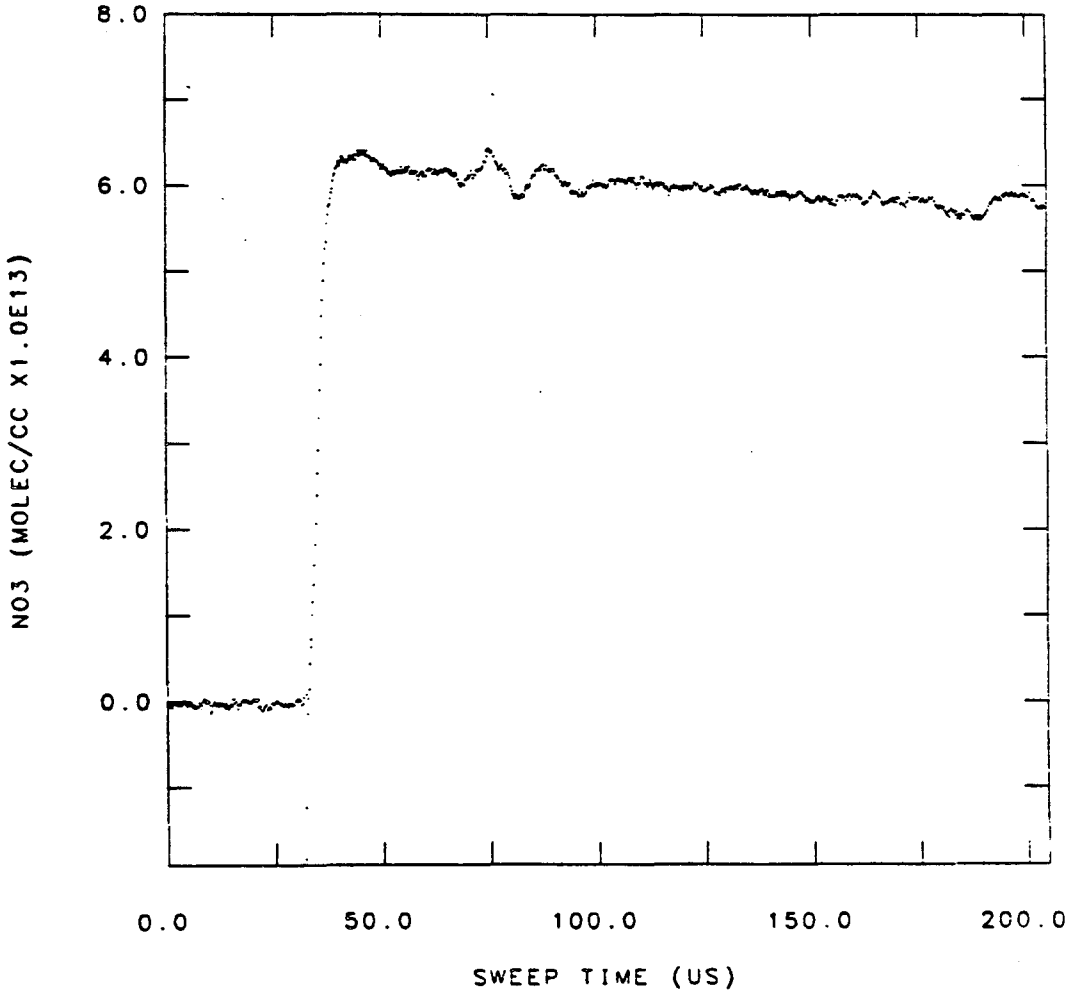

Figure 5. $[NO_3]$ versus time; 0.2 μsec/ channel

section at this wavelength[38] is 1.9×10^{-17} cm^2. The concentration was also calculated from Beer's law. I_o was taken as the average laser intensity in the pre-trigger period, typically channels 1-100. The maximum amount of NO_3 was produced shortly after the photolysis pulse. For experiments in which the decay was followed for longer time periods (Figure 6), the maximum amount of NO_3 was assumed to be present at the maximum in the absorption.

In addition to information on the quantum yield, these spectra provide kinetic information on the appearance and decay of NO_3. Initial experiments showed that the appearance of NO_3, when probed at 662 nm, was not instantaneous. For each condition, two spectra were recorded, one at a time resolution of 0.2 µsec/channel and another at 2 µsec/channel. The initial rise of the faster spectra was then fit to an exponential function to obtain the appearance rate constant.

$$[NO_3]/[NO_3]_o = 1 - e^{-k_r t} \qquad k_r = 1/\tau,\ \tau \equiv \text{risetime} \tag{11}$$

The decay rate was obtained by fitting the "slow" spectra to a single exponential decay.

$$[NO_3]/[NO_3]_{max} = e^{-k_d t} \tag{12}$$

The results of each series of experiments are given in the sections which follow.

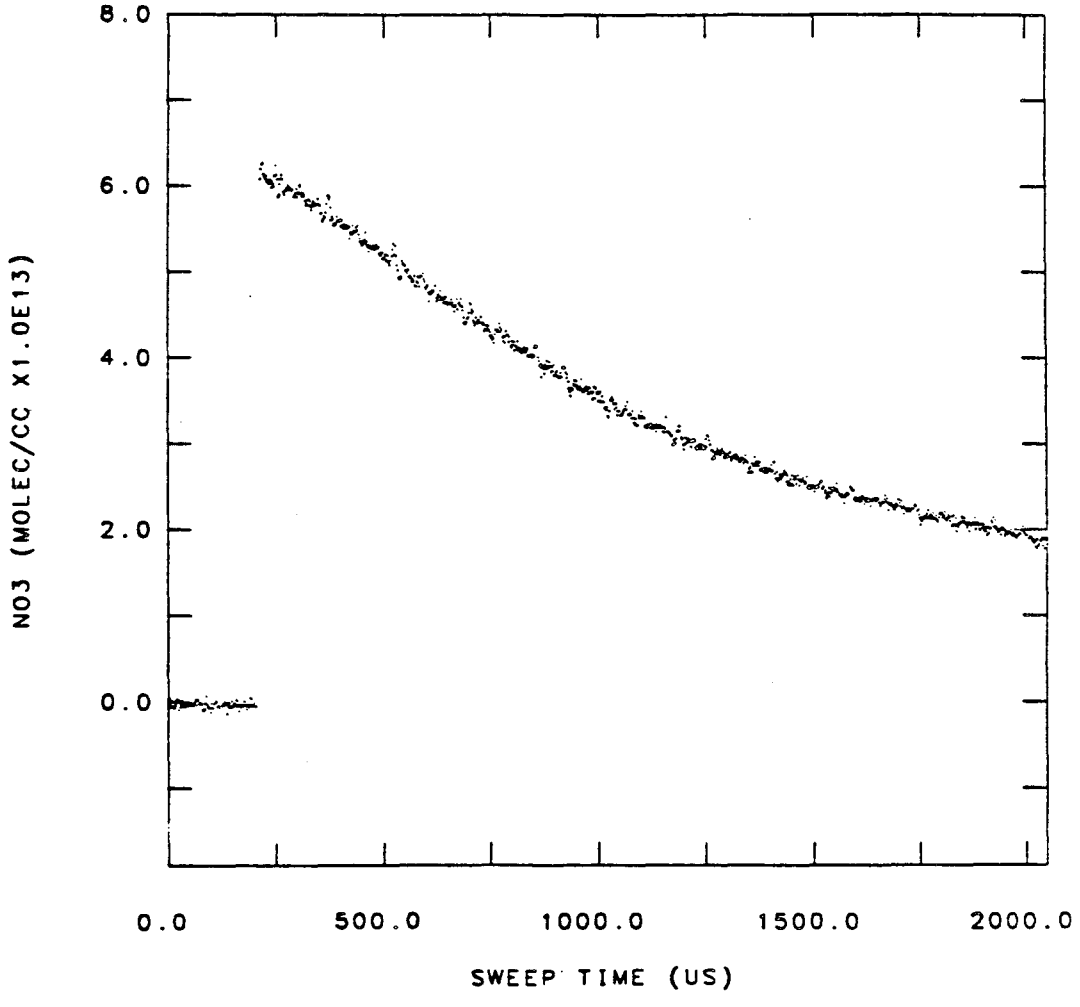

Figure 6. $[NO_3]$ versus time; 2.0 μsec/ channel

B. NO_3 Quantum Yields

1. Quantum Yield versus Pressure

In a series of experiments, the NO_3 quantum yield was measured as a function of pressure in the range 10-100 torr. The N_2O_5 concentration was kept fairly constant and ranged from 1.0 to 1.7 X 10^{16} cm^{-3} with an average concentration of 1.5 X 10^{16} cm^{-3}. Either N_2 or O_2 was used as a carrier gas. The results of the experiments are listed in Table 5. These data are plotted as quantum yield versus pressure in Figure 7. From the plot, several things are readily seen. The quantum yield is high, near unity for all cases. No dependence on pressure was observed, and no difference was seen between using N_2 or O_2 as a carrier gas. For this entire series of experiments, the average quantum yield was found to be 0.82 ± 0.12.

2. Quantum Yield versus Concentration

Another series of experiments was done in order to determine whether varying the N_2O_5 concentration affected the production of NO_3. The N_2O_5 concentration was varied two orders of magnitude from 2.6 X 10^{14} cm^{-3} to 5.0 X 10^{16} cm^{-3}. The lower limits were effectively determined by limitations on the ability to measure N_2O_5 UV and NO_3 visible absorptions. The upper limit was determined by difficulties in maintaining a steady flow at high concentrations. (All of these experiments were done at 20 torr

Table 5 Pressure Dependence Results at 249 nm

Carrier Gas	Pressure /torr	$[N_2O_5]/10^{16}$ cm^{-3}	ϕ	$k/10^5$ sec^{-1}	k_d/sec^{-1}
N_2	10.5	0.52	0.56	2.01	514
N_2	10.5	1.52	0.82	1.44	856
N_2	20.3	1.61	0.94	----	---
N_2	21.0	1.08	0.79	3.92	783
N_2	18.8	0.95	0.98	2.29	759
N_2	39.5	1.27	0.71	4.63	413
N_2	60.3	1.08	0.95	5.62	667
N_2	64.2	0.70	0.72	4.77	390
N_2	80.8	1.64	0.76	----	---
N_2	83.5	0.64	0.70	4.52	550
N_2	101.4	1.43	0.89	6.92	---
O_2	18.1	0.97	0.82	3.78	627
O_2	20.2	0.89	0.51	1.62	867
O_2	40.6	1.51	0.86	3.60	697
O_2	60.9	1.59	0.87	4.27	---
O_2	80.8	1.73	0.86	5.27	594
O_2	100.9	1.59	0.90	6.58	378

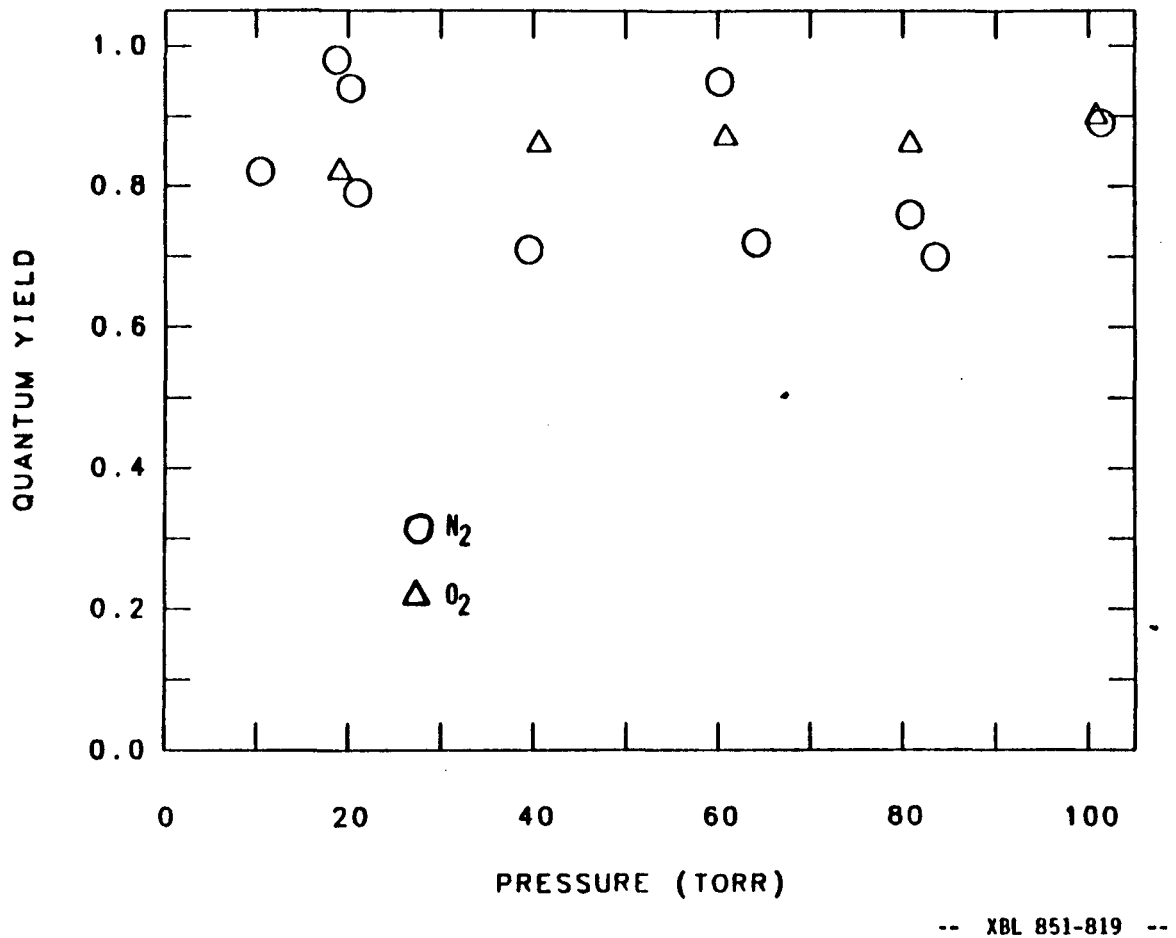

Figure 7. Quantum yield versus pressure

nitrogen total pressure.) The results of these experiments are listed in Table 6. The quantum yield is plotted against the N_2O_5 concentration in Figure 8. This plot shows that there is little or no dependence of the quantum yield on N_2O_5 concentration. The average quantum yield over this set of experiments was 0.97 ± 0.15.

3. Quantum Yield versus Photolysis Wavelength

A few experiments were conducted at photolysis wavelengths other than 249 nm. The results of these experiments are listed in Table 7. Because the absorption cross-section for N_2O_5 drops off rapidly at longer wavelengths, high N_2O_5 concentrations were necessary in order to produce enough NO_3 to measure. The average quantum yield at 308 nm was found to be 1.60 ± 0.83. The large scatter in this experiment was due not only to a decreased absorption cross-section, but also to the very low output power of the excimer laser used. At 350 nm, the average quantum yield was found to be 0.83 ± 0.15. In this case, the error is an estimate based on the signal-to-noise ratio of the NO_3 absorption and the poor stability of the N_2O_5 flow. In both cases, the average quantum yields were within the experimental error of the value determined at 249 nm.

4. Quantum Yield versus Laser Fluence

The results of several experiments to determine whether the

Table 6 Concentration Dependence Results

$[N_2O_5]/10^{15}$ cm^{-3}	ϕ	$k/10^5$ sec^{-1}	k_d/sec
0.26	1.16	----	---
0.31	1.17	----	---
0.51	1.34	1.63	---
0.52	0.90	1.54	122
1.20	1.02	2.26	212
1.90	0.96	1.46	319
2.00	1.20	1.63	201
3.10	0.79	----	---
3.50	1.06	----	---
4.11	0.85	1.78	194
5.30	0.88	2.44	519
6.40	0.84	2.01	575
6.40	0.94	2.34	685
12.0	0.80	3.92	783
21.3	0.89	3.39	---
30.5	0.90	4.02	1010
47.0	0.90	2.41	1200
49.5	0.83	4.57	1090

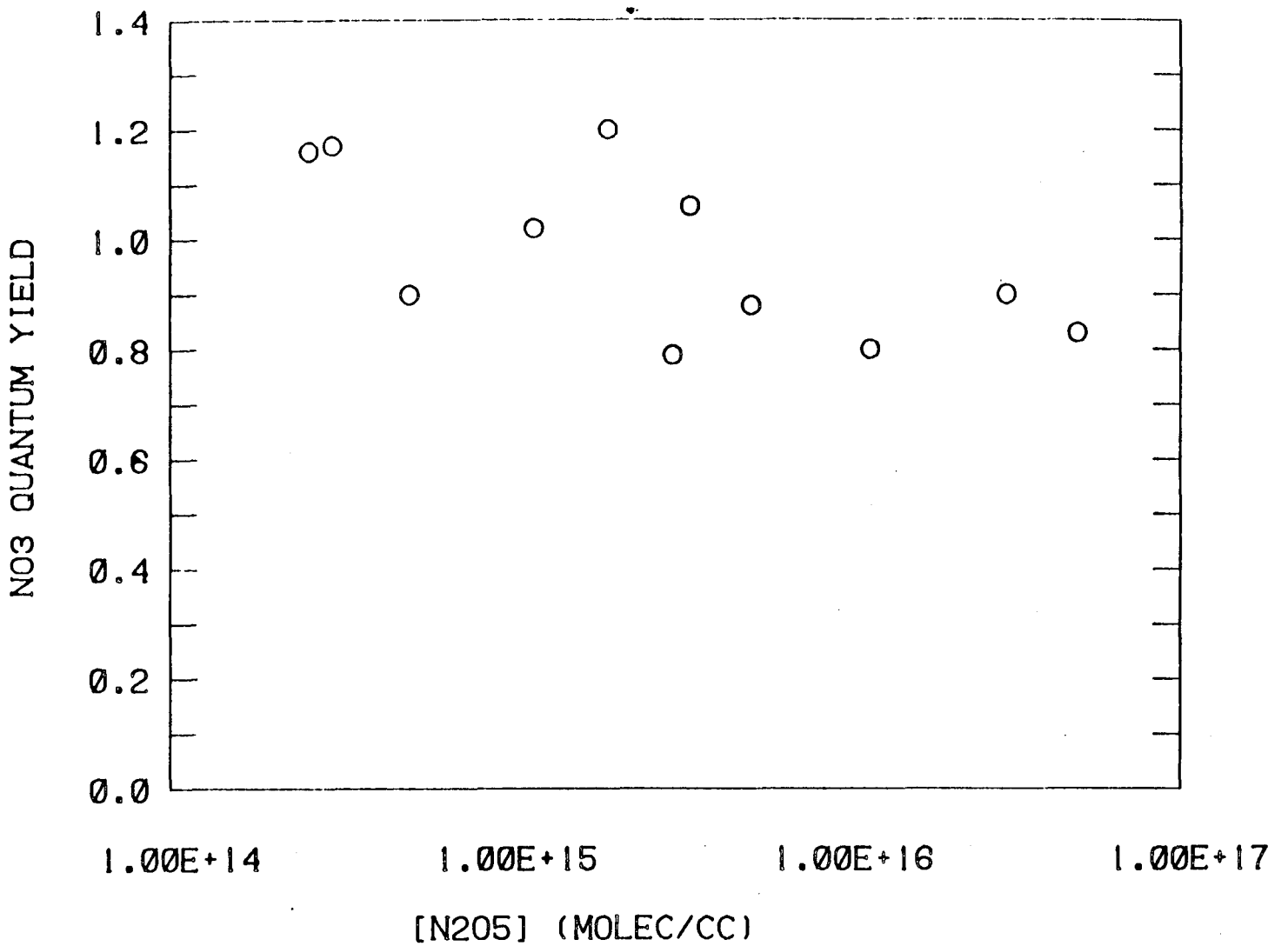

Figure 8. Quantum yield versus $[N_2O_5]$; 20 torr N_2 carrier gas

Table 7 N_2O_5 Photolysis Results at Wavelengths Other Than 249 nm

λ/nm	Pressure/torr	$[N_2O_5]/10^{16}$ cm^{-3}	ϕ
350	19	10.0	0.87
350	18.9	6.8	0.79
308	10.1	13.0	2.1
308	35.6	15.0	2.7
308	70.5	9.5	1.2
308	4.4	12.0	1.4
308	4.6	12.0	0.6

quantum yield is dependent on laser fluence are listed in Table 8. The average quantum yield was found to be 0.84 ± 0.09. This average is the same as the averages for the previous series and indicates that the quantum yield is not dependent on laser fluence at λ = 249 nm.

5. Discussion

As was mentioned in the introduction, four possible product channels for N_2O_5 photolysis in this wavelength region have been considered.

Channel 1.	$N_2O_5 + h\upsilon \rightarrow NO_2 + NO_3$		$\lambda < 1300$ nm
Channel 2.	$\rightarrow NO_2 + NO + O_2$		$\lambda < 1125$ nm
Channel 3.	$\rightarrow 2\ NO_2 + O$		$\lambda < 401$ nm
Channel 4.	$\rightarrow NO_3 + NO + O$		$\lambda < 307$ nm

In contrast to the results of previous studies, the experiments reported here demonstrate that NO_3 is the primary photochemical product of N_2O_5 photolysis at wavelengths between 249 and 350 nm. The average quantum yield over all the experiments at 249 nm was found to be 0.90 ± 0.14. The absence of a laser fluence dependence implies that this photolysis is a single photon process.

A previous study[3] suggested that N_2O_5 forms a metastable complex after excitation. The lifetime of such a species was estimated at 10 μsec with deactivation presumed to occur by

Table 8 Fluence Dependence Results (λ = 249 nm)

$[N_2O_5/10^{15}$ cm^{-3}	Laser Fluence/mJ cm^{-2}	ϕ
4.1	5.0	0.85
6.2	9.7	0.87
2.0	14.0	0.94
2.6	19.0	0.71

collision.

$$N_2O_5 + h\upsilon \rightarrow [N_2O_5]^* \quad (13)$$

$$[N_2O_5]^* \rightarrow \text{products} \quad (14)$$

$$[N_2O_5]^* + M \rightarrow N_2O_5 \quad (15)$$

$$N_2O_5 + [N_2O_5]^* \rightarrow 2\ N_2O_5 \quad (16)$$

If this were the case, one would expect the observed quantum yield to be pressure dependent. At higher pressures, the deactivation by collisions with the carrier gas would compete with the product channel. Similarly, increasing the N_2O_5 concentration would increase the self-deactivation, and again the observed quantum yield would be decreased. The absence of a dependence on either N_2O_5 concentration or the total pressure rules out the suggested mechanism involving a metastable species.

During the course of these experiments, two other studies were reported on attempts at determining the products of N_2O_5 photolysis. Photoacoustic techniques were used by Barker, et al.[35] For photolysis at 290 nm, the quantum yield was reported to be near unity although a specific number was not reported. A quantum yield for oxygen atom production was reported to be $\leqslant 0.1$ as determined by resonance fluorescence techniques.[35]

A recent study by Ravishankara[36] involved looking at both NO_3 and oxygen atom yields by visible absorption and resonance fluorescence, respectively. The quantum yield for NO_3 was found to be unity at all wavelengths studied. The oxygen atom yield

was found to be small at wavelengths longer than 290 nm, and increasing from 0.1 to 0.7 between 290 and 249 nm.

Both these studies confirm, as presented here, that NO_3 is a primary photochemical product of N_2O_5 photolysis. The results of Ravishankara suggest that channel 4 is important. This channel had been previously ruled out on the basis of experiments of Magnotta[4] which indicated quantum yields of ≤ 0.1 for NO (λ = 290-300 nm). The threshold observed for the experiments of Ravishankara agrees fairly well with that calculated from thermodynamics.[37] These results support the conclusion that there are two channels (Channels 1 and 4) involved in photolysis of N_2O_5. At wavelengths above 250 nm, channel 1 is dominant. Below this, channel 4 is the primary process. For all wavelengths, the quantum yield of NO_3 is unity.

Based on the plots, one could argue that there is a slight downward trend in ϕ for higher N_2O_5 concentrations. If so, this may be due to errors in fitting the curves. As the N_2O_5 concentration increased, the decay rate also increased (as will be shown in Section II.C.2). The assumption that the NO_3 concentration reaches its maximum before it can start to decay becomes somewhat less true, and a slight downward trend is expected. The quantum may be reduced by several percent. However, since the values of ϕ at higher concentrations are within the experimental error, it is not clear that such a trend is real.

C. Decay Rates of NO_3 after Photolysis

1. Decay Rate versus Pressure

The same series of experiments used to determine the effect of pressure on quantum yields was used to determine k_d, the rate of decay of NO_3 after photolysis. The results are listed in Table 5. Blanks in the table indicate cases where the data, which had been stored on paper tape were not able to be read back because of mispunching errors. The results obtained are plotted in Figure 9. The decay rate (k_d) appears to decrease slightly at higher pressures. For loss by reaction, the rate would be expected to increase with higher pressures if it were affected at all. The slight trend may therefore be due to diffusion of the NO_3 products out of the region being probed.

2. Decay Rate versus $[N_2O_5]$

For the experiments listed in Table 5, the decay rate k_d was calculated from the fit to a single exponential decay. The rates are also listed in Table 5. A plot of decay rate versus N_2O_5 concentration is shown in Figure 10. A definite trend in the decay rate was seen in these experiments. The decay rate increased non-linearly with N_2O_5 concentration. This suggests that destruction of NO_3 occurs by reaction with other products of the photolysis. Oxygen atoms, NO and NO_2 are all produced in the

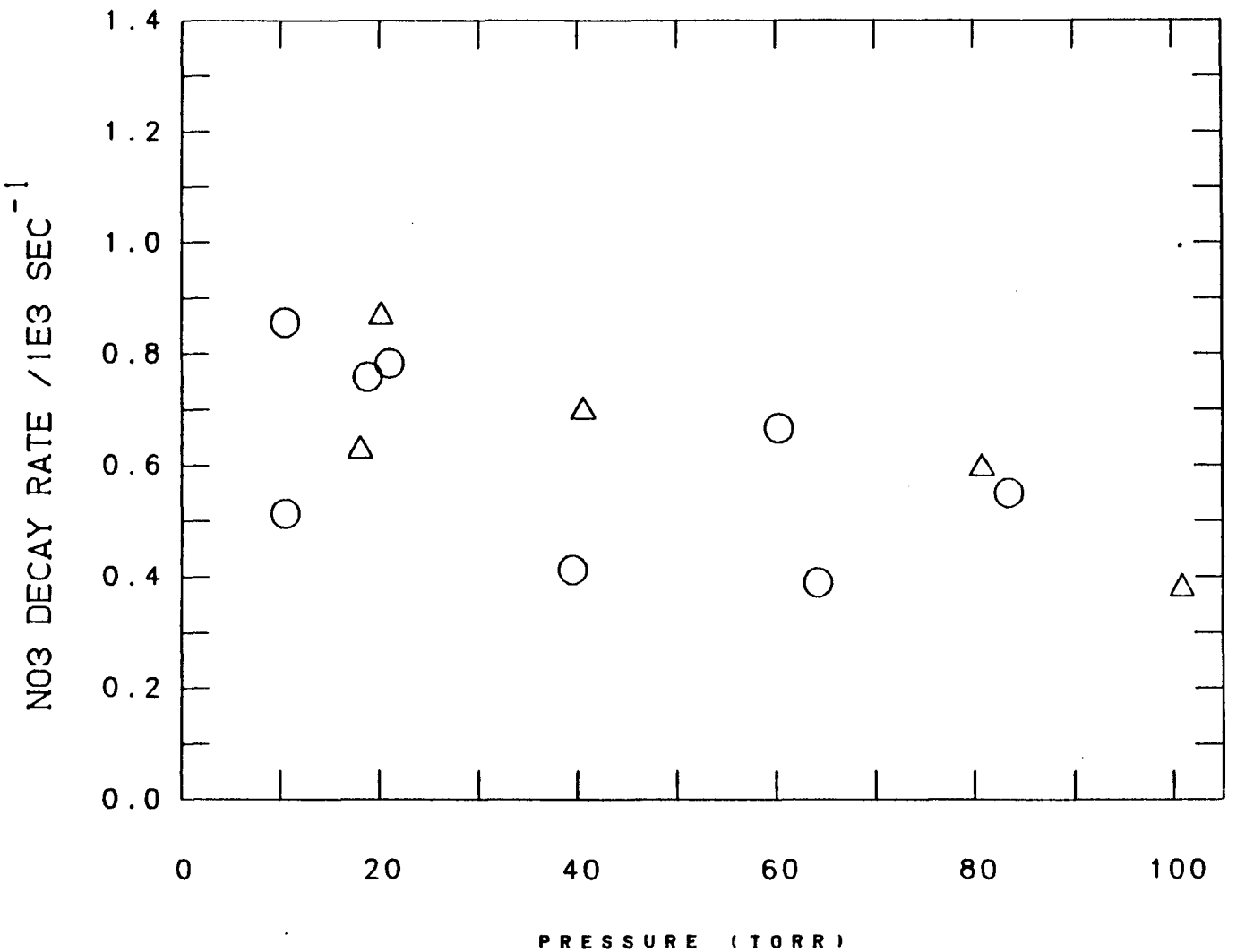

Figure 9. Decay rate, k_d, versus pressure

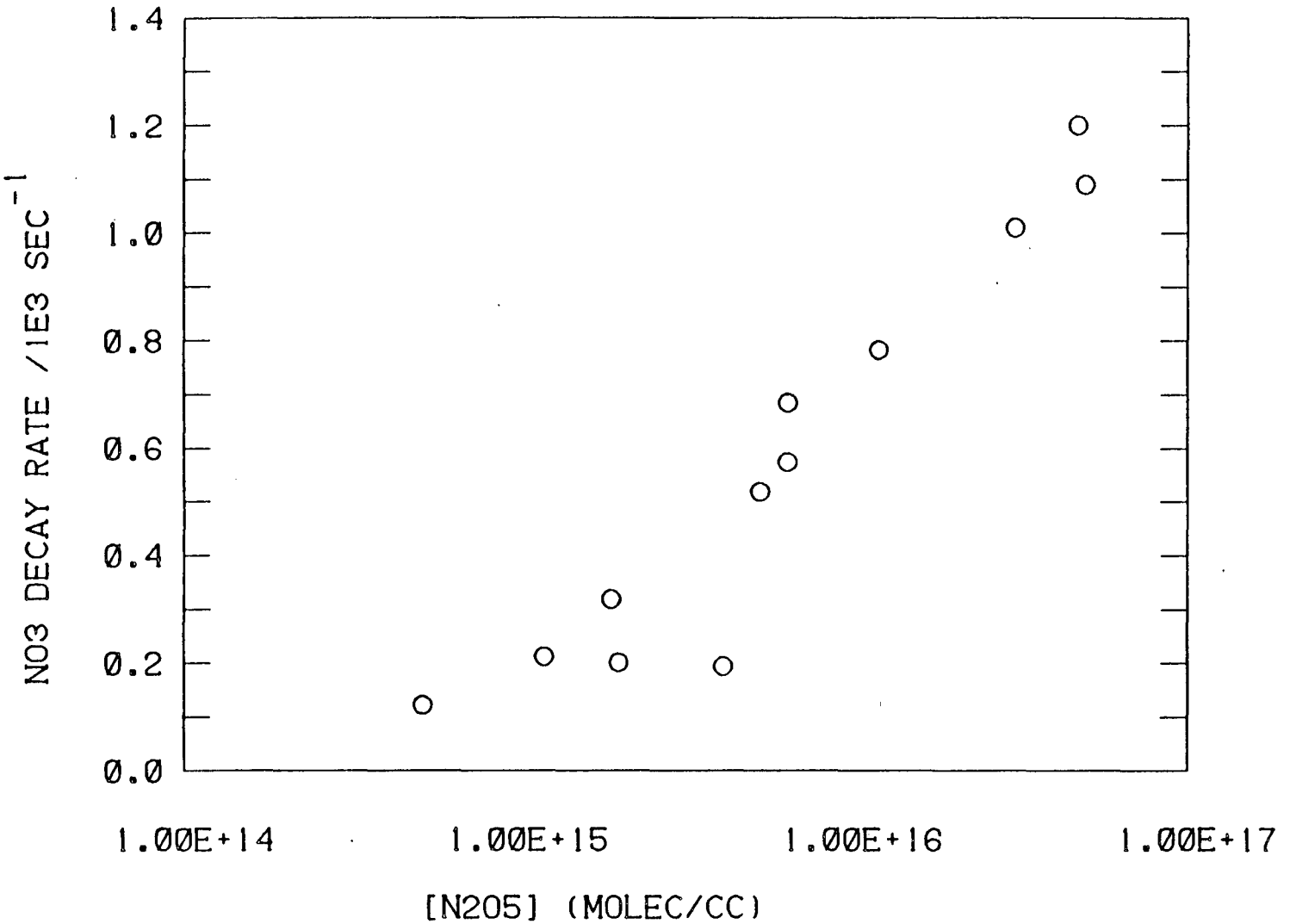

Figure 10. Decay rate, k_d, versus $[N_2O_5]$

photolysis of N_2O_5, and all can react with NO_3.

$$NO_3 + NO_2 \rightarrow N_2O_5 \qquad k_1[M] = 3.55 \times 10^{-13}\ cm^3sec^{-1},\ 20\ torr \quad (17)$$

$$NO_3 + O \rightarrow NO_2 + O_2 \qquad k_2 = 6.2 \times 10^{-12}\ cm^3sec^{-1} \quad (18)$$

$$NO_3 + NO \rightarrow 2\ NO_2 \qquad k_3 = 2.0 \times 10^{-11}\ cm^3sec^{-1} \quad (19)$$

The rate constant k_1 for reaction 17 is a function of pressure. The value at 20 torr shown above was calculated using an equation for third-body rate constants.[39] Because reaction 17 is much slower[6] than reactions 18 and 19, it can be neglected. Self-reaction of NO_3 is also negligibly slow[6].

The expression for the rate of reaction of NO_3 is given by Eq. 20.

$$-d[NO_3]/dt = k_2[O]\{NO_3] + k_3[NO][NO_3] \quad (20)$$

The initial concentrations of reactant species, O and NO, are proportional to the concentration of NO_3 produced in the photolysis.

$$[O]^o = [NO]^o = 0.7[NO_3]^o \quad (21)$$

Because the two reactions are competing, at a given time the loss of O atoms ($[O] - [O]^o$) will be smaller than the loss of NO by the factor k_2/k_3. Substituting these relations into equation 20 leads to equation 22.

$$-d[NO_3]/dt = [NO_3]^2\{0.7(k_2 + k_3) + A\} \quad (22)$$

where,

$$A = \{[NO_3]^o/[NO_3] - 1\}\{0.7(k_2 + k_3) - (k_2^2 + k_3^2)/(k_2 + k_3)\}.$$

For short times, $[NO_3] \cong [NO_3]^o$, so the equation reduces to a second-order rate expression (Eq. 23).

$$-d[NO_3]/dt = 0.7(k_2 + k_3)[NO_3]^2 \quad (23)$$

or,

$$1/[NO_3] - 1/[NO_3]^o = 0.7(k_2 + k_3)t = k't \quad (24)$$

A plot of $1/[NO_3]$ versus time is shown in Figure 11, with the value of $1/[NO_3]$ in the pretrigger period, where $[NO_3] = 0$, set equal to 1.0. The curvature in the plot at longer times shows that the second term of equation 22 becomes important. Although diffusion out of the probe region would also cause curvature, this has been shown to be small for carrier gas pressures $\geq$20 torr (Secs. III.C.1 and IV.C.3) Substituting the values of k_2 and k_3 into equation 23 gives $k' = 1.83 \times 10^{-11}$ sec^{-1} near $t = 0$. For t = 2.0 msec, $[NO_3]^o \cong 3[NO_3]$. Substituting this into equation 22 gives a slope $k' = 2.15 \times 10^{-11}$ sec^{-1}. Therefore, the rate constant k' obtained by fitting the data should be in the range $k' = 1.83 - 2.15 \times 10^{-11}$ sec^{-1}.

The data from all the experiments were fitted to a function

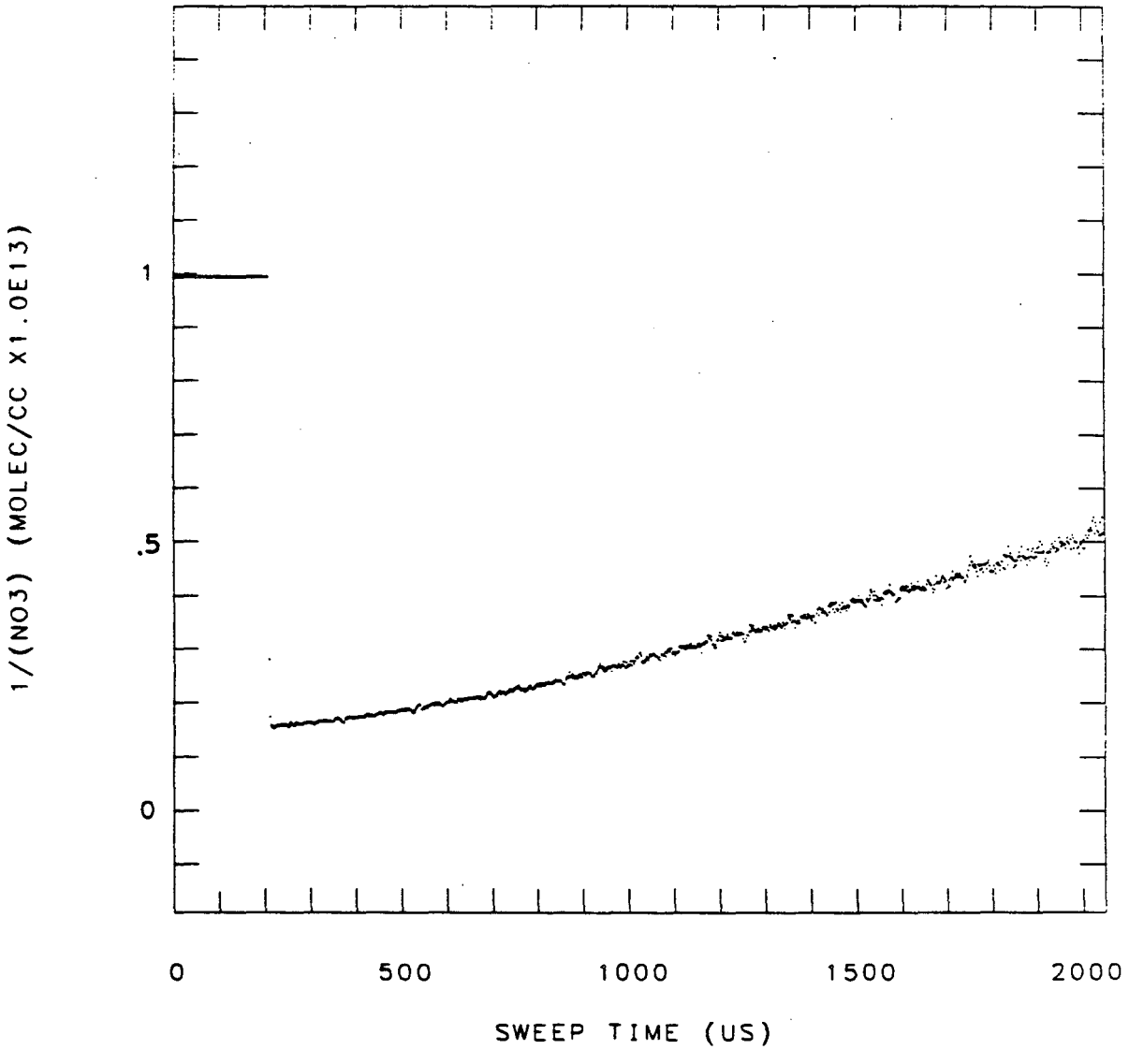

Figure 11. $1/[NO_3]$ versus time

of the form of Equation 24 giving a rate constant k'. These values are listed in Table 9 along with the initial values of NO_3 concentration observed Figure 12 shows a plot of k' versus $[NO_3]$.The rate constant was found to be independent of N_2O_5 or NO_3 concentration. The average value was found to be 1.60 ± 0.45 X 10^{-11} cm^3sec^{-1}. This value agrees within experimental error with the calculated range of the value of k' and is therefore consistent with loss of NO_3 being due to reaction with oxygen atoms and NO.

D. Risetimes of NO_3 After N_2O_5 Photolysis

In initial experiments, it was observed that NO_3 (when probed at 662 nm) was not produced at the time of the laser pulse. A resolvable risetime, on the order of 1-10 μsec was found. This rate is too fast for the time scale of chemical reaction (for these experimental conditions) and suggests that the risetime is due to collisional deactivation. Deactivation of an excited N_2O_5 can been ruled out because of the pressure independence of ϕ. The risetime is presumably due to collisional deactivation of NO_3. After photolysis at 249 nm, a large amount of excess energy remains which must be distributed among the products, either as translational, rotational, vibrational or electronic energy.

Table 9 Results of Second-order Decay Rate Analysis (T = 298 K)

$[NO_3]/10^{13}$ cm^{-3}	$k'/10^{-11}$ cm^3 sec^{-1}	
1.32	2.06	
2.20	2.14	
2.25	1.20	
3.22	1.58	
3.40	1.35	
3.99	1.56	
4.08	2.09	
4.20	1.60	
5.05	1.65	
5.12	1.67	
5.96	2.06	
6.00	1.38	
6.40	1.14	
6.42	1.67	(a)
9.49	1.19	
10.2	1.33	
12.9	1.77	
13.5	2.03	(a)
13.8	2.11	
13.9	0.57	(a)
14.2	1.09	(a)

Table 9 Results of Second-order Decay Rate Analysis (Continued)

$[NO_3]/10^{13}$ cm^{-3}	$k'/10^{-11}$ cm^3 sec^{-1}	
15.2	0.81	(a)
15.2	2.15	
19.2	2.16	

(a) carrier gas = oxygen

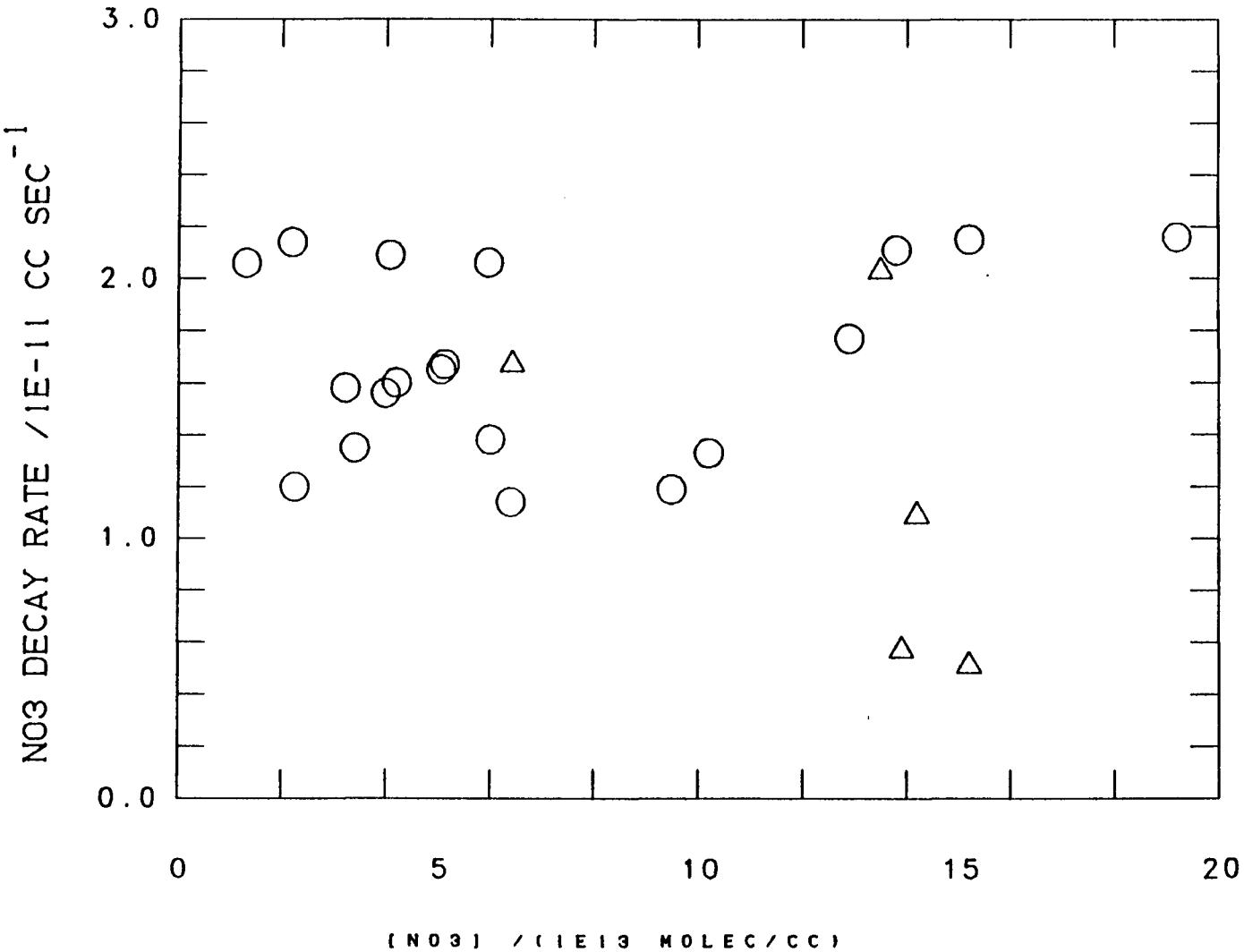

Figure 12. Decay rate, k', versus $[NO_3]$

$$N_2O_5 + h\upsilon \longrightarrow NO_3^* + \text{products} \qquad (25)$$

$$NO_3^* \xrightarrow{[M]} NO_3 \qquad k_q[M] = k_r \qquad (26)$$

This mechanism requires that the risetime be dependent on pressure and the collision partner. For this simple two step mechanism, the rate of appearance of NO_3 in its ground state is exponential. Therefore, each faster time resolution spectrum (0.2 μsec/channel) obtained was fit to a single exponential rise (Figure 5), and an appearance rate constant k_r (equals $1/\tau$, inverse lifetime) was obtained.

1. Appearance Rate versus Pressure

The deactivation rates obtained are listed in Table 5 and are plotted as reciprocal risetime ($1/\tau$) versus pressure in Figure 13. As the pressure was increased, the deactivation rate also increased. These data were fitted to a least-squares line. The slope of k_r versus [M] gave a deactivation rate, k_q, of 1.6 ± 0.3 X 10^{-13} cm^3sec^{-1}. The intercept of this line, 1.8 ± 0.1 X 10^5 sec^{-1}, is non-zero due to the contribution of deactivation by N_2O_5. No difference was seen between deactivation of NO_3 by O_2 and N_2 as expected since these gases have similar collisional cross-sections.

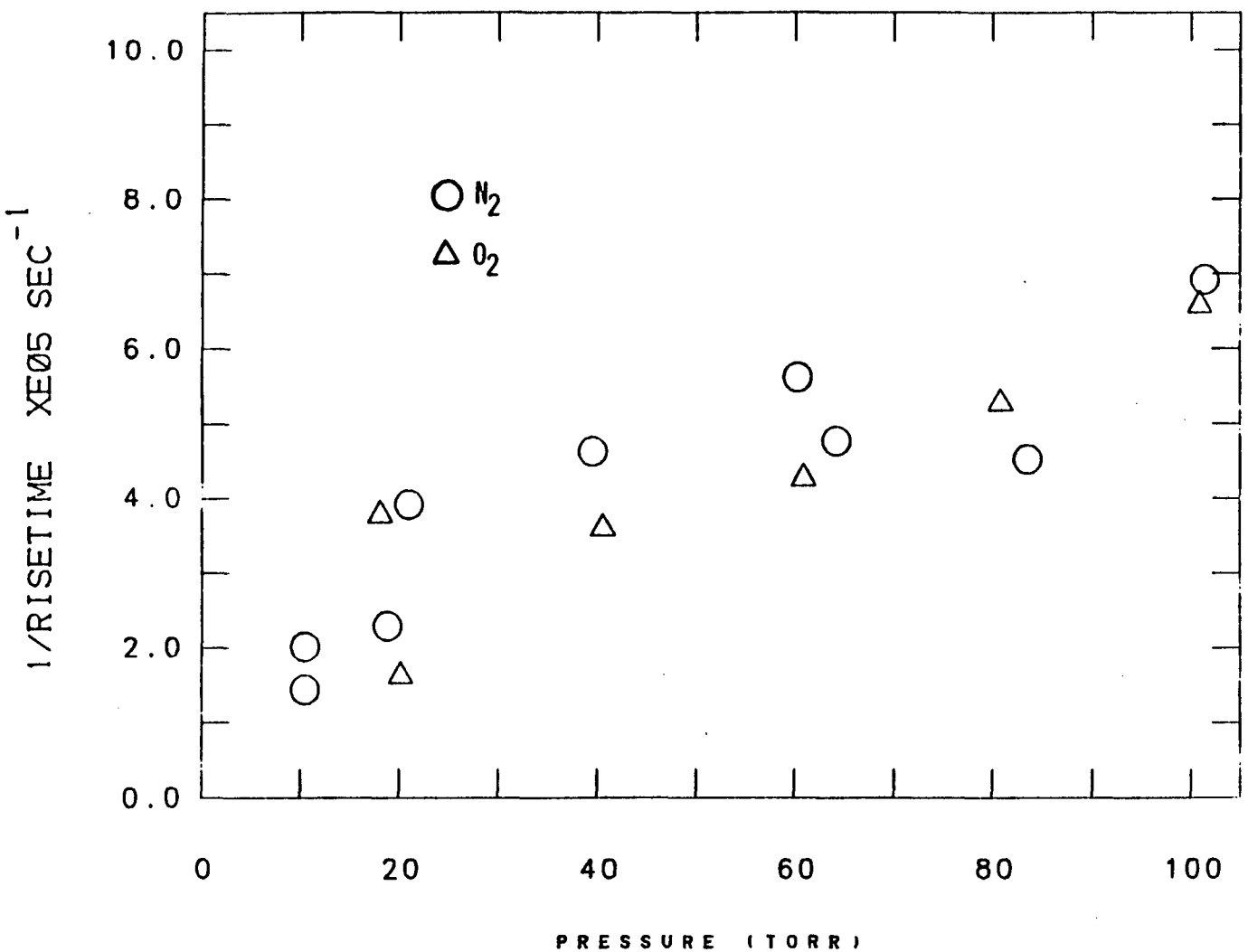

Figure 13. Inverse lifetime, k_r, versus pressure

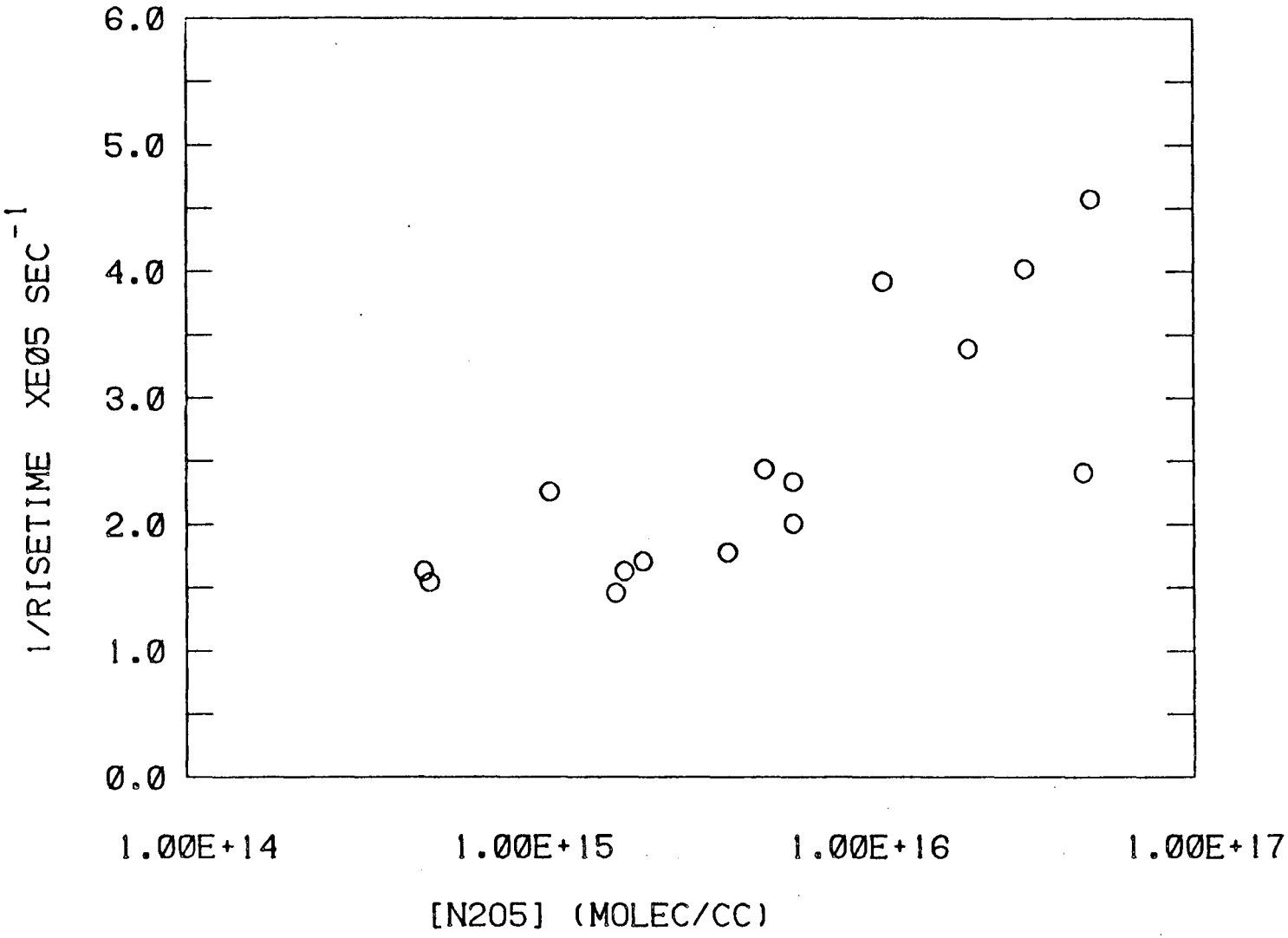

Figure 14. Inverse lifetime, k_r, versus $[N_2O_5]$

2. Appearance Rate versus N_2O_5 Concentration

The appearance rates, k_r, for the experiments varying N_2O_5 concentration are given in Table 6 and are plotted versus N_2O_5 concentration in Figure 14. From the slope, the rate constant k_q for deactivation by N_2O_5 was found to be $k_q = 4.0 \pm 1.0 \times 10^{-12}$ $cm^3 sec^{-1}$. The intercept is consistent with the contribution to this rate from the carrier gas (20 torr N_2). As expected, deactivation by N_2O_5 was found to be much more efficient than by nitrogen or by oxygen.

IV. DEACTIVATION OF NO_3

A. Introduction

It was shown in the previous chapter that the NO_3 produced from photolysis of N_2O_5 appears with a risetime of 1-10 μsec. Those experiments probed the NO_3 ($\upsilon = 0$) concentration only at 662 nm. The next series of experiments to be described probed NO_3 at 679 nm. The NO_3 absorption spectrum shows a hot band at 679 nm, which corresponds to a vibrational excitation of 378 cm^{-1}. These experiments, therefore, involved the first excited vibrational state of NO_3. Similar sets of experiments were conducted for this vibrational level as were conducted for the ground vibrational state. The quantum yields, risetimes, and decay rate constants were determined as a function of pressure and N_2O_5 concentration.

The simplest model for the kinetics requires a three-state system as shown in the following equations:

$$NO_3\ (\upsilon > 1) \xrightarrow{k_1} NO_3\ (\upsilon = 1) \tag{27}$$

$$NO_3\ (\upsilon = 1) \xrightarrow{k_2} NO_3\ (\upsilon = 0) \tag{28}$$

$$NO_3\ (\upsilon = 0) \xrightarrow{k_d} \text{products} \tag{29}$$

where k_1 is the rate of deactivation into NO_3 ($\upsilon = 1$), k_2 is the rate of deactivation from NO_3 ($\upsilon = 1$) to NO_3 ($\upsilon = 0$), and k_d is the disappearance rate of ground state NO_3 due to reaction. Because there is some population in NO_3 ($\upsilon = 1$) for a relaxed

(Boltzmann) distribution, k_{-2} is necessary to model the equilibrium between NO_3 ($\upsilon = 1$) and NO_3 ($\upsilon = 0$).

Solving the rate equations for NO_3 in both $\upsilon = 0$ and $\upsilon = 1$ gives the following, assuming that k_1 is much faster than k_2:

$$[NO_3(0)] = [NO_3(0)]_{eq}(e^{-k_d t} - e^{-(k_2 + k_d)t}) \tag{30}$$

$$[NO_3(1)] = [NO_3(1)]_{eq}(e^{-k_d t} - e^{-k_1 t}) + [NO_3(0)]_{eq}(e^{-(k_2 + k_{-2} + k_d)} - e^{-k_1 t}) \tag{31}$$

where $[NO_3(i)]_{eq}$ represents the equilibrium population of NO_3 in $\upsilon = i$. At equilibrium, the following relation will hold:

$$[NO_3(0)]_{eq}/[NO_3(1)]_{eq} = k_2/k_{-2} \tag{32}$$

The results of a typical experiment at $\lambda = 679$ nm are shown in Figure 16. The time dependence found in these experiments was consistent with the prediction of equation 31. A fast initial rise (k_1) was followed by an initial decay (k_2) and then a much slower decay (k_d). The NO_3 concentrations were calculated using an absorption cross-section $\sigma = 5.9 \times 10^{-19}$,[1] for $\lambda = 679$ nm.

B. <u>Probe of NO_3 ($\upsilon = 1$)</u>

1. Quantum Yields

The quantum yields (ϕ) were calculated, as for $\lambda = 662$ nm, from the NO_3 absorption maximum and from the measured photolysis energies and N_2O_5 concentrations (see Section III.A). A series

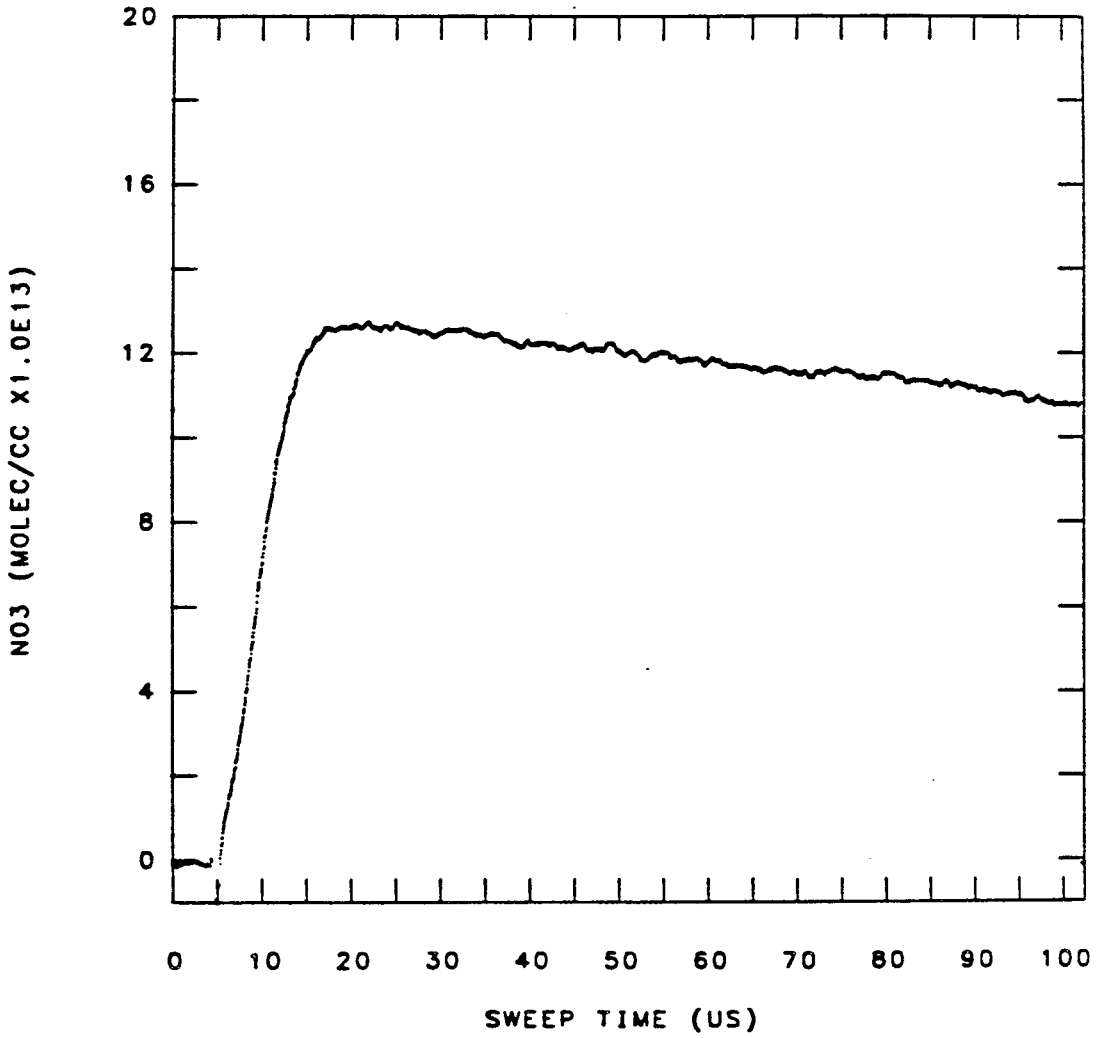

XBL 851-898

Figure 15. $[NO_3(0)]$ versus time ; λ = 662 nm

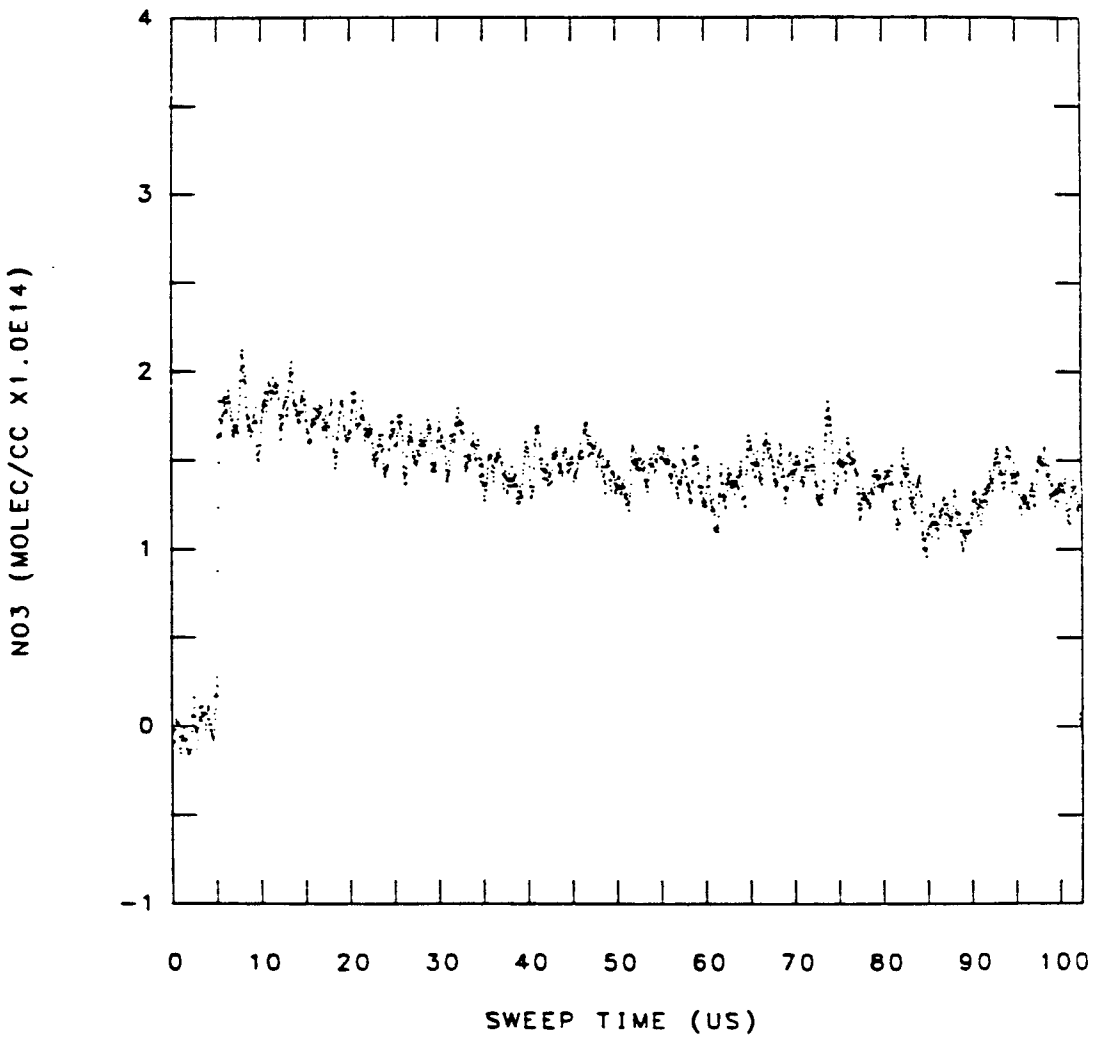

XBL 851-900

Figure 16. $[NO_3(1)]$ versus time ; λ = 679 nm

of experiments was done for N_2O_5 concentrations from 2.0 X 10^{15} to 3.1 X 10^{16} cm^{-3} at a pressure of 9.6 torr. The results of the quantum yield calculations are listed in Table 10. Figure 17 shows a plot of quantum yield versus N_2O_5 concentration. A large amount of scatter was observed. Much of this was due to the low absorption cross-section at λ = 679 nm. No trend was evident. The average quantum yield was found to be 1.87 ± 0.47.

In another series of experiments, the pressure was varied from 0.3 to 95 torr, with a constant N_2O_5 concentration of either 5.0 or 8.0 X 10^{15} cm^{-3}. These results are listed in Table 11. The resulting quantum yields as a function of pressure are shown in Figure 18. The average quantum yield was found to be 1.75 ± 0.34 in agreement with the concentration studies mentioned above. Again, no trend was apparent.

The important point here is that the quantum yield was found to be significantly different from unity. A quantum yield of one would indicate that the population in υ = 1 is that of an equilibrium distribution at 298 K. It was seen that for times less than about 10 µsec after the photolysis pulse, the population in υ = 1 was enhanced relative to the equilibrium population. For a Boltzmann distribution at 298 K, the relative populations of υ = 1 and υ = 0 can be calculated. Approximately 13% of the population is in υ = 1, 85% in υ = 0, and the remaining few percent are in higher vibrational levels. The observed quantum yield of 1.8 indicates that for short times about 23% of the population is in

Table 10 Concentration Dependence Results for Probing NO_3 (υ = 1), λ = 679 nm

$[N_2O_5]/10^{15}cm^{-3}$	ϕ	$k_1/10^6sec^{-1}$	$k_d/10^3sec^{-1}$	$k_2/10^4sec^{-1}$
2.04	1.92	0.82	2.69	
2.08	2.08	0.92	1.91	
2.82	2.30	0.77	2.78	
3.46	1.73	1.19	1.93	
4.93	2.33	0.82	2.68	
4.94	1.10	1.07	1.39	
5.06	2.18	1.89	3.32	9.40
5.79	2.78	0.65	2.37	17.2
7.03	2.43	1.40	3.51	
7.37	1.28	3.31	3.30	9.63
7.42	2.37	5.36	6.06	
8.20	1.79	0.83	2.75	
9.83	2.06	0.95	3.14	
10.1	1.34	3.31	2.70	5.89
10.2	1.78	2.66	3.75	3.67
20.0	2.15	1.28	3.48	
20.8	1.30	4.07	3.17	9.74
26.4	1.43	1.97	1.62	6.79
30.9	1.26	4.68	4.93	
31.4	1.73	0.87	3.03	

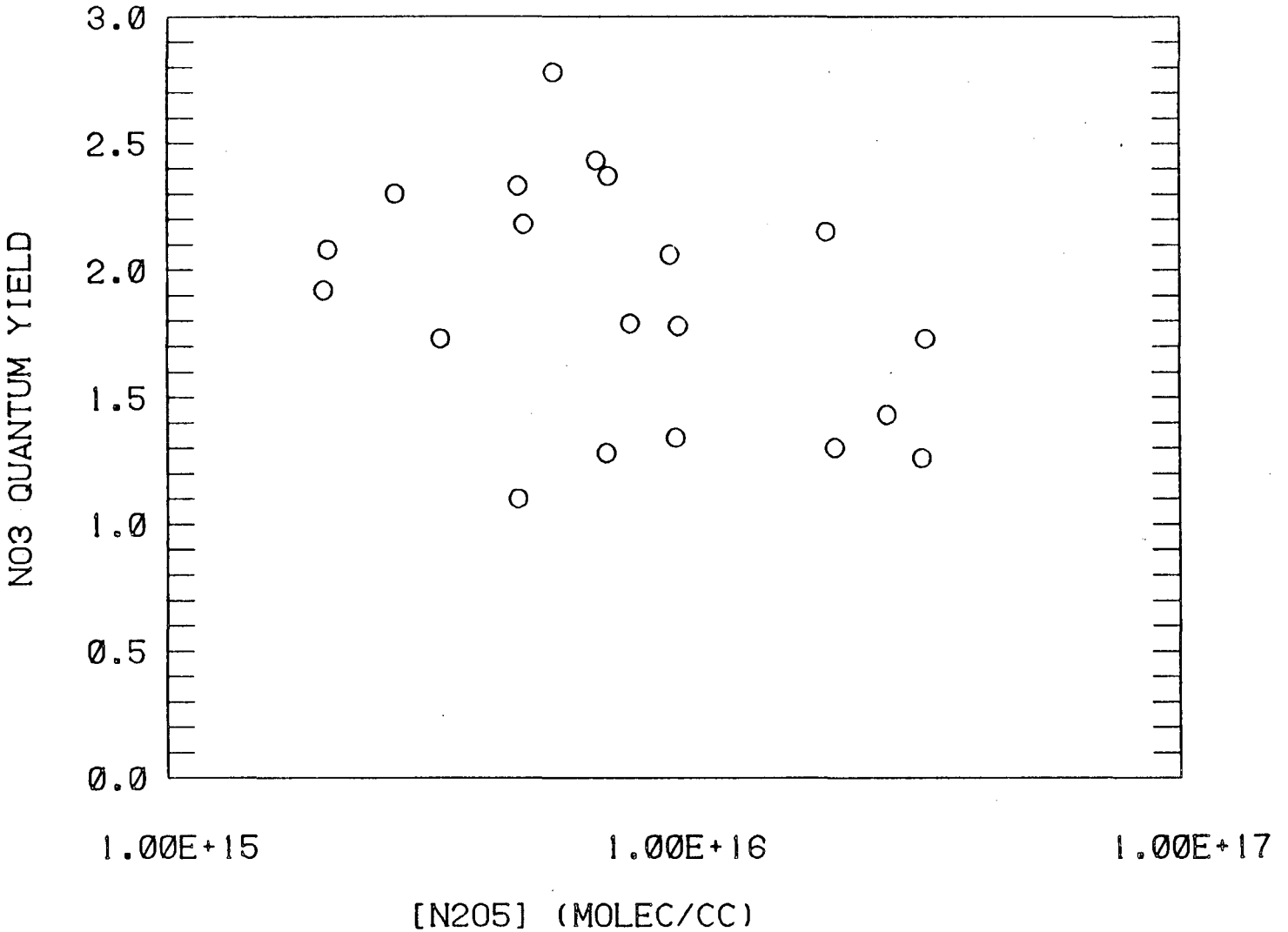

Figure 17. Quantum yield of $[NO_3(1)]$ versus $[N_2O_5]$

Table 11 Pressure Dependence Results for NO_3 (υ = 1), λ = 679 nm

P/torr	ϕ	rise $k_1/10^6 sec^{-1}$	slow decay $k_d/10^3 sec^{-1}$	fast decay $k_2/10^4 sec^{-1}$
* 0.28	1.60	0.92	9.75	
0.33	1.75	0.61	8.71	
0.31	1.15	1.32	7.71	1.89
1.5	1.98	0.59	5.71	
* 1.7	1.97	0.79	5.42	
3.3	1.98	0.99	4.57	
* 3.3	2.13	1.15	4.10	
* 4.9	2.05	1.49	3.87	
5.2	1.89	0.79	2.77	
5.1	1.43	2.80	---	2.77
8.6	1.97	1.13	1.93	
* 9.2	2.34	1.03	2.82	
11.0	1.48	3.40	0.92	4.68
20.1	1.39	3.33	1.20	5.03
*20.2	1.59	1.36	2.66	
20.8	1.73	1.56	1.58	
*30.2	2.17	1.04	1.45	
30.3	2.13	0.95	1.31	
49.8	1.52	1.98	1.28	12.8
*50.0	1.81	0.94	1.83	

Table 11 Pressure Dependence Results for NO_3 (υ = 1), λ = 679 nm (Continued)

P/torr	ϕ	rise $k_1/10^6 sec^{-1}$	slow decay $k_d/10^3 sec^{-1}$	fast decay $k_2/10^4 sec^{-1}$
72.8	1.31	2.44	2.66	15.0
95	1.22	2.04	0.67	9.13

* $[N_2O_5] = 8 \times 10^{15}\ cm^{-3}$

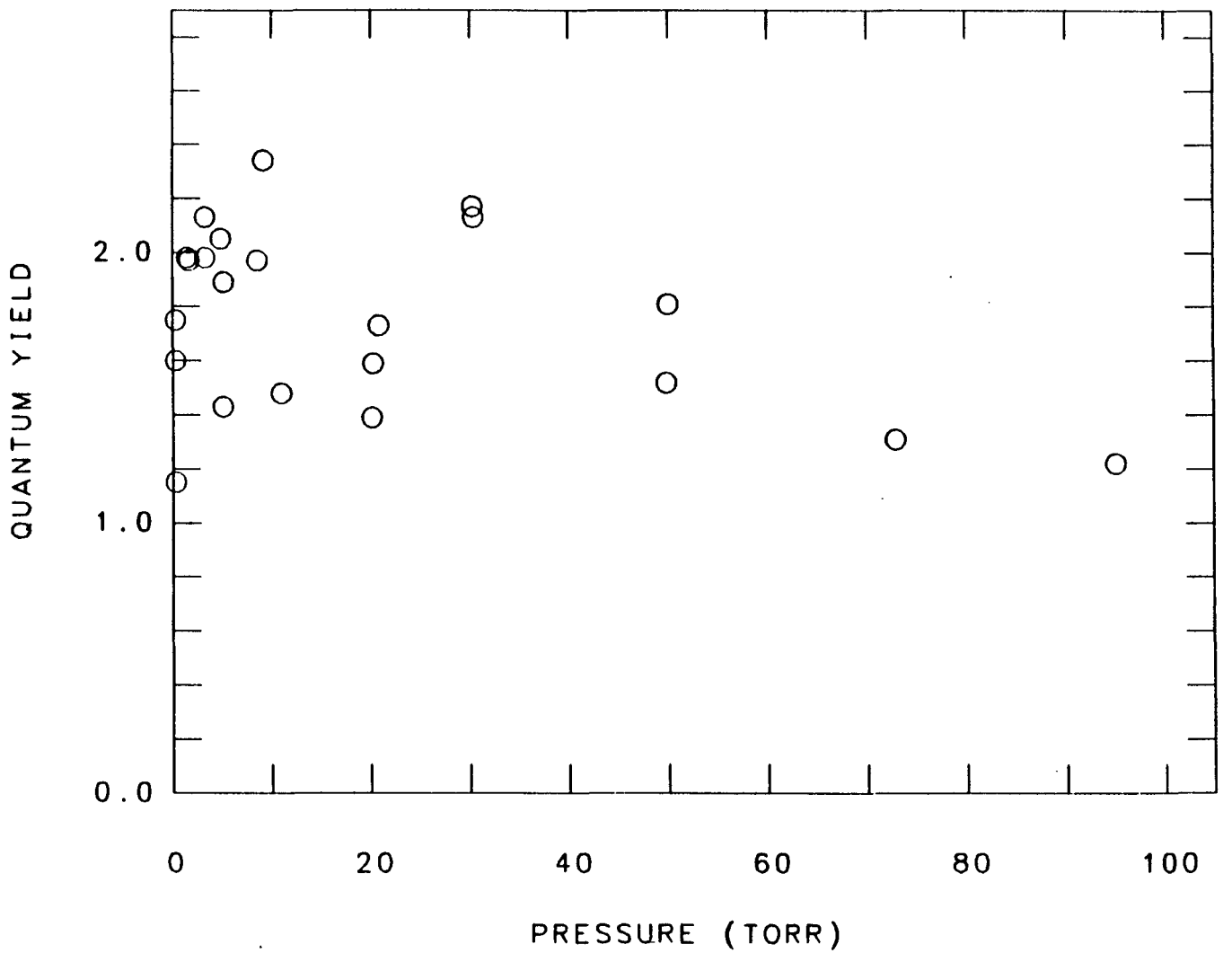

Figure 18. Quantum yield of $NO_3(1)$ versus pressure

$\upsilon = 1$, or about 23% of the deactivation occurs through $\upsilon = 1$.

In the calculation of population, it was assumed that the states were non-degenerate. If NO_3 is of D_{3h} symmetry, the vibrational state being probed would correspond to a doubly degenerate bending mode. In this case, the equilibrium population would be greater, about 23%. The enhanced population observed would correspond to 41% of the deactivation occuring through $\upsilon = 1$.

2. Risetimes

As shown in Figure 16, the appearance of NO_3 ($\upsilon = 1$) was instantaneous on the time scale of the experiments. The time resolution of these experiments was 50 ns/channel, but the real limitation occurred because of noise due to the laser pulse. Typically 250 ns were obscured. The data from the same series of experiments described above were fit to a triple exponential of the form corresponding to Equation 33, where $\alpha_1 = k_d$, $\alpha_2 \cong k_2$ and $\alpha_3 = k_1$.

$$[NO_3] = c_1(e^{-\alpha_1 t} - e^{-\alpha_3 t}) + c_2(e^{-\alpha_2 t} - e^{-\alpha_3 t}) \qquad (33)$$

In many cases the data could not be fit uniquely to a triple exponential due to the noise in the data. In these cases, the data were fit to a double exponential, where $\alpha_1 \cong k_d$ and $\alpha_3 = k_1$.

$$[NO_3] \cong c_1(e^{-\alpha_1 t} - e^{-\alpha_3 t}) \qquad (34)$$

The results of fitting the data for all the experiments are listed in Tables 10 and 11 for the concentration and pressure dependent studies, respectively. The tabulated risetimes are approximately constant. The average appearance rate (for the pressure studies) was $1.5 \pm 0.8 \times 10^6$ sec^{-1}, or an average risetime of 0.7 µsec. Besides being limited by the laser noise, the limit also depended on the ability to fit a small number of data points. A meaningful risetime was not obtained in cases where the rise was comprised of less than about 15 channels (data points) in these experiments.

3. Decay Rates

From the same double or triple exponential fits to the data, the rate constant for vibrational deactivation, k_2, and the rate of disappearance, k_d, were obtained. These results are listed in Tables 10 and 11.

The slower decay, k_d, is expected to be due mainly to reaction, and should be equivalent to the decay rates observed for NO_3 ($\upsilon = 0$). Since the reactions involved should not depend on collisions with the carrier gas, a pressure dependence is not expected. A plot of k_d versus pressure is shown in Figure 19. The plot shows that between 10 and 100 torr, k_d was independent of pressure. At pressures below 10 torr, the decay rate began to increase. At these lower pressures, the rate of diffusion of the

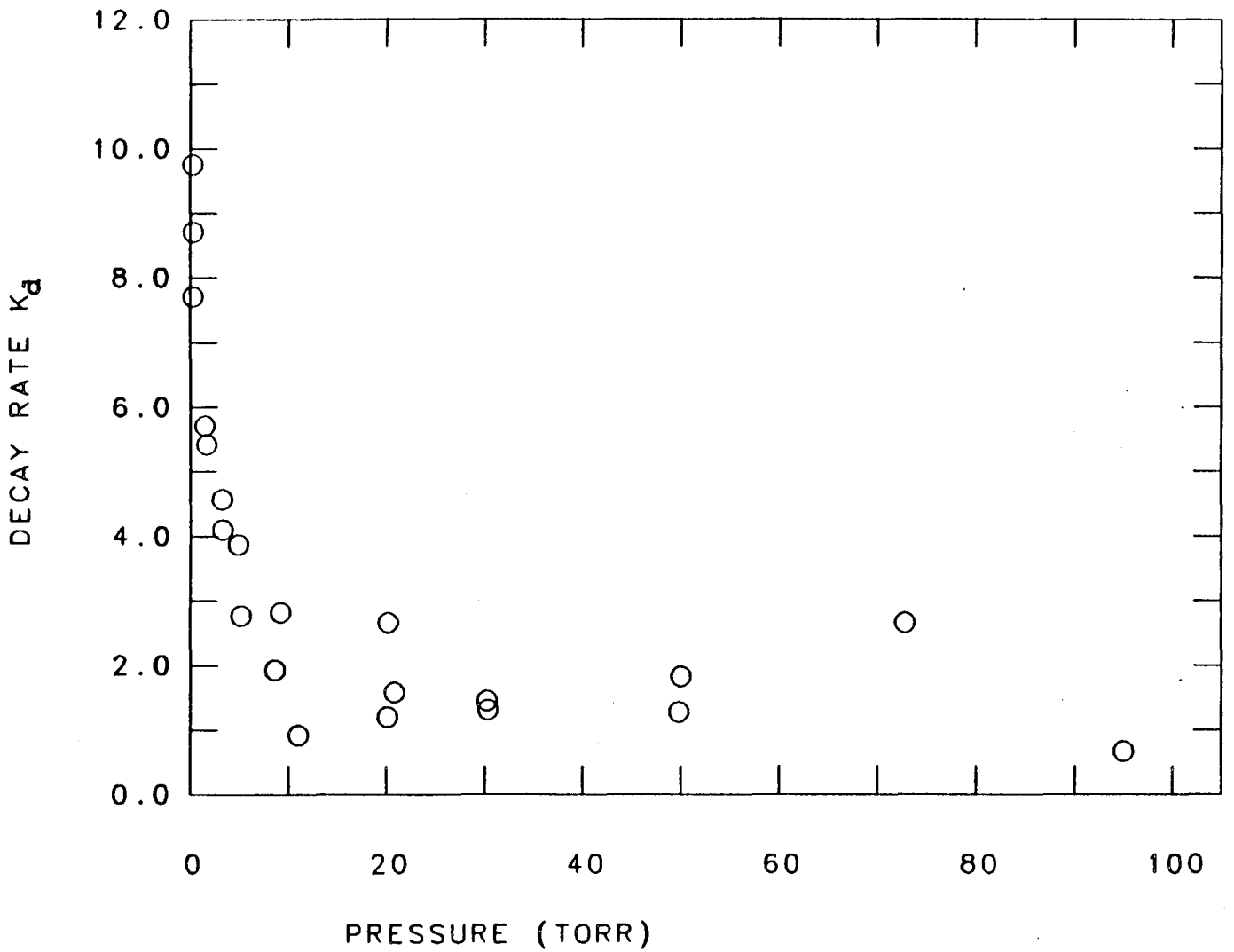

Figure 19. Decay rate, k_d, versus pressure

NO_3 reaction products out of the lasing region became significant.

It was seen for NO_3 ($\upsilon = 0$) that the decay rate was dependent on N_2O_5 concentration, and that this dependence was justified as being caused by reaction of NO_3 with other photolysis products (NO and oxygen atoms)(Sec.III.C.2). The slower decay of NO_3 ($\upsilon = 1$) should show this same N_2O_5 concentration (NO_3 concentration) dependence. The relation between k_d and NO_3 concentration is tabulated in Table 12 and plotted in Figure 20. A trend was seen toward higher decay rates at higher NO_3 concentrations. The values obtained were generally in agreement with those for the NO_3 ($\upsilon = 0$) results. Because of the scatter, no attempt to obtain actual reaction rate constants was made.

The faster initial decay, which corresponds to collisional deactivation of NO_3 ($\upsilon = 1$) is expected to show both concentration and pressure dependence in an analogous fashion to the dependence observed for the ground vibrational state of NO_3. The values of the decay rate, k_2, from the N_2O_5 concentration studies show no clear trend. The results of the pressure dependent studies are shown in Figure 21 plotted as k_2 versus pressure. Although it was not explicitly stated previously, the deactivation rate k_2 is the product of the deactivation rate constant k_v and the pressure.

$$NO_3\ (\upsilon = 1) \xrightarrow{k_v[M]} NO_3\ (\upsilon = 0); \quad k_2 = k_v[M] \qquad (35)$$

Table 12 Results of Decay Analysis

$[NO_3]/10^{14}$ cm^{-3}	$k_d/10^3$ sec^{-1}
1.61	3.32
2.40	2.70
3.74	3.17
1.70	3.30
1.52	2.37
1.98	6.06
2.34	1.62
1.71	3.75
0.57	1.93
0.49	2.69
1.97	2.68
1.12	2.78
2.51	3.51
2.92	3.14
4.75	3.45
4.76	3.03
0.72	1.91
2.14	2.75
0.933	1.39
3.57	4.93

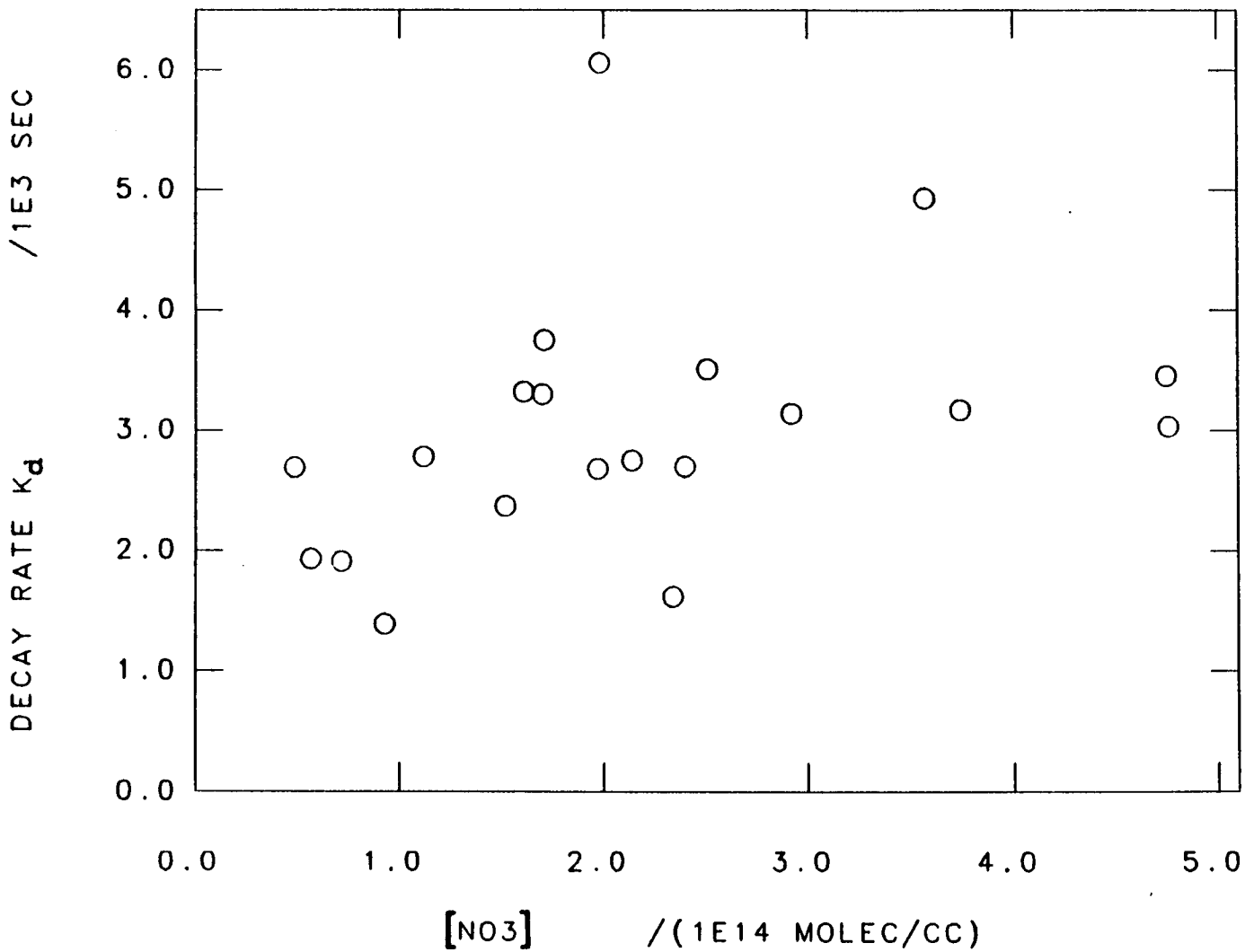

Figure 20. Decay rate, k_d, versus $[NO_3(1)]$

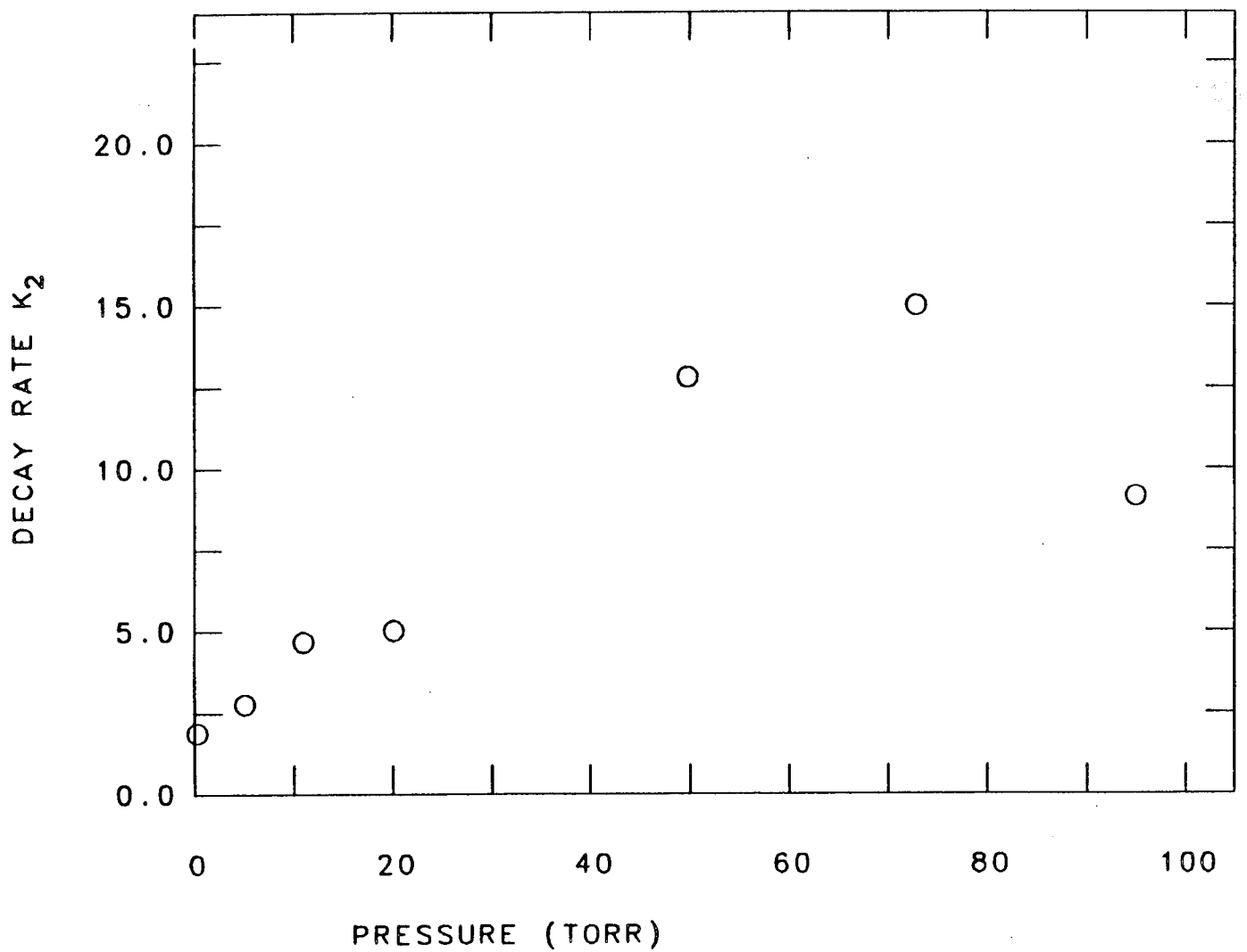

Figure 21. Decay rate, k_2, versus pressure

A plot of k_2 versus pressure will therefore have a slope of k_v. From the results shown, a rate $k_v = 6.3 \pm 1.5 \times 10^{-14}$ $cm^{-3}sec^{-1}$ was obtained. If the appearance of NO_3 ($\upsilon = 0$) occurred entirely by collisional deactivation of NO_3 ($\upsilon = 1$), the quenching rate of NO_3, k_q, would be equal to the deactivation rate k_v. The value of k_q obtained from the previous section (Section III.C) was $k_q = 1.6 \pm 0.3 \times 10^{-13}$ $cm^{-3}sec^{-1}$, a factor of 2.5 higher than the value of k_v obtained. It was also shown (Section IV.B.2) that less than about 40% of the deactivation to $\upsilon = 0$ occurs through $\upsilon = 1$. The initial population in $\upsilon=0$, although partially obscured by the laser pulse, was seen to be $\leq$5%. The remaining population may be in higher vibrational states. Deactivation from these states is expected to be faster, and may account for the higher value of k_q relative to k_v.

C. Variation of Probe Beam Wavelength

In order to try to get a more complete picture of the energy distribution and deactivation of NO_3 after N_2O_5 photolysis, a set of experiments was conducted in which the probe laser wavelength was varried from 662 nm to 697 nm. The pressure was kept constant at 9.0 torr. The N_2O_5 concentration was kept constant at either 5.0×10^{15} cm^{-3} for λ = 662-679 nm or 8.0×10^{15} cm^{-3} for λ = 679-697 nm. The higher N_2O_5 concentrations for longer wavelengths were necessary because of the decline in the absorption cross-sections. The concentration of NO_3 was recorded as a

function of time at each of the wavelengths probed. From these measurements, information on the quantum yields, appearance rates and decay rates was obtained.

1. Quantum Yields

Two distinct types of behavior were seen in the spectra. For wavelengths near 662 nm, the concentration of NO_3 rose relatively slowly to a maximum, then leveled off and began to decay. The maximum of this curve corresponds to the quantum yield for a relaxed population and has been shown to be unity (Section II.B). For wavelengths near 697 nm, a sharp rise and decay was seen. At times after relaxation (about 10 μsec) little or no absorption was seen. The quantum yield calculated at the peak absorption corresponds to the enhancement of the population for short times. At intermediate wavelengths both types of behavior were seen. A fast rise and decay was seen, followed by a slow decay due to absorption of the relaxed population. From this type of spectra two yields can be calculated. A quantum yield for the relaxed population (ϕ_r) was calculated at this peak absorption for short times. This corresponds to the ratio of populations before and after relaxation has occurred.

The quantum yields (ϕ_r) for each of the experiments are reported in Table 13 and are plotted versus wavelength in Figure 22. For longer wavelengths, the absorption cross-sections are

Table 13 Wavelength Dependence Results

λ/nm	ϕ_r	$k_1/10^6 sec^{-1}$	$k_d/10^3 sec^{-1}$	$k_2/10^4 sec^{-1}$	$\phi_p - \phi_r$
662	1.03	0.208	3.35		
662	1.23	0.184	2.42		
663	1.19	0.186	2.25		
664	1.11	0.178	2.41		
665	0.93	0.211	2.35		
666	1.04	0.194	1.84		
666	1.21	0.253	2.07		
667	0.94	0.284	3.31		
667	1.21	0.254	2.21		
668	1.01	0.785	2.81		
669	1.27	0.905	1.77		
670	2.88	1.13	3.21		
671	1.80	2.74	2.29	7.90	
674	0.57	4.00	9.62		
677	1.80	3.02	5.70		
* 679	1.52	---	3.44		
* 679	1.13	---	4.69		
680	1.82	2.39	2.44	6.33	0.57
* 682	1.79	---	4.81		0.65
* 682	3.17	---	4.20		1.4
683	3.41	3.08	2.05	8.81	2.1

Table 13 Wavelength Dependence Results (Continued)

λ/nm	ϕ_r	$k_1/10^6 sec^{-1}$	$k_d/10^3 sec^{-1}$	$k_2/10^4 sec^{-1}$	$\phi_p - \phi_r$
* 685	4.44	---	---	5.27	9.4
* 685	6.00	---	---	6.53	10.
686	19.2	1.32	2.95	2.96	20.
* 688	3.98	---	---	5.77	8.
* 688	5.73	---	---	3.93	10.
689	34.1	2.67	1.47	6.73	20.
* 691	16.8	---	---	6.69	40.
* 691	0.95	---	---	8.62	20.
* 694	16.9	---	---	8.04	30.
* 694	12.2	---	---	5.24	30.
* 697	3.68	---	---	6.92	5.
* 697	2.17	---	---	4.67	7.

* $[N_2O_5] = 8.0 \times 10^{15}\ cm^{-3}$

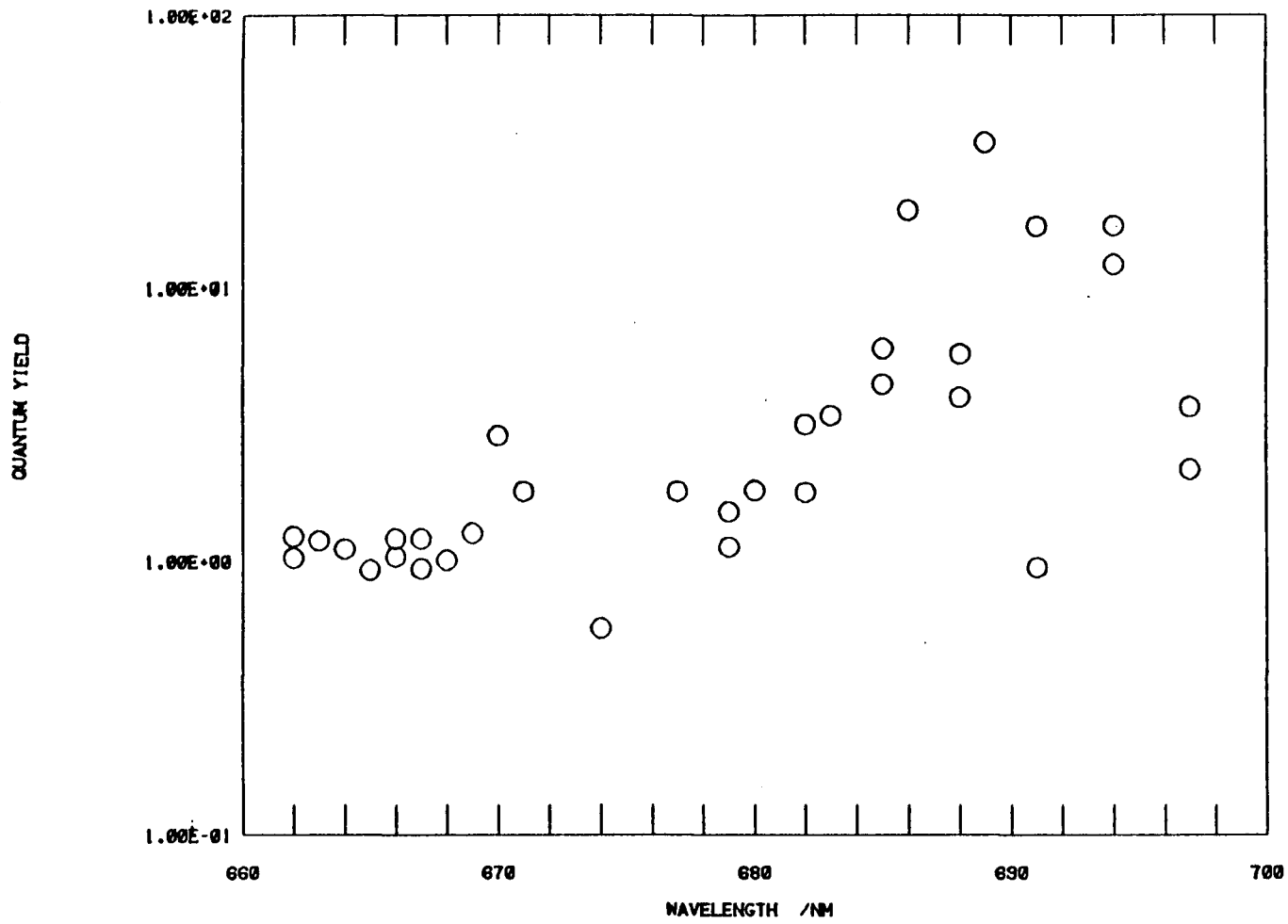

Figure 22. Quantum yield versus wavelength

small, and small amounts of noise led to high yields. The quantum yields are therefore unreliable. For shorter wavelengths, however, the quantum yields were found to be unity as expected.

The differences between the peak yield and the relaxed yield ($\phi_p - \phi_r$) are listed in Table 13 for wavelengths longer than 679 nm, where significant. These values were extremely sensitive to the accuracy of the values used for the absorption cross-section. For this reason, these values are listed with as many significant figures as used for the absorption cross-sections. In general, it was observed that the relative population enhancement increases with wavelength.

The enhancement for $\upsilon = 1$ at $\lambda = 679$ nm has already been discussed (Section IV.B). It was found that about 40% of the total population is in $\upsilon = 1$. The absorption spectrum of NO_3 shows a relative maximum at 697 nm, or 759 cm^{-1} above $\upsilon = 0$. A frequency of 750 cm^{-1} has been reported[16] for υ_4. This peak in the absorption spectrum may correspond to $\upsilon_4 = 1$. The first overtone of υ_1 is also expected to occur in this region at about 700 cm^{-1} or $\lambda = 694$ nm. At these wavelengths, a room temperature distribution predicts about 2.5% of the total population to be in these states. For an average enhancement factor of about 20, as much as 50% of the total population may be in these states at short times. Although this value is quite uncertain, it is clear that the spectra represent deactivation through states at these energies.

energies.

2. Risetimes

Just as in the case of the experiments at λ = 679 nm, the data in these experiments for λ = 662-697 nm were fit to a triple exponential when possible, or a double exponential otherwise (Equations 33 and 34). The values of the appearance rate, k_1, for experiments for which $[N_2O_5] = 5.0 \times 10^{15}$ cm^{-3} are listed in Table 13. Figure 23 shows a plot of k_1 versus wavelength for λ = 662-690 nm. From 662-670 nm, the appearance rate was seen to increase steadily. These probe wavelengths occur within the rotational contour of $\upsilon = 0$. This implies that the deactivation process also involves highly rotationally excited levels of υ = 0, which then relax. Because the visible absorption spectrum showed no rotational structure, it was not possible to get detailed information concerning individual rotational states with this experimental method.

For wavelengths longer than 670 nm, the appearance rates reached a constant value of about 4×10^6 sec^{-1}. As was discussed before, this limit was reached because of noise from the photolysis pulse, and because fitting the data required a minimum number of data points. For the experiments with $[N_2O_5] = 8.0 \times 10^{15}$ cm^{-3}, the laser noise was reduced. The rise was seen to be instantaneous and was too fast to be fit to an exponential. This

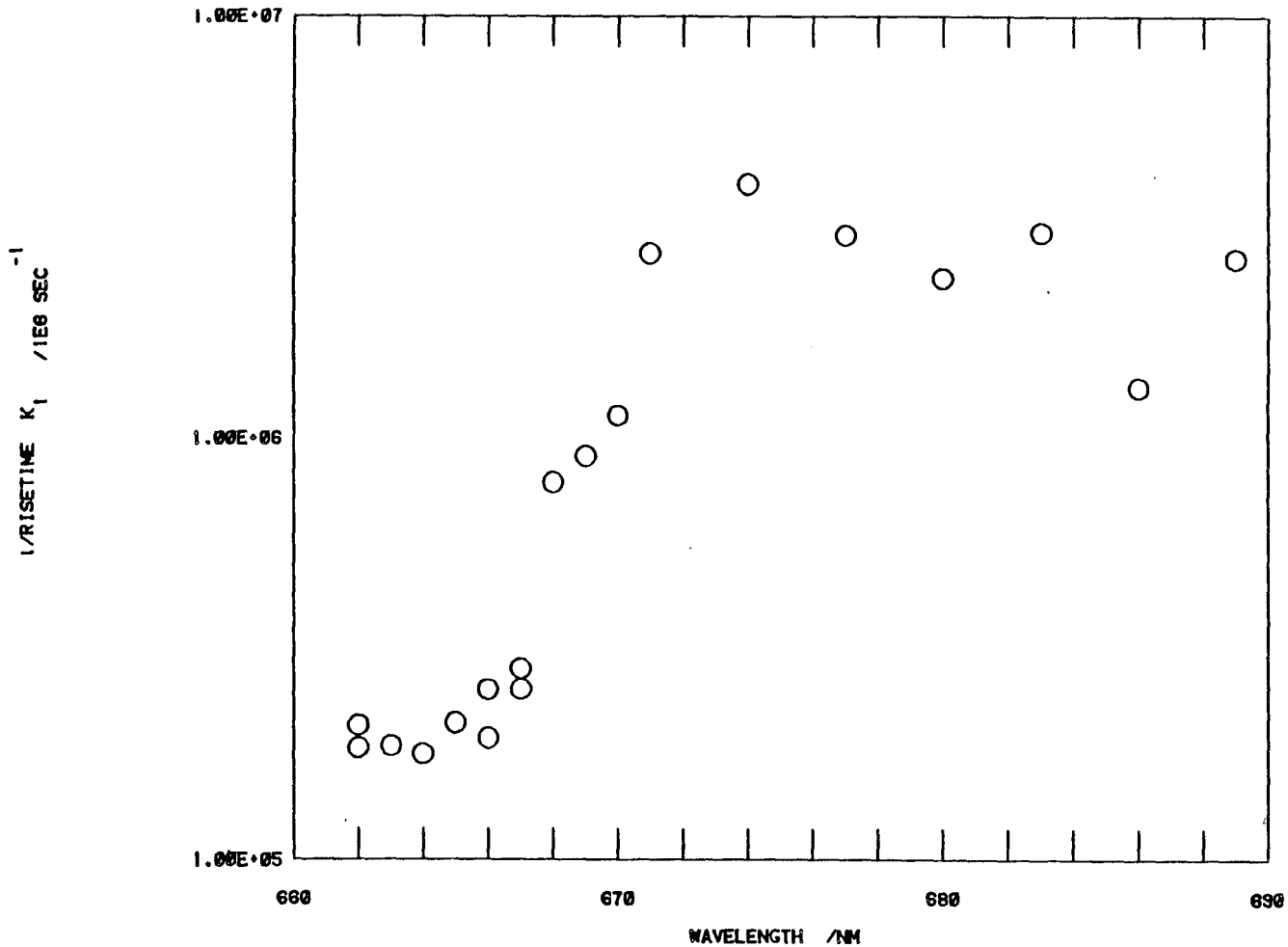

Figure 23. Appearance rate, k_1, versus wavelength

instantaneous rise was observed for wavelengths longer than 679 nm, and occurred within 100 nsec.

3. Decay Rates

For wavelengths from 662-670 nm, the spectra were fit according to Equation 8. A rise (k_1) was followed by a slow decay (k_d) due to reactions of NO_3. From 670 to about 683 nm, a faster decay (k_2) due to collisional deactivation was seen. Where possible, the data was fit to Equation 7 to obtain both k_d and k_2. In most cases, however, a unique solution could not be obtained and the data were fit according to Equation 8, and a value of k_d was obtained. For the experiments at $[N_2O_5] = 8.0 \times 10^{15}$ cm^{-3}, the rise was too fast to be fit. Taking k_1 as infinity in Equation 33 gives Equation 36, where again $\alpha_1 = k_d$ and $\alpha_2 = k_2$.

$$[NO_3] = c_1 e^{-\alpha_1 t} + c_2 e^{-\alpha_2 t} \tag{36}$$

An attempt was made to fit the data at this concentration to Equation 36, however, unique fits were not obtained. The data were then fit to a single exponential to obtain k_d. For wavelengths longer than about 683 nm, the decay of the thermally excited NO_3 could not be observed because of the low absorption cross-sections. Because of this, the data were fit to a single exponential decay to obtain k_2. The results of these analyses

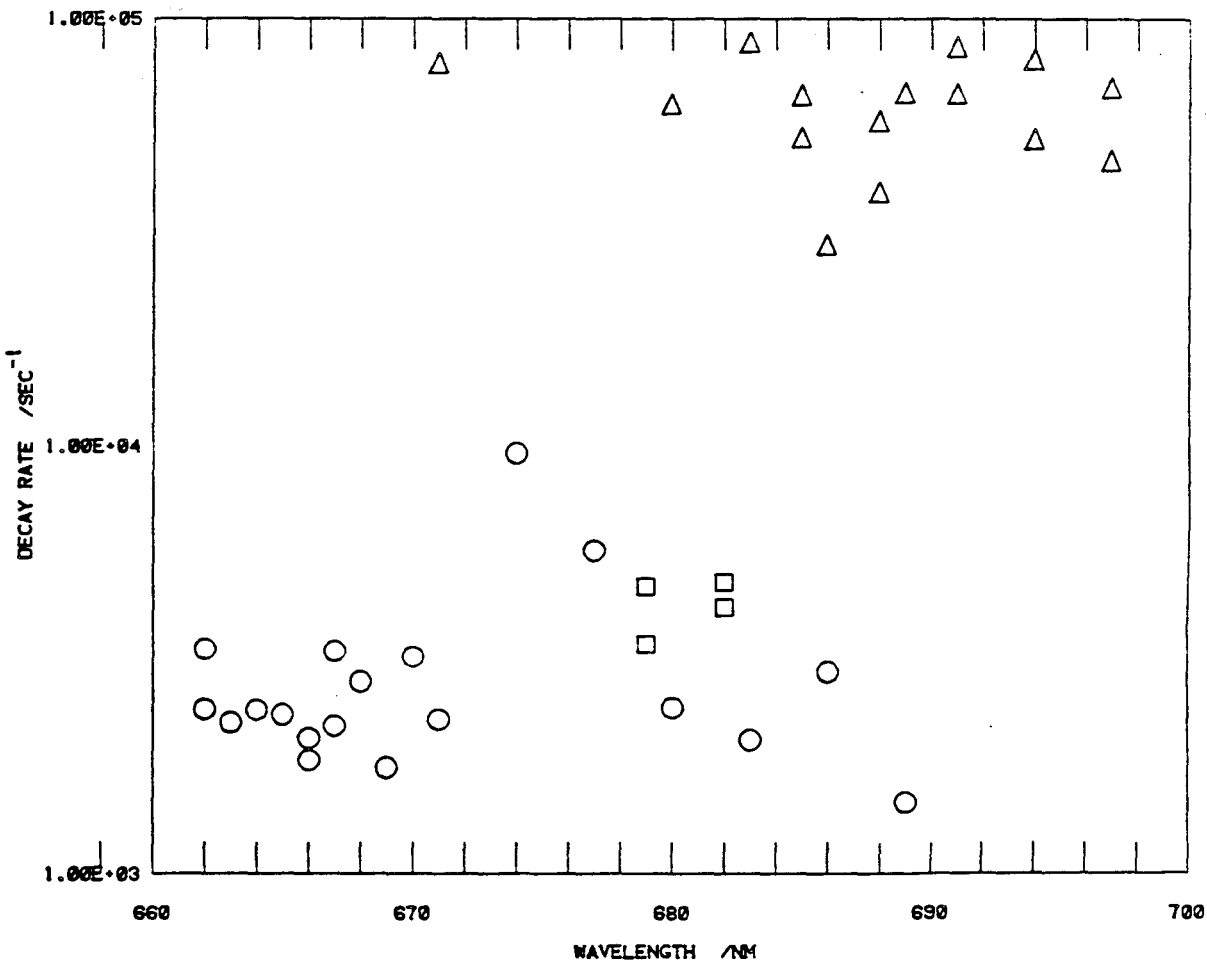

Figure 24. Decay rates versus wavelength;

O = k_d, $[N_2O_5]$= 5.X10^{15} cm^{-3}
□ = k_d, $[N_2O_5]$= 8.X10^{15} cm^{-3}
Δ = k_2

for k_2 and k_d are listed in Table 13. Both k_2 and k_d are plotted in Figure 24.

The rates, k_d, were seen to be independent of wavelength with an average value of $2.4 \pm 0.5 \times 10^3$ sec^{-1} for $[N_2O_5] = 5.0 \times 10^{15}$ cm^{-3}. These values are consistent with the earlier results at $\lambda = 679$ nm. The dependence on N_2O_5 concentration is consistent with the decay being due to reaction of NO_3 with the other photolysis products (oxyen atoms and NO).

The collisional deactivation rate constant, k_2, also was seen to be independent of wavelength from 680 to 697 nm. The average value obtained was $k_2 = 6.2 \pm 1.7 \times 10^4 sec^{-1}$. The deactivation rates obtained[41] at 662 nm were $4.0 \pm 1.0 \times 10^{-12}$ $cm^3 sec^{-1}$ for N_2O_5 and $1.6 \pm 0.3 \times 10^{-13}$ $cm^3 sec^{-1}$ for N_2. The constant k_2 should be the sum of deactivation from both these sources.

$$k_2 = k_{N_2O_5}[N_2O_5] + k_{N_2}[N_2] \tag{37}$$

For these experiments at a pressure of 9.0 torr and an N_2O_5 concentration of 8.0×10^{15} cm^{-3}, the calculated value of k_2 was found to be $7.8 \pm 1.7 \times 10^4$ sec^{-1}. Therefore, the value observed in these experiments was found to be within the experimental error of the 662 nm results. This implies that states 350 to 750 cm^{-1} higher in energy than $\upsilon = 0$ are deactivated directly to $\upsilon = 0$. Within experimental error, the deactivation rates were not different for states within this energy range.

V. RATE OF REACTION: $O + NO_3$

A. Analysis

1. Calculation of Rate Constant

In measuring the rate of a reaction, an ideal system would include only reactants, and the concentrations of reactants and products would be directly measureable as a function of time. In practice, this is not often the case, especially for radical species.

For these experiments, the reactants, oxygen atoms and NO_3, are both produced by photolysis at 249 nm. The photolysis products of O_3 at this wavelength are known to be O_2 and $O\ (^1D)$.[1]

$$O_3 \xrightarrow{h\nu} O_2 + O\ (^1D) \qquad (38)$$

$$O\ (^1D) \xrightarrow{[M]} O\ (^3P) \qquad (39)$$

However, it is also known that quenching of $O\ (^1D)$ to its ground electronic state $O\ (^3P)$ is fast. For the experimental conditions (20 torr nitrogen) quenching is complete in about 1 μsec. As was discussed in the preceeding section (Section III), N_2O_5 photolysis produces a mixture of products at 249 nm. The NO_3 produced is also excited and is quenched within 10 μsec.

$$N_2O_5 \xrightarrow{h\nu\ (249)} NO_3 + NO_2 \quad 30\% \qquad (40)$$

$$NO_3 + NO + O \quad 70\% \qquad (41)$$

In order to determine the rate constant (k_1) of interest, it is preferable to have pseudo-first order kinetics. Since the concentration of NO_3 is determined by the FP/LA technique, pseudo-first order kinetics is obeyed as long as oxygen atoms are present in large excess.

$$O + NO_3 \xrightarrow{k_1} O_2 + NO_2 \qquad (42)$$

$$O + NO_2 \xrightarrow{k_2} NO + O_2 \qquad (43)$$

$$NO + NO_3 \xrightarrow{k_3} 2\ NO_2 \qquad (44)$$

The rate constants for Reactions 43 and 44 are $k_2 = 9.3 \times 10^{-12}$ cm^3/sec and $k_3 = 2.0 \times 10^{-11}$ cm^3/sec.[38] In addition to the reaction of interest (Reaction 42), there are many side reactions. Most of these reactions are too slow to be important. Reaction 43, which occurs at a similar rate to Reaction 42,[31] will not affect the measured concentration of NO_3, although it will serve to consume oxygen atoms. As long as the oxygen atoms are present in excess of both NO_3 and NO_2($\leq NO_3 3$), this will not cause a problem.

Reaction 44 is also fast enough to affect the determination of the desired rate constant, k_1. The rate of disappearance of NO_3 is given by Equation 45, where k_d is a term due to other processes such as diffusion out of the probe beam and slower chemical reactions.

$$-d[NO_3]/dt = \{k_1[O] + k_3[NO] + k_d\}[NO_3] \qquad (45)$$

In order for pseudo-first order kinetics to prevail, the concentration of NO must be constant. As stated above, the concentration of oxygen atoms is assumed to be large and constant. Although NO is not present in excess, its concentration remains fairly constant since Reaction 44 should destroy NO at a rate comparable to the rate at which Reaction 43 produces it.

The results of a typical experiment are shown in Figure 25. The observed rate constants, k′, were then obtained by fitting the decay of $[NO_3]$ to an exponential.

$$[NO_3] = [NO_3]_o \exp(-k't) \tag{46}$$

$$k' = k_1[O] + k_3[NO] + k_d \tag{47}$$

A plot of $\ln[NO_3]$ versus time with slope k′ is shown in Figure 26. Because the concentration of N_2O_5 and the photolysis energy were kept fairly constant throughout the experiments, the concentration of NO produced was fairly constant. Several sets of experiments were therefore conducted at a constant N_2O_5 concentration. By plotting k′ against [O], the rate constant k_1 was obtained.

2. Calculation of Reactant Concentrations

For a mixture of two components, both of which absorb, the total absorption is given by Equation 48, where the subscripts refer to the two different components. I, I_o, σ, N and L are the light intensities with and without absorption, the cross-section,

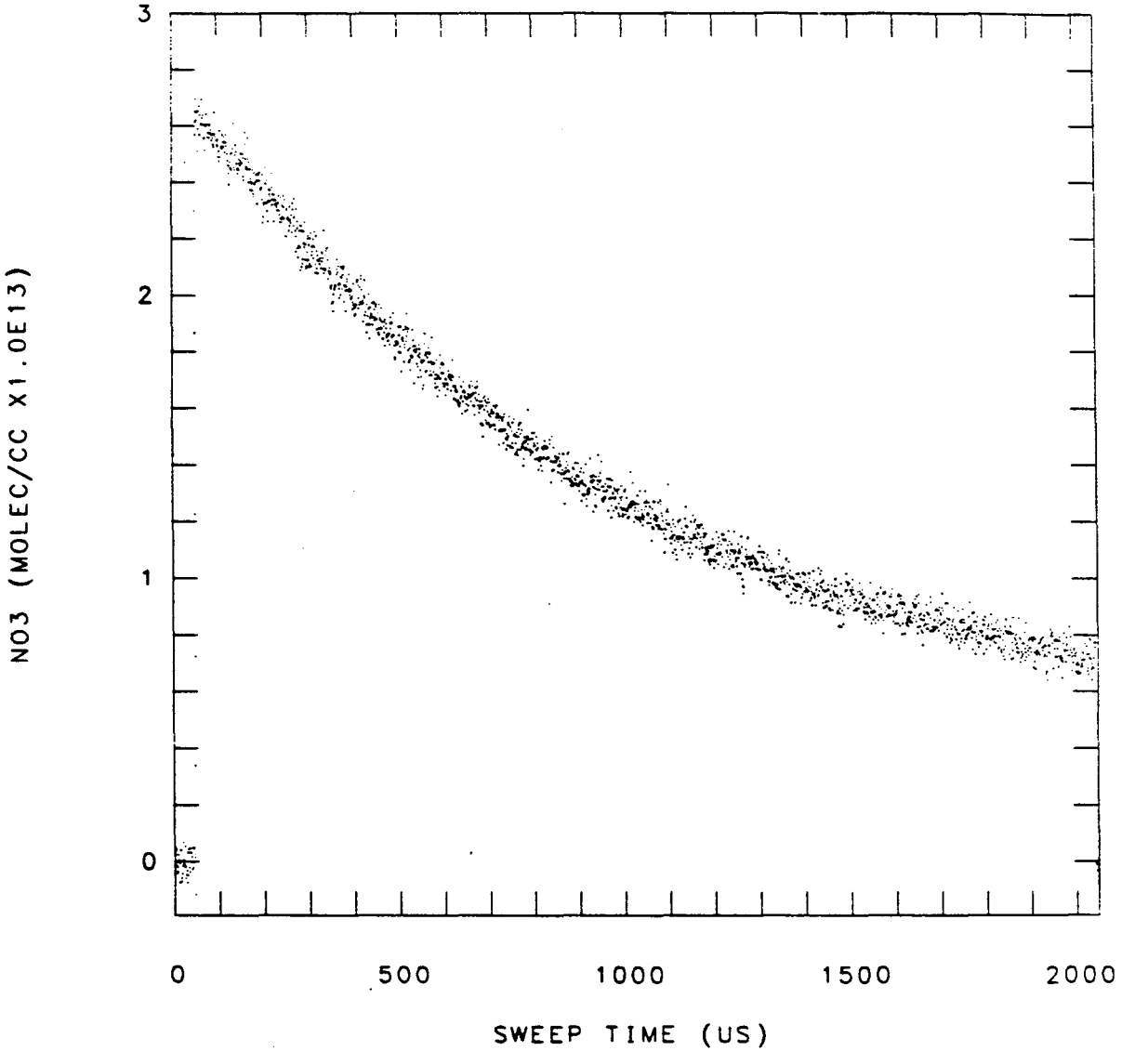

Figure 25. $[NO_3]$ versus time

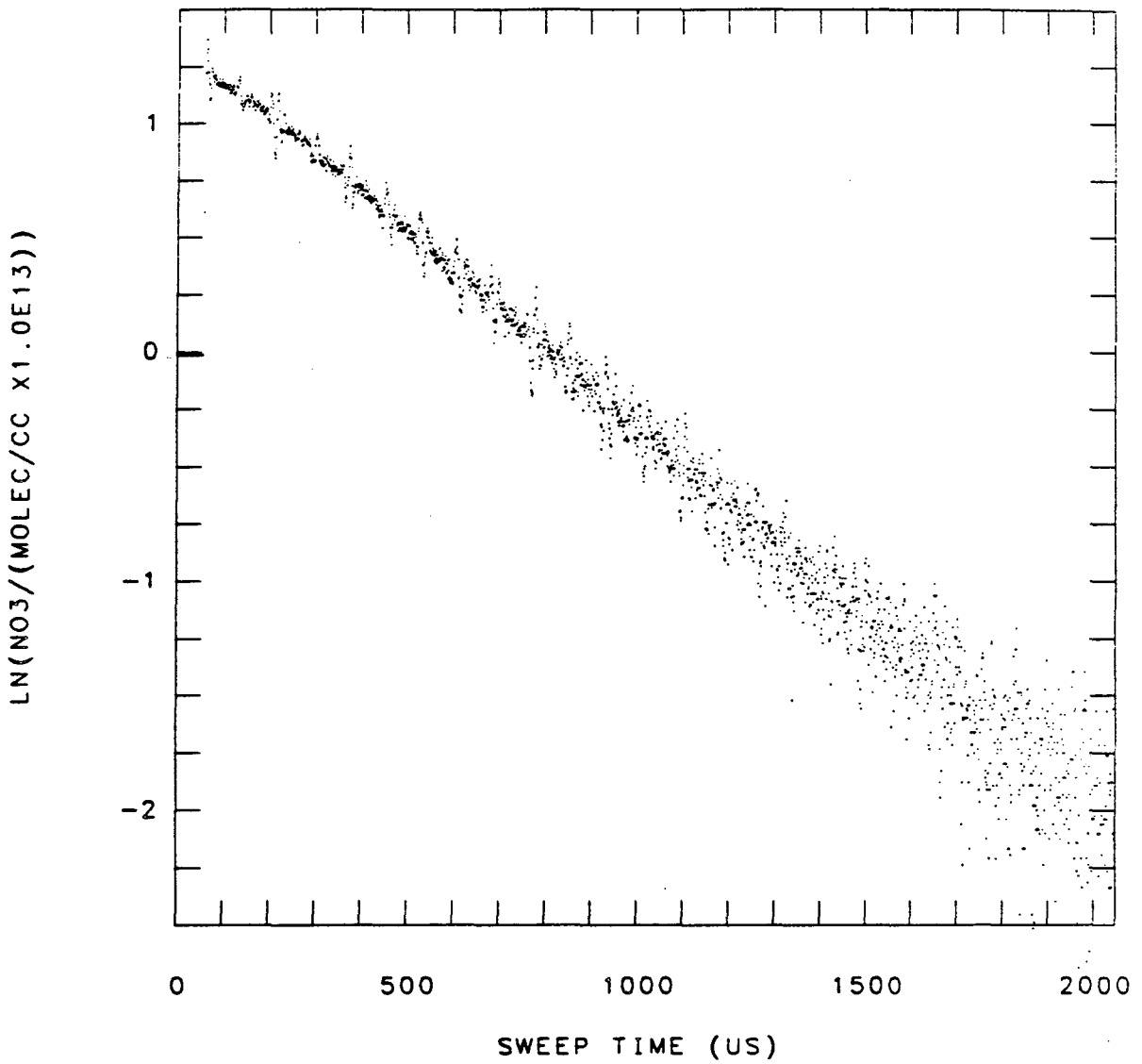

Figure 26. ln([NO_3]) versus time

the concentration and pathlength, respectively.

$$\ln (I_o/I) = (\sigma_1 N_1 + \sigma_2 N_2)L \tag{48}$$

For these experiments, two absorbing species were present, N_2O_5 and O_3. In order to solve for the concentrations of these species, for each experiment the absorption was measured at two wavelengths. At 250 nm, the O_3 neared its absorption maximum such that most of the total absorption at this wavelength was due to O_3. At 220 nm, the absorption cross-section of N_2O_5 is larger than that of O_3. The set of two simultaneous equations was then solved to calculate the concentrations of both N_2O_5 and O_3. The cross-sections used are shown in Table 14. The concentration of oxygen atoms for an individual experiment was then calculated from the O_3 concentration and photolysis energies using Beer's law.

$$[O] = I_o - I = I_o(1 - e^{-\sigma[O_3]L}) \tag{49}$$

The intensities (I and I_o) are in units of photons/cm^3 (the total pulse energy divided by the photolysis volume). The contribution to the total concentration of oxygen atoms from N_2O_5 photolysis can be calculated in a similar way. The total [O] is then the sum of contributions from both O_3 and N_2O_5 photolyses.

Table 14 UV Absorption Cross-sections of Precursors

Wavelength (nm)	σ/cm^2 O_3	N_2O_5
220	1.8×10^{-18}	2.2×10^{-18}
250	1.1×10^{-17}	4.0×10^{-19}

B. Results

The results of all the experiments at 20 torr total pressure are summarized in Table 15. In order to determine the rate constant k_1, k′ must be plotted against oxygen atom concentration. These results are shown in Figure 27. A linear least-squares analysis of the slope of the line gave $k_1 = 6.9 \pm 0.5 \times 10^{-12}$ cm^3/sec. The intercept was found to be 460 sec^{-1}. Under the experimental conditions, 60% of the intercept can be accounted for by Reaction 44.

1. Calculation of NO_3 Concentration

Although is is not necessary to know the NO_3 concentration to analyze the kinetics, it is useful to compare the concentration calculated from the N_2O_5 concentration to the concentration of NO_3 observed in the probe beam. The ratio NO_3(calc)/NO_3(obs) is shown in Table 15 for the last several entries. The ratio was generally about 20% too low. Half of this can be accounted for by realizing that no correction was made for reflection off the rear cell window. This correction would cause the calculated values of [NO_3] and [O] to increase, and would therefore reduce the value of k_1. The remainder may be due to errors in measuring correct N_2O_5 concentrations from the ultraviolet absorption measurements. Because the ozone cross-sections are larger than those of N_2O_5 by at least a factor of five, the error in measuring the ozone concentrations is expected to be much smaller

Table 15 O + NO_3 Kinetics Results at 20 torr

$[O_3]$ $/10^{14}cm^{-3}$	$[N_2O_5]$ $/10^{15}cm^{-3}$	$[O]$ $/10^{14}cm^{3}$	k' $/10^{-3}$ sec^{-1}	$[NO_3]$ $/10^{13}cm^{-3}$	$\frac{[NO_3](calc)}{[NO_3]\ (obs)}$
8.25	0.72	2.99	2.84	1.54	
14.19	0.48	3.55	2.85	1.00	
6.38	1.01	2.49	2.36	2.14	
5.33	0.96	2.26	2.26	1.95	
0.17	0.83	0.65	0.93	0.86	
6.52	1.01	1.23	1.75	0.99	
7.01	1.12	1.42	1.66	1.20	
9.30	1.12	1.53	2.05	1.18	
17.31	1.04	2.03	2.21	1.14	
7.36	1.14	1.48	1.70	1.24	
5.42	1.16	1.21	1.61	1.22	
3.72	1.12	0.91	1.39	1.14	
0.08	0.79	0.16	0.71	1.62	
1.50	0.79	0.89	1.38	1.64	
2.37	0.78	1.27	1.41	1.61	
3.32	0.86	1.80	1.60	1.93	
3.94	0.90	2.05	1.67	2.05	
4.43	0.91	2.18	1.73	2.03	
5.44	0.97	2.45	1.81	2.11	

Table 15 O + NO_3 Kinetics Results at 20 torr (Continued)

$[O_3]$ $/10^{14}cm^{-3}$	$[N_2O_5]$ $/10^{15}cm^{-3}$	$[O]$ $/10^{14}cm^{-3}$	k′ $/10^{-3}$ sec^{-1}	$[NO_3]$ $/10^{13}cm^{-3}$	$\frac{[NO_3](calc)}{[NO_3]\ (obs)}$
1.95	0.94	1.15	1.00	1.98	
0.14	0.96	0.22	0.48	2.02	
3.80	0.72	1.65	1.31	1.36	
5.22	1.38	2.18	2.18	2.64	
2.13	1.53	1.18	1.49	2.86	
7.04	0.86	2.43	1.86	1.60	
1.30	1.12	0.76	1.07	2.07	
0.69	1.00	0.48	0.81	1.87	
0.00	1.05	0.14	0.57	1.95	
3.50	1.13	1.60	1.58	2.11	
1.75	0.55	0.86	0.81	1.01	0.88
4.52	0.64	1.74	1.35	1.14	0.83
2.86	0.89	1.25	1.14	1.55	0.86
6.40	0.84	2.18	1.61	1.49	0.93
1.33	0.74	0.68	0.73	1.28	0.76
0.65	0.75	0.39	0.57	1.29	0.72
0.05	0.95	0.14	0.45	1.63	0.72
1.60	1.07	7.14	1.00	1.87	0.83

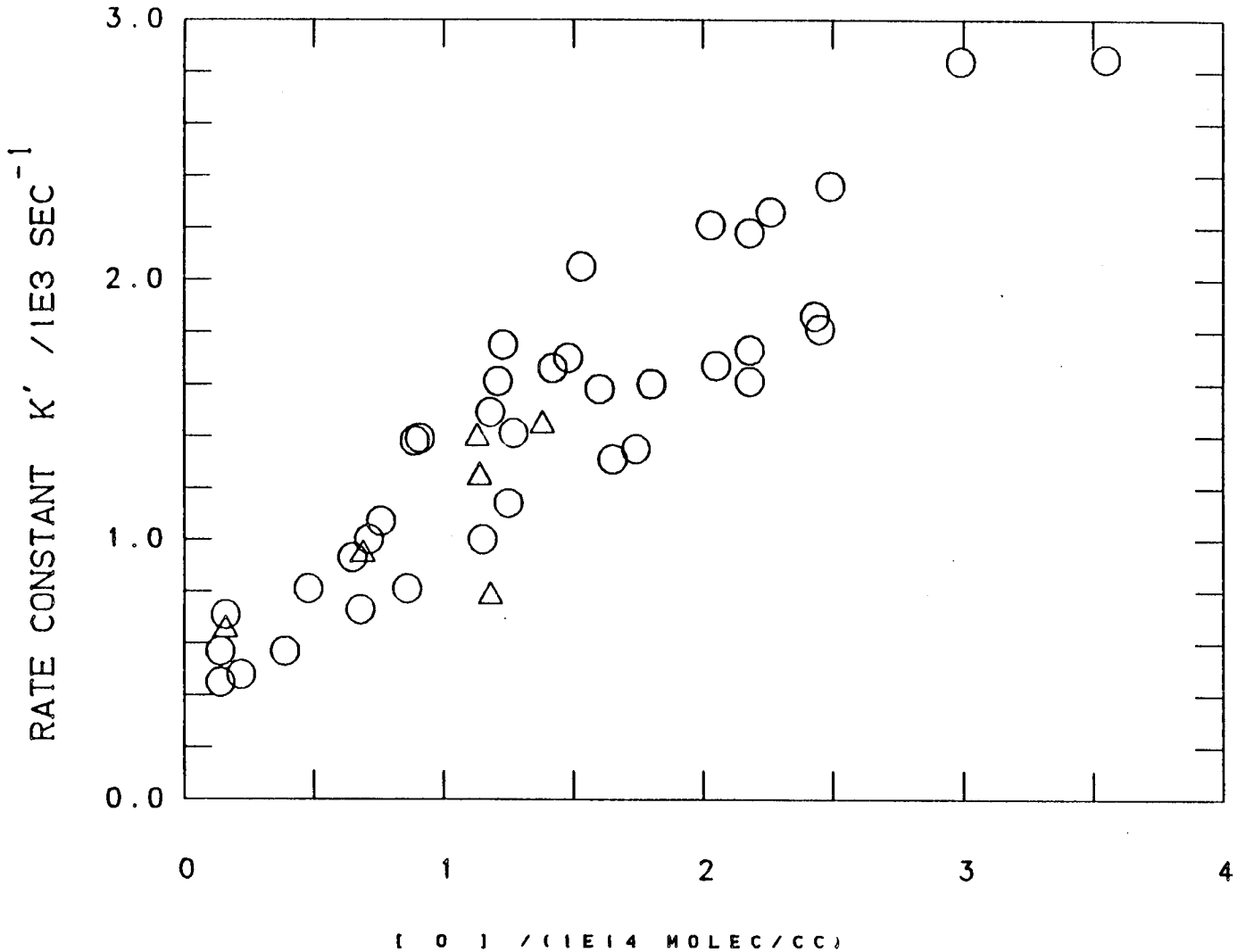

Figure 27. Rate constant, k', versus [O]

($\leq$ 2%) and can be neglected. Applying a 10% correction for reflection gives $k_1 = 6.2 \pm 0.5 \times 10^{-12}$ $cm^3 sec^{-1}$.

2. Pressure Dependence of the Rate Constant

If the reaction were to involve a third body, the rate constant obtained would be dependent on total pressure; therefore, a set of experiments was conducted at a higher pressure (100 torr). The results of these experiments are shown in Table 16. The analysis was carried out in the same manner as for the 20 torr experiments. The observed rate constants, k′, for both pressures are plotted in Figure 27. A fit of the line from the data at 100 torr gave a slope $k_1 = 6.7 \pm 0.3 \times 10^{-12}$ cm^3/sec. This value does not differ significantly from the value at 20 torr. No pressure dependence of the rate constant k_1 was observed for pressures between 20-100 torr.

C. Discussion

In order to test the assumption that the NO_3 concentration data fits a single exponential decay, the system was numerically modeled using the CHEMK[42] chemical kinetics program. CHEMK uses rate constants and initial concentrations as input, solves the rate equations numerically, and outputs concentration versus time for all species involved. In this case the set of equations and the rate constants used were those listed in Table 17. The

Table 16 O + NO_3 Kinetics Results at 100 torr

$[O_3]$ $/10^{14}cm^{-3}$	$[N_2O_5]$ $/10^{15}cm^{-3}$	$[O]$ $/10^{14}cm^{-3}$	k' $/10^{-3}\ sec^{-1}$	$[NO_3]$ $/10^{13}cm^{-3}$
2.77	1.36	1.38	1.44	2.51
5.28	1.00	1.13	1.39	1.87
0.64	1.05	1.18	0.78	1.87
2.09	1.22	1.14	1.24	2.33
0.00	1.26	0.16	0.65	2.28
1.15	1.06	0.69	0.94	1.97

Table 17 Reactions Used in Modeling (T = 298 K)

Reaction			k (20 torr) /$cm^3 sec^{-1}$
$NO_2 + NO_3$	$\xrightarrow{[M]}$	N_2O_5	3.55×10^{-13}
$O + NO_3$	$\longrightarrow$	$NO_2 + O_2$	1.0×10^{-11}
$O + NO_2$	$\xrightarrow{[M]}$	NO_3	5.37×10^{-14}
$O + NO_2$	$\longrightarrow$	$NO + O_2$	9.3×10^{-12}
$NO + NO_3$	$\longrightarrow$	$2\ NO_2$	2.0×10^{-11}
$O + NO$	$\xrightarrow{[M]}$	NO_2	7.17×10^{-14}
$O_3 + NO$	$\longrightarrow$	$NO_2 + O_2$	1.8×10^{-14}
$O_3 + O$	$\longrightarrow$	$2\ O_2$	8.0×10^{-15}
$O_3 + NO_2$	$\longrightarrow$	$NO_3 + O_2$	3.2×10^{-17}
$NO_3 + NO_3$	$\longrightarrow$	$2\ NO_2 + O_2$	2.3×10^{-16}

initial concentrations chosen were typical of an actual experiment and were 7.0×10^{12}, 3.0×10^{12}, and 1.0×10^{13} cm^{-3} for NO, NO_2 and NO_3, respectively. For the four simulations, the initial oxygen atom concentration was varied between 0.5 and 3.0×10^{14} cm^{-3}. The initial ozone concentration varied from $0.8\text{-}9.0 \times 10^{14}$ cm^{-3}. The appropriate ozone concentration was determined by assuming an average pulse energy of 20 mJ, and calculating the concentration of ozone required for the desired oxygen atom concentration. The simulation data were then fit to a single exponential function resulting in a rate constant k' (= $k_1[O] + k_3[NO]$). The results of these calculations are shown in Table 18. The value of k_1 calculated from these results was 9.90×10^{-12} cm^{-3}. Since this value differs from the value input into CHEMK by only 1.0%, the assumption of first-order kinetics is valid. This implies that one is justified in using first-order kinetics to obtain k_1 from the actual data.

The value of k_1 previously measured[6] was given as $1.0 \pm 0.4 \times 10^{-11}$ cm^3sec^{-1}. This differs from the value obtained in this study, $k_1 = 6.2 \pm 0.5 \times 10^{-12}$ cm^3sec^{-1}. The value measured here is lower than that previously reported, but is within the previous error estimates. The previous experiment was indirect and relied on values from many independent photolysis and reaction rates. Because of this, it seems reasonable that the value of k_1 determined in this study is more accurate.

Table 18 Results of Computer Modeling

$[O]/10^{14}$ cm^{-3}	k'/sec^{-1}
0.5	618 ± 0.5
1.0	1112 ± 0.7
2.0	2101 ± 1.1
3.0	3093 ± 1.1

VI. NO_3 LASER INDUCED FLUORESCENCE YIELDS

A. Results

The aim of this experiment was to measure fluorescence yields of NO_3 relative to NO_2. The fluorescence intensity showed a maximum at the time of the excitation pulse and decayed from this point logarithmically. This intensity is proportional to the number of photons absorbed, the yield, and a factor dependent on the geometry and sensitivity of the detection system used.

$$I \propto (\text{photons absorbed})(\phi)(\text{detector factor}) \qquad (50)$$

The relative yield for NO_3 compared to NO_2 is then given by

$$\phi_{NO_3}/\phi_{NO_2} = (\text{phot. abs.})_{NO_2} I_{NO_3}/(\text{phot. abs.})_{NO_3} I_{NO_2} \qquad (51)$$

The concentration of photons absorbed (which is equivalent to the change in intensity of the exciting pulse, ΔI_{ex}) can be calculated using Beer's law (Equation 52):

$$\Delta I_{ex} = I^{o}_{ex} - I_{ex} = I^{o}_{ex}(1 - e^{-\sigma_{ex} NL}) \qquad (52)$$

where σ is the absorption cross-section of the molecule at the exciting wavelength in cm^2, N is the concentration of the molecule in the beam path in cm^{-3}, and L is the path length in cm.

For these experiments, the intensity of the exciting laser was kept constant for a given set of NO_3 and NO_2 determinations.

Therefore, the intensity of the exciting laser factors out of the expression for the relative yields.

$$\phi_{NO_3}/\phi_{NO_2} = (1 - e^{-\sigma_{ex}NL})_{NO_2} I_{NO_3}/(1 - e^{-\sigma_{ex}NL})_{NO_3} I_{NO_2} \quad (53)$$

The steady state concentration (N) can also be calculated using Beer's law, from the absorption of the probe beam (the Nernst glower).

$$N = \ln (I_o/I)/\sigma L \quad (54)$$

A typical spectrum (Figure 28), in this case taken with a chart recorder, clearly shows the NO_3 absorption maximum at 662 nm. A typical NO_2 spectrum is shown in Figure 29.

The results of the nine sets of data taken are listed in Table 19. For each set, the fluorescence intensity obtained with NO_2 can be compared to that for NO_3. The cross-sections used in calculating the relative yields are given in Table 20. The data shown was obtained by subtracting a spectrum of the scattered laser light from the total intensity observed. The corresponding NO_3 spectrum is shown in Figure 30. In all cases the fluorescence intensity for NO_3 was below the noise level of the experiment. The values for NO_3 fluorescence intensity given in the table are an estimate of the noise level observed.

From these data, an upper limit for the NO_3/NO_2 total fluorescence ratio was found to be 4×10^{-3} for λ_{ex} = 623 nm. Because of large scattered light problems, only one data set was

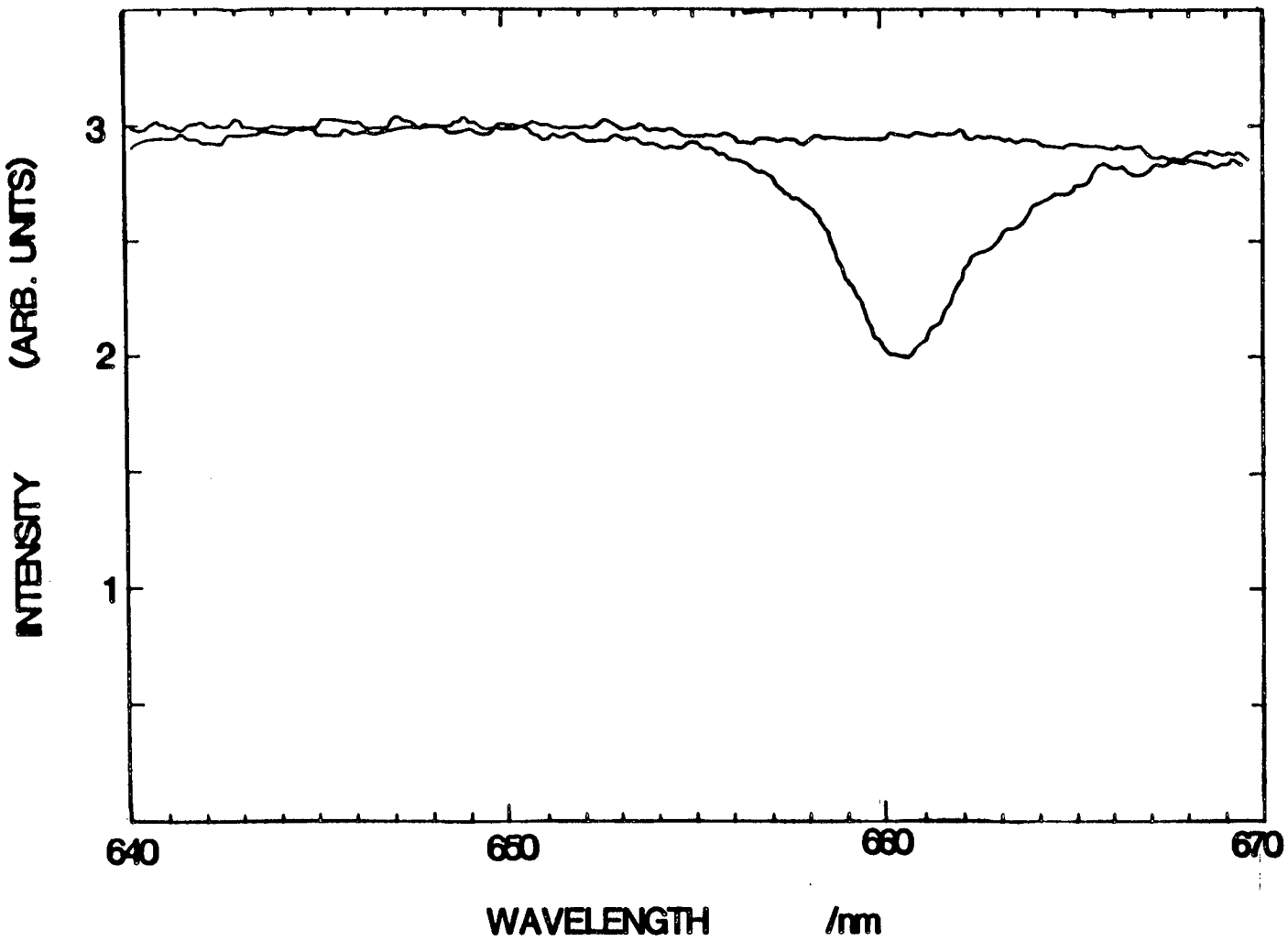

Figure 28. Spectrum showing NO_3 absorption in LIF experiments

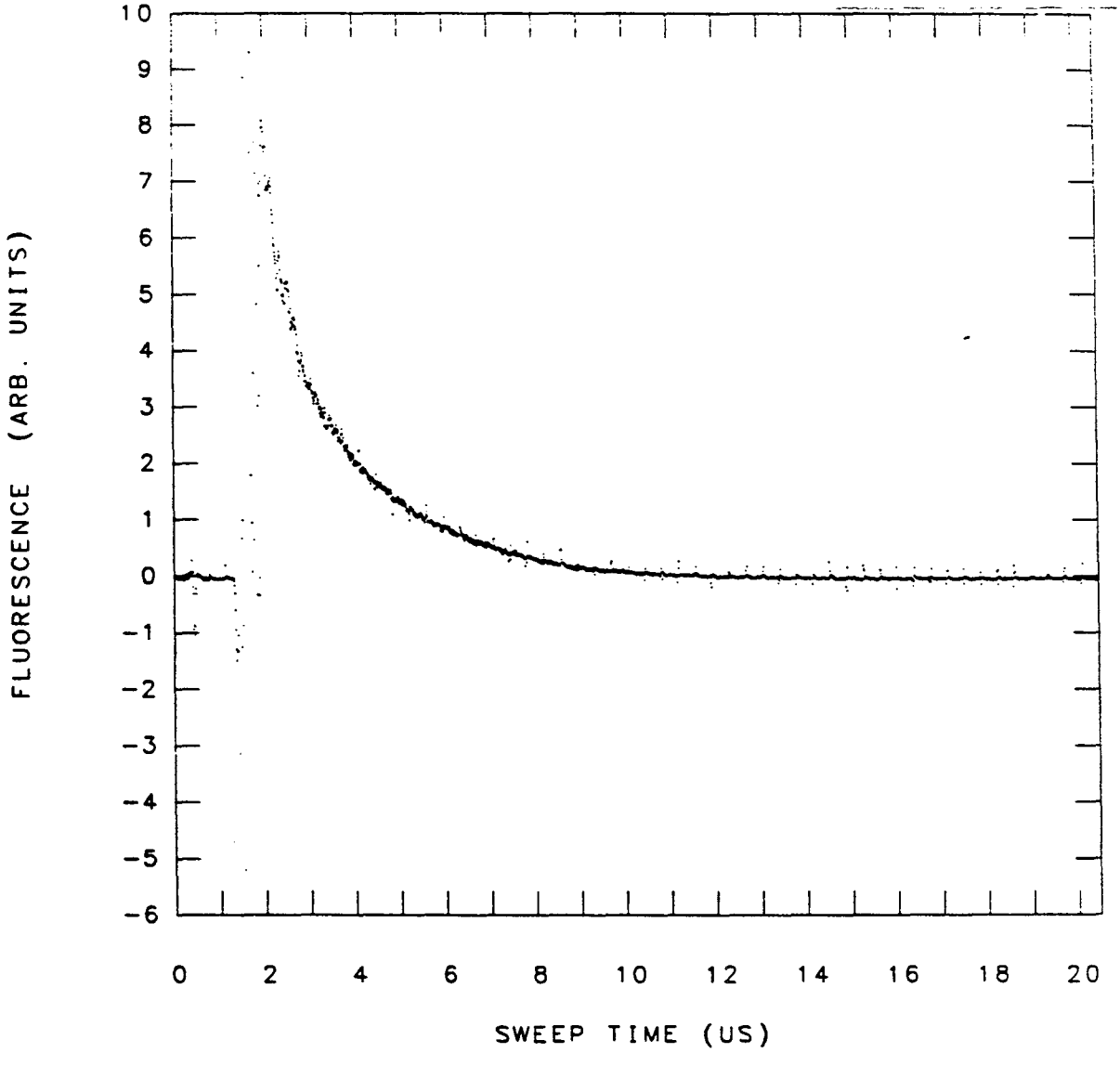

Figure 29. NO_2 fluorescence versus time

Table 19 Laser Induced Fluorescence Results

Set	$[NO_2]/10^{15}\ cm^{-3}$	$[NO_3]/10^{12}\ cm^{-3}$	I_{max} (arb.)	$1 - e^{-\sigma_{ex}NL}$	ϕ_{NO_3}/ϕ_{NO_2}
1	0.5		671	0.0155	
		9.5	67	0.226	0.007
		8.9	118	0.239	0.011
2	1.9		130	0.0336	
		4.0	≤40	0.0560	0.19
		4.0	≤40	0.0560	0.19
		4.5	≤20	0.0627	0.08
3	8.7		1640	0.269	
		6.6	113	0.173	0.11
		6.2	85	0.163	0.15
4	3.8		1000	0.128	
		4.2	≤20	0.113	0.023
5	9.8		1500	0.297	
		6.1	10	0.162	0.012
6	4.0		5128	0.136	
		8.0	130	0.205	0.017
7	4.1		8100	0.136	
		6.8	≤40	0.177	0.004
8	6.0		1600	0.019	
		2.9	≤50	0.123	0.005

Table 20 Visible Cross-sections for NO_2 and NO_3

λ/nm	σ_{NO_2}/cm^2	σ_{NO_3}/cm^2
623	1.5×10^{-20}	1.2×10^{-17}
650	1.6×10^{-20}	3.2×10^{-19}
662	2.0×10^{-21}	1.9×10^{-17}

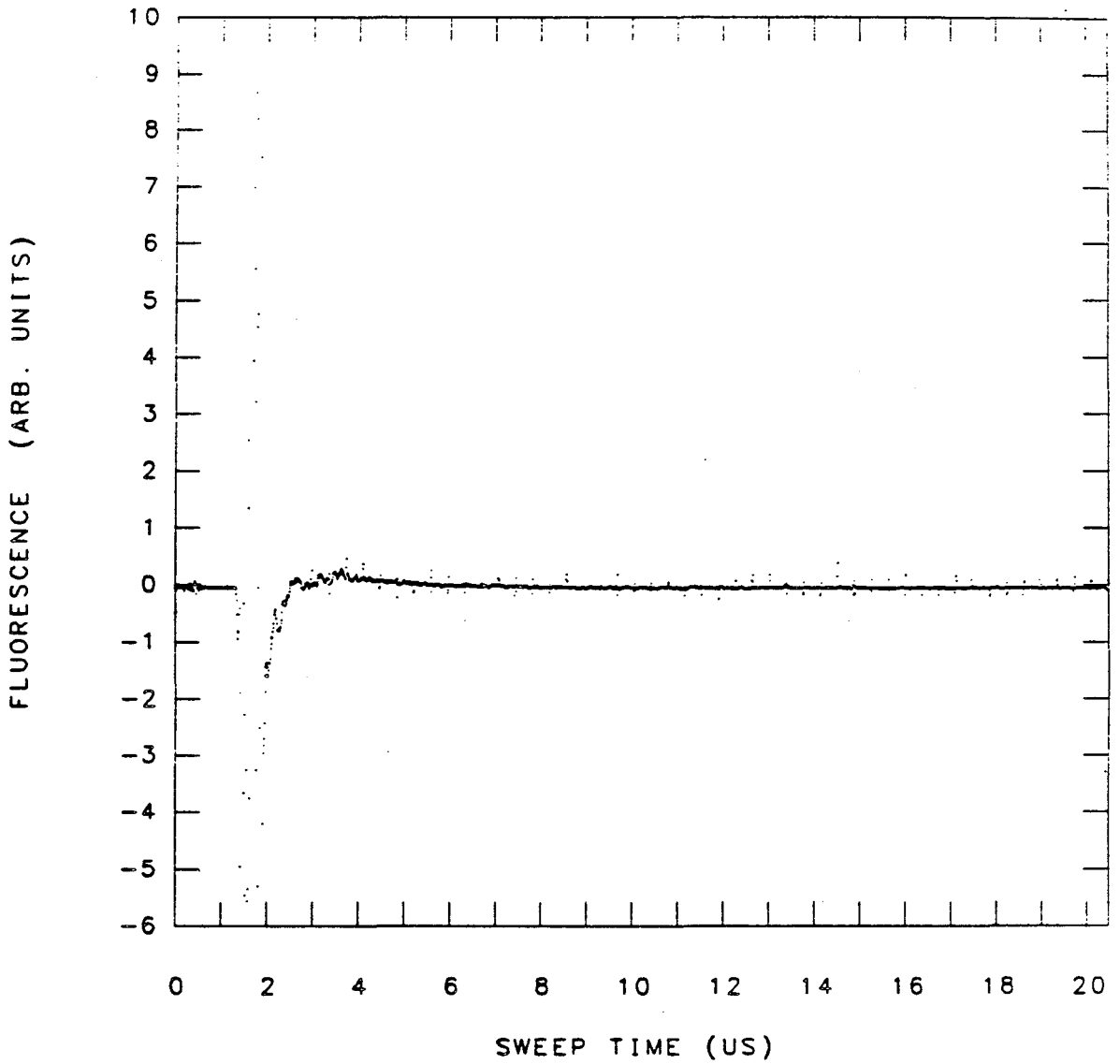

Figure 30. NO_3 'fluorescence' versus time. The peak is due to incomplete subtraction of the laser pulse.

taken at λ = 662 nm. The ratio at this wavelength did not differ substantially from those found at λ = 623 nm.

B. Consideration of Fluorescence Lifetimes

The scattered light problems encountered also serve to obscure the part of the spectra immediately after the laser pulse. This interference lasts for approximately 0.5 µsec. It is therefore necessary to consider whether the fluorescence lifetime is so short that the signal was obscured by the laser pulse and could not be observed.

In general, the fluorescence quenching rate, k_q, which is the inverse of the lifetime, τ, is given by Equation 55.

$$1/\tau = k_q = f + k_q[M] \tag{55}$$

where f is the collisionless fluorescence rate, k_q is the collisional quenching rate, and [M] is the total concentration of molecules present.

For NO_2, the fluorescence lifetime has been reported by Schwartz[43] to be about 70 µsec. Although the quenching rate at this exciting wavelength was not given, it can be estimated to be 1.6×10^{-10} cm^3/sec. The calculated fluorescence lifetime at 0.1 torr total NO_2 pressure will then be 1.9 µsec. One of the NO_2 spectra (set #8) was submitted to a least squares analysis of the decay rate. The observed lifetime was found to be 3.0 µsec, in

rough agreement with the calculated value. Lifetimes in the sets did not appear to differ substantially. This shows that fluorescence decays with lifetimes on the order of a few μsec are easily observable.

The fluorescence lifetime and collisional deactivation rates have also been measured by Nelson , et al., for NO_3.[44] The collisionless lifetime obtained was 340 μsec. Deactivation by nitric acid (one of the precursors) was found to be important, with a rate $k_q = 3.1 \times 10^{-10}$ cm^3/sec. Deactivation by O_2 was found to be 0.21×10^{-11} cm^3/sec. Assuming that the quenching rates of other NO_X species are similar to that for nitric acid, and that the O_2 deactivation is similar to O_3, one calculates an observed lifetime of 1.3 μsec for NO_3 fluorescence under typical experimental conditions. A comparison can also be made to the lifetimes observed by Ishiwata, et al.,[17] who used a similar chemical system for producing NO_3. At 0.5 torr total pressure, a lifetime of about 1.0 μsec was observed. Because the collision-free lifetime observed (2.8 μsec) was much shorter than that obtained by Nelson, et al.,[44] it is possible that the lifetime at 0.5 torr is also somewhat short. But by either estimation, the observed NO_3 lifetime should be long enough to permit detection of the fluorescence.

C. Discussion

As mentioned in the introduction (Section I.D), the diffuseness of the absorption spectrum of NO_3 and the absence of dissociation products in the region 660-662 nm can be explained by the Douglas effect.[14] If this is the case, visible fluorescence could be observed. The fluorescence is expected to have a long lifetime and a yield near unity. The upper limit on the fluorescence yield obtained in this work was 4×10^{-3} (λ= 623 nm). However, other studies have observed fluorescence.[16,17] A long collision-free lifetime of 340 µsec has been obtained.[44] The lifetime measurements give further evidence for the Douglas effect and suggest that redetermination of the fluorescence yield, under conditions such that fluorescence is observed, is necessary.

VII. *Ab initio* CALCULATIONAL STUDIES ON NO_3

A. Methods

All *ab initio* calculations were carried out on the Lawrence Berkeley Laboratory CDC 7600 computer system. The first set of calculations was done using an early version of HONDO/GAMESS.[45] The second set of calculations was done using a version of the Ohio State University Symmetry by Equal Contribution Molecular Integrals Program.[46] This program, however, could not handle basis sets large enough to include polarization functions. The final group of computations were done using an updated version of HONDO.[47] In all cases, standard basis sets were used. The optimized geometries from lower levels of calculation were used as initial guess geometries for higher levels. Geometry optimizations were carried out with a gradient optimization routine except in those cases for which the energy of a symmetric (D_{3h}) geometry was calculated from C_{2v} orbitals. In those cases, the optimum geometry was found by calculating single point energies for different bond lengths. The force constant calculations at the 4-31G level were done by moving the atoms along the internal coordinates and calculating the resulting gradient of the energy. The Wilson FG matrix method[48] was then used to solve for the vibrational frequencies. Calculations of the vibrational frequencies at the [4s-2p-1d] level were accomplished using a HONDO routine which first calculated the cartesian force constant

matrix and then used that matrix in determining the vibrational frequencies.

B. Results

The results of the geometry optimization calculations are listed in Table 21. For each basis set, the geometries, total electronic energies and electronic state are given. For the spin unrestricted Hartree-Fock (UHF) calculations, the resulting total spin density S^2 is also listed. In the case of the double-zeta plus polarization basis set [4s, 2p, 1d] calculation, two states are listed with different geometries and energies. The higher energy state was the one that the geometry optimization originally converged upon. When trying to calculate the vibrational frequencies for that state, a negative frequency was found indicating that the state was a local minimum. The geometry was then reoptimized such that the lower energy state was obtained.

The value of ΔE listed in Table 21 is the difference in energy between the lowest energy D_{3h} state and the lowest C_{2v} state for a particular basis set. These calculations predict that the preferred geometry for NO_3 is of distorted C_{2v} symmetry with a $^2B_2$ ground state energy 33.6 kcal/mol below that of the symmetric D_{3h} state (DZ + P).

Two other points are worth mentioning. First, the lowering of the energy on relaxing the symmetry restrictions was found to

Table 21 Geometry Optimization Results

Basis Set	Symmetry	R_1/Å	R_2,R_3/Å	$\theta_{2,3}$/deg	-E/au	ΔE/kcal	S^2	State
STO-3G UHF	C_{2v}	1.340	1.344	106.4	278.04955		1.528	$^2B_1$
4-31G UHF	D_{3h}	1.22			278.30210	22.7		$^2A_2'$
	C_{2v}	1.21	1.29	106.9	278.33849		1.11	$^2B_2$
[4s-2p]	D_{3h}	1.25			278.48921			$^2A_2'$
	D_{3h}^*	1.26			278.65925	10.6		($^2B_2$)
	C_{2v}	1.20	1.29	104.8	278.67571			$^2B_2$
[4s-2p-1d]	D_{3h}	1.19			278.72462			$^2A_2'$
	D_{3h}^*	1.21			278.82728			
	C_{2v}	1.17	1.24	104.6	278.8444	10.8		$^2B_2$
	C_{2v}	1.34	1.18	131.5	278.88074	33.6		$^2B_2$

be large. On going from the more restrictive D_{3h} to C_{2v} symmetry, greater orbital mixing occurred. In this case, the resulting energy difference ($E_{D_{3h}} - E_{D_{3h}}*$) was found to be 64 kcal/mol. Second, there appear to be many low lying states. This was shown in part by the fact that two $^2B_2$ states were found to be only 22.8 kcal/mol different in energy. The fact that the calculated values of S^2 were so high for the UHF calculations implies that interactions with low lying quartet states may also be important.

The results of calculations of the vibrational frequencies of NO_3 are shown in Table 22. Also listed in Table 22 are the frequencies which were experimentally observed,[16] subsequent to these calculations. The table shows a possible assignment of these frequencies compared to the best calculated values. At this level of calculation, the vibrational frequencies are expected to be about 20% too high[49]. Considering this, the calculated and experimental values show good agreement.

C. Discussion

A simple molecular orbital picture for the NO_3 radical, which considers only the p-orbitals perpendicular to the plane of the molecule, is shown in Figure 31. This simple model predicts that the lowest D_{3h} electronic state will be $^2E''$. The Jahn-Teller effect, however, predicts that the molecule will distort to C_{2v} symmetry. The calculations reported here, along with previous calculations,[50] have shown that this simple picture is

Table 22 Vibrational Analysis Results

	mode	frequency/cm^{-1} 4-31G	[4s-2p-1d]	experimental[16]
υ_1	symmetric stretch	1864	1592	1489
υ_2	symmetric bend	657	739	---
υ_3	N-O stretch	909	1129	1050
υ_4	out-of-plane bend	1086	880	754
υ_5	asymmetric stretch	681	1874	---
υ_6	asymmetric bend	349	617	360

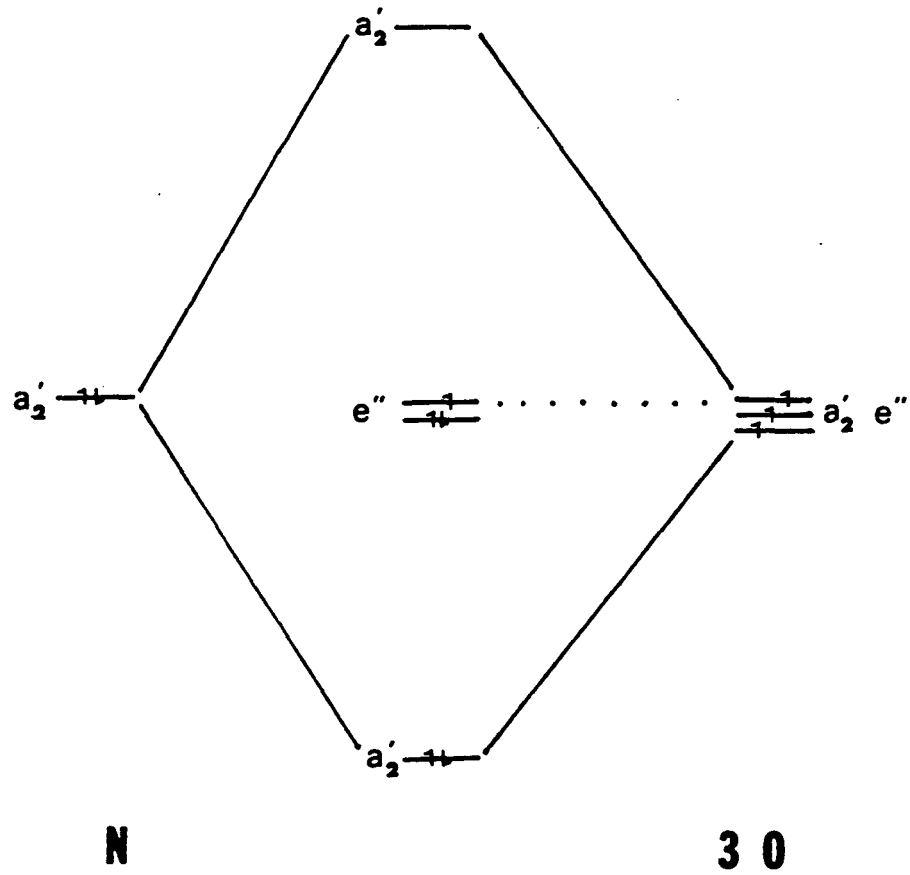

Figure 31. Simplified molecular orbital diagram for NO_3 with D_{3h} symmetry. Only the p_z (out-of-plane) orbitals are shown.

inadequate. The lowest energy state of D_{3h} symmetry was found by these calcualtion to be $^2A_2'$. Because this state is non-degenerate, the molecule would not be expected to distort. Some previous calculations assumed that knowledge of the D_{3h} ground state would be sufficient to predict the molecular geometry. The present calculations show that knowledge of this state alone is not sufficient. In fact, the energy of the lowest C_{2v} state was found to be below that of the D_{3h} states.

Before these calculations were completed, no conclusive experimental studies had been reported on either the geometry or vibrational frequencies of NO_3. Recently, however, two studies of NO_3 laser induced fluorescence[16,17] have provided the vibrational frequencies given in Table 22. These frequencies were found to be consistent with those calculated here for the C_{2v} symmetry; however, they are also fairly consistent with vibrational frequencies of similar molecules known to have D_{3h} symmetry.[51] Subsequently, a high-resolution diode laser study (of the 1480 cm^{-1} band) has been reported.[52] Assignment of the individual rotation-vibration lines has led to the conclusion that NO_3 is of D_{3h} symmetry. Perturbations of the lines were explained as being due to a low lying electronic state.

The calculations have shown that many low-lying configurations exist. These results and the recent experimental studies suggest that single configuration SCF calculations of this molecule are inadequate.

REFERENCES

1. H. H. Holmes, and F. Daniels, J. Am. Chem. Soc., 56, 630 (1934).

2. R. Murphy, Ph.D. Thesis, University of California, Los Angeles (1969).

3. P. S. Connell, Ph.D. Thesis University of California, Berkeley (1979).

4. F. Magnotta, Ph.D. Thesis University of California, Berkeley (1979).

5. D. L. Bauch, et al., Evaluated Kinetic and Photochemical Data for Atmospheric Chemistry, J. Phys. Chem. Ref. Data, 9, 295 (1980).

6. R. A. Graham and H. S. Johnston, J. Phys. Chem., 82, 254 (1978).

7. E. J. Jones and O. R. Wolf, J. Chem. Phys., 5, 873 (1937).

8. D. A. Ramsey, Proc. Colloq. Spectroscopy Int., 10th, 583 (1962).

9. G. Schott and N. Davidson, J. Am. Chem. Soc., 80, 1841 (1958).

10. W. J. Marinelli, D. M. Swanson and H. S. Johnston, J. Chem. Phys., 76, 2864 (1982).

11. A. R. Ravishankara and P. H. Wine, Chem. Phys. Lett., 101, 73 (1983).

12. H. S. Johnston and R. A. Graham, Can. J. Chem., 52, 1415 (1974).

13. D. M. Mitchell, R. P. Wayne, P. J. Allen, R. P. Harrison and R. J. Twin, J. Chem. Soc. Faraday II, 76, 785 (1980).

14. A. E. Douglas, J. Chem. Phys., 45, 1007 (1966).

15. For a review see D. K. Hsu, D. L. Monts, R. N. Zare, "Spectral Atlas of Nitrogen Dioxide 5530 to 6480 Å", Academic Press: New York, 1978.

16. H. H. Nelson, L. Pasternak and J. R. McDonald, J. Phys. Chem., 87, 1286 (1983).

17. T. Ishiwata, I. Fujiwara, Y. Naruge, K. Obi and I. Tanaka, J. Phys. Chem., 87, 1349 (1983).

18. D. E. Wood and G. P. Lozos, J. Chem. Phys., 64, 546 (1976).

19. A. Reuveni and Z. Luz, J. Magn. Reson., 23, 271 (1976).

20. G. W. Chantry, A. Horsfield, J. R. Morton and D. H. Whiffen, Mol. Phys., 5, 589 (1962).

21. T. K. Gunda Rao, K. V. Lingam and B. N. Bhattacharya, J. Magn. Reson., 16, 369 (1974).

22. R. M. Golding and M. Henchman, J. Chem. Phys., 40, 1554 (1964).

23. A. D. Walsh, J. Chem. Soc., 2306 (1953).

24. J. F. Olsen and L. Burnelle, J. Am. Chem. Soc., 92, 3659 (1970).

25. T. E. H. Walker and J. A. Horsley, Mol. Phys., 21, 939 (1971).

26. R. Lefebvre and E. Ressayre, Theoret. Chim. Acta, 18, 391 (1970).

27. A. Lund and K. Thomas, Chem. Phys. Lett., 44, 569 (1976).

28. W. J. Marinelli, Ph.D. Thesis, University of California, Berkeley (1981).

29. Exciton Chemical Company.

30. F. Paschen, Ann. Phys., 40, 27 (1919).

31. For a complete description, see Ref. 28, p. 59.

32. Written by Brian Kan, revised by Diane M. Swanson.

33. J. U. White, J. Opt. Soc. Am., 32, 285 (1942).

34. D. L. Littlejohn, Ph.D. Thesis University of California, Berkeley (1980).

35. J. R. Barker, M. J. Rossi, P. L. Trevor and D. M. Golden, preprint.

36. A. R. Ravishankara, private communication.

37. D. L Bauch, et al., Evaluated Kinetic and Photochemical Data for Atmospheric Chemistry, J. Phys. Chem. Ref. Data, 9, 295 (1980).

38. Chemical Kinetic and Photochemical Data for Use in Stratospheric Modeling Evaluation Number 5 (NASA-Jet Propulsion Laboratory, 1982).

39. See Ref. 38, p. 88.

40. F. Yao, I. Wilson and H. S. Johnston, J. Phys. Chem., (1982).

41. D. Swanson, B. Kan and H. S. Johnston, J. Phys. Chem., 88, 3115 (1984).

42. G. Z. Whitten and J. P. Meyer, CHEMK: A Computer Modeling Scheme for Chemical Kinetics (Systems Applications, Inc., 1979).

43. S. F. Schwartz and H. S. Johnston, J. Chem. Phys., 51, 1286 (1969).

44. H. H. Nelson, L. Pasternak and J. R. McDonald, J. Chem. Phys., 79, 4279 (1983).

45. M. Dupuis, J. Rys and H. F. King, GAMESS version 1.0 (1980).

46. Written by H. L. Hsu and R. M. Pitzer, with revisions by H. F. Schaefer, III and P. Saxe.

47. H. F. King, M. Dupuis and J. Rys, HONDO version 6.0 (1981).

48. E. B. Wilson, Jr., J. C. Decius and P. C. Cross, "Molecular Vibrations", McGraw-Hill Book Co.: New York, 1956.

49. H.F. Schaefer, personal communication

50. See Refs. 22-26.

51. For example NO_3^-.

52. T. Ishiwata, I. Tanaka, K. Kawaguchi and E. Hirota, J. Chem. Phys., 82, 2196 (1985).